

Optimizing withdrawal from drinking water reservoirs to
combine downstream river demands with a sustainable raw
water management

by Michael Weber

from Leipzig

Accepted Dissertation thesis for the partial fulfillment of the requirements for a

Doctor of Natural Sciences

Fachbereich 7: Natur- und Umweltwissenschaften

Universität Koblenz-Landau

Thesis examiners:

Prof. Dr. Andreas Lorke, University of Koblenz-Landau

Dr. Bertram Boehrer, Helmholtz Centre for Environmental
Research - UFZ, Magdeburg

Date of the oral examination: 21 December 2017

This dissertation is based on the following research articles:

Weber, M., Rinke, K., Hipsey, M.R., Boehrer, B., accepted 07 March 2017. Optimizing withdrawal from drinking water reservoirs to reduce downstream temperature pollution and reservoir hypoxia. *Journal of Environmental Management* 197, 96-105. doi:10.1016/j.jenvman.2017.03.020

Weber, M., Boehrer, B., Rinke, K., in review since July 2017. Minimizing environmental impact whilst securing drinking water quantity and quality demands from a reservoir. *River Research and Applications*.

Hipsey, M.R., Weber, M., et al., in review since November 2017. A General Lake Model (GLM 2.4) for linking with high-frequency sensor data from the Global Lake Ecological Observatory Network (GLEON). *Geoscientific Model Development*.

Table of contents

Abstract	1
Chapter 1: Introduction	2
1.1 The worldwide dam boom	2
1.2 Dam impact on downstream rivers – the release of hypolimnetic, cold waters.....	3
1.3 Selective withdrawal to mitigate the temperature disruption.....	4
1.4 Withdrawal strategies for the combination of downstream and in-reservoir water quality objectives	6
1.5 Research Objectives and Questions	7
1.6 Outline of the thesis	8
Chapter 2: A General Lake Model (GLM 2.4) for linking with high-frequency sensor data from the Global Lake Ecological Observatory Network (GLEON)	10
Abstract.....	10
2.1 Model background	11
2.2 Adaptive offtake dynamics	13
2.3 Dynamic coupling with biogeochemical and ecological model libraries	14
Chapter 3: Optimizing withdrawal from drinking water reservoirs to reduce downstream temperature pollution and reservoir hypoxia.....	16
Chapter 4: Minimizing environmental impact whilst securing drinking water quantity and quality demands from a reservoir	17
Abstract.....	17
4.1 Introduction.....	17
4.2 Methods.....	20
4.2.1 Study site	20
4.2.2 Model description and source code modifications	21
4.2.3 Input data.....	22
4.2.4 Scenario definitions.....	23
4.3 Results.....	25
4.3.1 Initial scenario	25
4.3.2 Management parameter improvement.....	28

4.3.3	Optimized reservoir management	29
4.4	Discussion	31
4.5	Conclusion	35
	Acknowledgements	35
Chapter 5:	Major findings and discussion	36
5.1	Numerical models in realistic reservoir simulations	38
5.2	Temperature as a key factor in regulated rivers	39
5.3	Hypolimnetic oxygen as a key factor for in-reservoir water quality	41
5.4	Improved reservoir withdrawal strategy to mitigate the dam impact whilst securing raw water quality.....	42
5.5	Implications for reservoir modelling.....	43
5.6	Decision support for Integrated Water Resources Management.....	45
Chapter 6:	Conclusions	47
	References	48
	Author contributions	56
	Other contributions.....	57
	Declaration	58
	Curriculum Vitae.....	59
	Danksagung.....	60
	Appendix 1	62

Abstract

Fresh water resources like rivers and reservoirs are exposed to a drastically changing world. In order to safeguard these lentic ecosystems, they need stronger protection in times of global change and population growth. In the last years, the exploitation pressure on drinking water reservoirs has increased steadily worldwide. Besides securing the demands of safe drinking water supply, international laws especially in Europe (EU Water Framework Directive) stipulate to minimize the impact of dams on downstream rivers. In this study we investigate the potential of a smart withdrawal strategy at Grosse Dhuenn Reservoir to improve the temperature and discharge regime downstream without jeopardizing drinking water production. Our aim is to improve the existing withdrawal strategy for operating the reservoir in a sustainable way in terms of water quality and quantity. First, we set-up and calibrated a 1D numerical model for Grosse Dhuenn Reservoir with the open-source community model “General Lake Model” (GLM) together with its water quality module “Aquatic Ecodynamics” library (AED2). The reservoir model reproduced water temperatures and hypolimnetic dissolved oxygen concentrations accurately over a 5 year period. Second, we extended the model source code with a selective withdrawal functionality (adaptive offtake) and added operational rules for a realistic reservoir management. Now the model is able to autonomously determine the best withdrawal height according to the temperature and flow requirements of the downstream river and the raw water quality objectives. Criteria for the determination of the withdrawal regime are selective withdrawal, development of stratification and oxygen content in the deep hypolimnion. This functionality is not available in current reservoir models, where withdrawal heights are generally provided *a priori* to the model and kept fixed during the simulation. Third, we ran scenario simulations identifying an improved reservoir withdrawal strategy to balance the demands for downstream river and raw water supply. Therefore we aimed at finding an optimal parallel withdrawal ratio between cold hypolimnetic water and warm epilimnetic or metalimnetic water in order to provide a pre-defined temperature in the downstream river. The reservoir model and the proposed withdrawal strategy provide a simple and efficient tool to optimize reservoir management in a multi-objective view for mastering future reservoir management challenges.

Chapter 1: Introduction

1.1 The worldwide dam boom

Human population growth and economic development under a changing climate increases the need for a safe electricity and drinking water supply. As water reservoirs are a booming source of renewable energy, thousands of large dams are either planned or under construction (Zarfl et al., 2015). According to the definition of the International Commission on Large Dams (2011), 58.519 dams were registered worldwide until May 2017, but thousands were still unrecorded. The main purpose of these large water reservoirs is irrigation water supply (~20.000 dams), electric power generation (~10.000 dams), drinking water supply (~7600 dams) and flood protection (~7.300 dams). Besides the single use of dams and reservoirs, a large number of dams were used in multiple ways e.g. for combining irrigation and raw water supply. Zarfl et al. (2015) showed that hydropower projects involve about 3.700 large dams currently planned or under construction worldwide. In conclusion, the large numbers of dams worldwide demonstrate that reservoirs play an important role producing “green” energy or supplying water for different demands.

However, dam operations have a decisive impact on freshwater ecosystems worldwide. Almost 60% of the large river systems are regulated by dams (Nilsson et al., 2005). Prominent examples are the Yangtse River (Asia), Colorado River and Rio Negro (America), as well as rivers Congo, Zambesi and Nile (Africa). Nearly 80% of the world’s population (4.8 billion, in 2000) live in areas where water security or biodiversity is threatened. Additionally, Vörösmarty et al. (2010) found that the habitat diversity in riverine ecosystems of 65% of the global river discharge is under moderate to high threat. Obstructions like dams play a major role for this habitat loss due to different impacts on rivers upstream and downstream of reservoirs. Inundation as an upstream effect, endangers terrestrial ecosystems, accelerates greenhouse gas emissions or leads to a massive resettlement. Especially the large dam projects in India and China have forced millions of people to leave their homes and to relocate. As a result of the Three Gorges Dam Project in China, for example, more than 1 million people have undergone an involuntary resettlement (Wilmsen, 2016).

1.2 Dam impact on downstream rivers – the release of hypolimnetic, cold waters

The disruption of the river continuum plays a crucial role for the downstream parts of rivers. Dams severely affect water temperature, flow discharge, aquatic communities, sediment transport and nutrient content downstream the dam. Then, the demands of regulated rivers on water quality and quantity, primarily for a natural temperature and flow discharge, cannot be fulfilled. The effect of temperature pollution can be classified in warm water and cold water pollution. Warm water pollution can be found in rivers downstream hydro-power dams, whereas cold water pollution appears downstream water supplying reservoirs (e.g. drinking water). On a temporal scale, we can distinguish between long term and short term temperature pollution. Long term temperature pollution is created by reservoir operations using only one withdrawal height especially to maintain the downstream water flow (e.g. via bottom outlet). This helps cold adapted fish species to establish, displacing native species (Sherman et al., 2007). In contrast, the short term temperature pollution is mostly related to operations of hydro-power dams with fluctuating discharges. This abrupt change in water temperature, also called thermopeaking, can be observed in many rivers downstream of (hydropower) reservoirs (Gore et al., 1989; Carolli et al., 2012). Together with huge variations in flow discharge (hydropeaking) it imposes serious consequences on the aquatic life. As water temperature is a key factor in rivers, temperature and flow manipulation may cause serious changes in biological communities or even a loss of populations. Sherman et al. (2007) found that year-round cold waters from Hume Dam, Australia, can support cold adapted fish species to establish, displacing native species. Bruno et al. (2013) investigated the responses of benthic invertebrates on hydropower dam releases and their abrupt temperature changes in flume experiments and found a severe drift. Long term observations in Green River downstream Flaming Gorge Dam (USA) showed a strong decline of invertebrates compared to pre-dam conditions (Vinson, 2001). Literature on the effect of dam operations on ecological community response over long or short time periods in the downstream river is still rather limited. We can conclude, however, that operations of large dams have a great potential to threaten the aquatic communities downstream.

Withdrawing cold water from the deepest layers of a reservoir (e.g. via bottom outlet) to downstream rivers is still a widely-used strategy. In drinking water reservoirs, bottom outlet withdrawal was implemented for water quality characteristics in the deep hypolimnion. There, the so called hypolimnetic withdrawal strategy is a relic from the times of cultural

eutrophication in Europe and North America. The aim was to maximize the export of phosphorus on the one hand and to protect hypolimnetic oxygen conditions on the other hand (Olszewski, 1961; Nürnberg, 1987). By hypolimnetic withdrawal low-oxygenated water from the deepest layers in the hypolimnion is removed and the oxygen content is increased by upper water layers with higher oxygen content. Maintaining sufficiently high oxygen concentrations in the hypolimnion and, hence preventing hypoxia or even anoxia avoids the release of nutrients and metals out of the sediment and a further eutrophication of the water body. Another advantage is the flushing of deposited sediments from hydro-power dams to preserve the storage capacity (Espa et al., 2016). However, there are negative effects of hypolimnetic withdrawal.

Besides the thermopeaking effect, the withdrawal of water from the deepest layers will also weaken the stratification in the reservoir. Large withdrawal leads to a dramatic shrinkage of the hypolimnion and the intensified vertical exchange will strongly influence the nutrient and phytoplankton dynamics (Barbiero et al., 1997). Furthermore, it will lead to a deepening of the thermocline and hence, to a warming of the hypolimnion (Gaugush, 1984) that accelerates oxygen depletion and reduces raw water quality in drinking water reservoirs. Above all, hypolimnetic withdrawal will lead to a loss of highly valuable raw water for drinking water production.

1.3 Selective withdrawal to mitigate the temperature disruption

The provisioning of economical aims, such as a sufficient electricity and raw water supply, whilst mitigating environmental impact on downstream rivers is essential for ecosystem services. In the last decades, further efforts, ranging from numerical simulations to structural changes (e.g. selective withdrawal structures), were made helping to reduce the disruption of the river continuum focusing on downstream water temperatures. The definition of selective withdrawal is “to use outlets placed at different levels in the dam to draw off selectively the water of desired quality according to a plan” (from Brooks and Koh, 1969). Specialized infrastructures for selective withdrawal can be multi-level intakes or pivoted pipes (Olden and Naiman, 2010). Fontane et al. (1981) used optimization techniques coupled with a 1D numerical reservoir model to control the discharge temperature by selective withdrawal. One of the first attempts to solve temperature pollution problem below large dams was the installation of a \$20 million multilevel outlet at Flaming Gorge Dam (USA) in

1978. Since the 1970's and 1980's, many reservoirs in the United States have been equipped with selective withdrawal structures for controlling the quality of the discharged water downstream (e.g. temperature). The Temperature Control Device (TCD) at Shasta Dam, for example, was built in 1997 for \$80 million to improve downstream fish habitats (Bartholow et al., 2001). Recently, a selective withdrawal structure was also installed at the Grosse Dhuenn Reservoir in Germany (Weber et al., 2017).

The withdrawal strategy was often modified to mitigate the river disruption. The impact on stratification and water quality of the reservoir water body was investigated by several numerical simulation studies. Selective withdrawal from the upper water layers (epilimnion/metalimnion) strengthened the thermal stability (stratification) during summer. Withdrawal height can control the thermocline depth and, hence, the hypolimnetic water volume (Casamitjana et al., 2003). According to their results, epilimnetic or metalimnetic withdrawal conserved cold water in the hypolimnion (Kennedy, 1999) usable for the drinking water supply. Moreno-Ostos et al. (2008) and Kerimoglu and Rinke (2013) provided evidence that a stronger stratification would lower the flux of hypolimnetic nutrients as a source for algae. Furthermore, Barbiero et al. (1997) suggested that stronger summer stratification can reduce the growth of cyanobacteria. In eutrophic (drinking) water reservoirs the selective withdrawal from the upper layers could be a viable strategy to reduce harmful algal blooms (Brookes and Carey, 2011).

However, predominant withdrawal from the upper layers can have a negative impact on the dissolved oxygen (DO) dynamics in the hypolimnion due to a higher thermal stability and minimal water renewal at the lake bottom (Çalışkan and Elçi, 2009; Zhang et al., 2013). During summer stratification the hypolimnion is isolated from oxygen-rich water layers in the epilimnion/metalimnion where atmospheric exchange and primary production takes place. Then, hypolimnetic DO is depleted by oxygen demanding processes (e.g. mineralization of organic material). If DO depletion continues long enough, hypoxic or even anoxic conditions occur. As a consequence nutrients and metals are increasingly released out of the sediments (Davison, 1993; Giles et al., 2016). Dissolved in lake water, the nutrients become available for primary producers. As a consequence, increased algal biomasses and stronger hypolimnetic oxygen depletion deteriorate the water quality.

In drinking water reservoirs, the concentration of dissolved manganese plays a crucial role for the costs of raw water treatment (Gantzer et al., 2009). As sufficiently high DO

concentrations suppress the release of manganese out of the sediments, low DO conditions in the hypolimnion should be avoided. In numerical simulations, Marcé et al. (2010) were optimizing the reservoir withdrawal strategy to better control the hypolimnetic DO dynamics and to avoid anoxia. So far, literature on combining downstream river demands with in-reservoir water quality requirements is still scarce (Kunz et al., 2013) and appropriate model tools are lacking.

1.4 Withdrawal strategies for the combination of downstream and in-reservoir water quality objectives

To the author's knowledge, the optimization potential in managing (drinking water) reservoirs in a way serving both, protecting raw water quality and quantity as well as minimizing the dam impact on the downstream river, has rarely been explored. Basic elements for combining the restoration of the quasi-natural temperature and flow conditions downstream with safeguarding reservoir water quality are the advantages and disadvantages of epilimnetic/metalimnetic and hypolimnetic withdrawal, mentioned in Chapter 1.2 and 1.3. Therefore, a smart mixing of cold hypolimnetic water with warm epilimnetic or metalimnetic water will provide a simple but powerful way to realize quasi-natural discharge temperatures and sufficiently high hypolimnetic DO concentrations at the same time. According to this, the goals for optimizing reservoir operation are:

- restoring temperature and flow regimes downstream without thermopeaking,
- protecting reservoir water quality to guarantee a safe raw water supply,
- minimizing the loss of valuable hypolimnetic water.

As all three goals are linked, they could not be altered without impacting the others (Figure 1.1).

Numerical models have been used to optimize selective withdrawal from reservoirs since 1980 (Fontane et al., 1981). The first optimization goals were downstream objectives like a desirable discharge water temperature. Later studies focused on flushing of deposited sediments (Espa et al., 2016) and other ecological parameters like salinity (Kerachian and Karamouz, 2006). In recent years, different optimization approaches using heuristic optimization algorithms, mostly genetic algorithms (GAs) and Reinforcement Learning (RL) have been applied (Kerachian and Karamouz, 2006; Castelletti et al., 2014). These

optimization approaches used in reservoir management are very effective, but may be too complex for operators to integrate them in real-time into the reservoir operation. Simple approaches, like demonstrated in Kunz et al. (2013) can easily and quickly be integrated into the operational strategy. However, there is a need for reservoir models with integrated management rules that are able to optimize management strategies for combining in-reservoir and downstream river objectives. The key for providing a near natural discharge temperature and flow for the downstream river without jeopardizing raw water supply for drinking water production is the smart balance between parallel withdrawal of cold hypolimnetic water with warm epilimnetic or metalimnetic water.

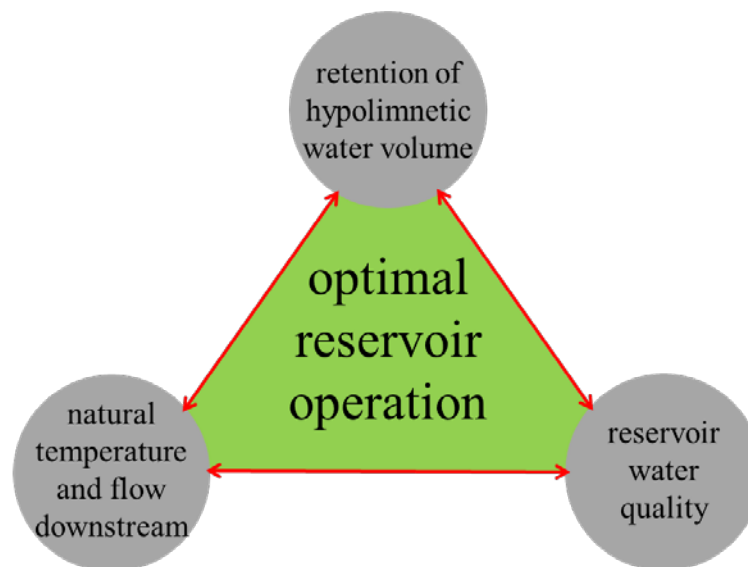


Fig. 1.1. Main goals in drinking water reservoir operation optimization in this study

1.5 Research Objectives and Questions

The purpose of this research was (i) the implementation of operational rules into the source code of an existing one-dimensional hydrodynamic model to (ii) reduce the impact of the reservoir on the downstream river temperature and flow while (iii) keeping raw water quality safe. The main management approach to fulfill these purposes was the (iv) optimization of the withdrawal strategy. We used the Grosse Dhuenn Reservoir, a major drinking water reservoir in western Germany, as a case study for exemplifying the outlined research agenda. Therefore, the focus of this modelling study was on drinking water

reservoirs. However, the numerical tool and the results of this thesis are partly transferable to reservoirs for hydro-power, irrigation and recreation (as discussed in Chapter 5.5).

Based on the gaps in the current state of reservoir modelling, we aimed at answering following research questions:

- Can we extend existing one-dimensional hydrodynamic models and integrate operational rules and management decisions into the simulation of reservoir water quality and stratification?
- Can we restore the quasi-natural temperature and flow conditions in downstream rivers by changing the current withdrawal strategy?
- What is the impact of a modified withdrawal strategy on stratification and water quality, especially hypolimnetic DO?
- Can we combine downstream river demands with a sustainable raw water supply by an optimal withdrawal strategy?

1.6 Outline of the thesis

This thesis is divided into three parts that consist of three research articles, either published in or submitted to peer-reviewed journals (Chapter 2-4). All articles are dedicated to the objectives in this thesis as stated above and to answer its research questions.

Chapter 2

In the first part of the thesis, we present an overview on the one-dimensional hydrodynamic model “General Lake Model” - GLM and the coupled water quality library “Aquatic EcoDynamics” - AED2. In detail, this method section consists of parts from the original description paper (see Appendix 1) and further explanations on the operational rules (source code modifications).

Hipsey, M.R., ... Weber, M. (in review, since November 2017), A General Lake Model (GLM 2.4) for linking with high-frequency sensor data from the Global Lake Ecological Observatory Network (GLEON), Geoscientific Model Development.

Chapter 3

The second part of the thesis presents the first application of the extended one-dimensional model (GLM/ AED2) applied on the Grosse Dhuenn Reservoir. Here, we investigated the impact of a modified reservoir withdrawal strategy on the stratification of the water body and the hypolimnetic dissolved oxygen content. Recommendations for future reservoir management are given.

Weber, M., Rinke, K., Hipsey, M.R., & Boehrer, B. (accepted 07 March 2017), Optimizing withdrawal from drinking water reservoirs to reduce downstream temperature pollution and reservoir hypoxia, Journal of Environmental Management.

Chapter 4

In the third part of the thesis we investigated the potential of withdrawal management of a large drinking water reservoir to alleviate the disruption of the river continuum by a reservoir dam with respect to the quasi-natural temperature and discharge. The reservoir model together with the proposed improved withdrawal strategy is provided as a simple and transferable tool for reservoir operators.

Weber, M., Boehrer, B., & Rinke, K. (in review, since July 2017), Minimizing environmental impact whilst securing drinking water quantity and quality demands from a reservoir, River Research and Applications.

Chapter 2: A General Lake Model (GLM 2.4) for linking with high-frequency sensor data from the Global Lake Ecological Observatory Network (GLEON)

In Chapter 2.1 we provide a general description of the “General Lake Model”-GLM. Then, in Chapter 2.2, we describe the new adaptive offtake functionality that was implemented in the model source code to simulate realistic selective reservoir withdrawal. In Chapter 2.3 we present the coupling ability of GLM to biogeochemical and ecological model libraries such as the Framework for Aquatic Biogeochemical Models (FABM) and the Aquatic Ecodynamics (AED2) Model Library.

Abstract

The General Lake Model (GLM) is a one-dimensional open-source model code designed to simulate the hydrodynamics of lakes, reservoirs and wetlands. GLM was developed to support the science needs of the Global Lake Ecological Observatory Network (GLEON), a network of lake sensors and researchers attempting to understand lake functioning and address questions about how lakes around the world vary in response to climate and land-use change. The scale and diversity of lake types, locations and sizes, as well as the observational data within GLEON, created the need for a robust community model of lake dynamics with sufficient flexibility to accommodate a range of scientific and management needs of the GLEON community. This paper summarizes the scientific basis and numerical implementation of the model algorithms, including details of sub-models that simulate surface heat exchange and ice-cover dynamics, vertical mixing and inflow/outflow dynamics. A summary of typical parameter values for lakes and reservoirs collated from a range of sources is included. GLM supports a dynamic coupling with biogeochemical and ecological modelling libraries for integrated simulations of water quality and ecosystem health. An overview of approaches for integration with other models, and utilities for the analysis of model outputs and for undertaking sensitivity and uncertainty assessments is also provided. Finally, we discuss application of the model within a distributed cloud-computing environment, and as a tool to support learning of network participants.

Keywords: lake, stratification, mixing, water balance climate change, water quality, observatory network

2.1 Model background

GLM adopts a 1D approach for simulating lake mixing processes by resolving a vertical series of layers that describe the variation in water column properties. Users may configure any number of inflows and outflows, and more advanced options exist for simulating aspects of the water and heat balance. Depending on the context of the simulation, either daily or hourly meteorological time-series data for surface forcing is required, and daily time-series of volumetric inflow and outflow rates can also be supplied. The model is suitable for operation in a wide range of climate conditions and is able to simulate ice formation, as well as accommodating a range of atmospheric forcing conditions.

Although GLM is a new model code written in the C programming language, the core layer structure and mixing algorithms is founded on principles and experience from model platforms including the Dynamic Reservoir Simulation Model (DYRESM; Imberger and Patterson, 1981; Hamilton and Schladow, 1997) and the Dynamic Lake Model (DLM; Chung et al., 2008). Other variations have been introduced to extend this underlying approach through applications to a variety of lake and reservoir environments, to which the reader is also referred (e.g., Hocking & Patterson, 1991; McCord & Schladow, 1998; Gal et al., 2003; Yeates and Imberger, 2003). The layer structure is numbered from the lake bottom to the surface, and adopts the flexible Lagrangian layer scheme first introduced by Imberger et al. (1978) and Imberger & Patterson (1981). The approach defines each layer as a ‘control volume’ that can change thickness by contracting and expanding in response to inflows, outflows, mixing with adjacent layers, and surface mass fluxes. Layer thickness limits are enforced to adequately resolve the vertical density gradient with fine resolution occurring in the metalimnion and thicker cells where mixing is occurring, as depicted schematically in Figure 2.1. Unlike fixed-grid (Eulerian) design of most 1D lake and ocean models, it has been reported that numerical diffusion at the thermocline can be restricted by this approach (depending on the user-defined minimum (h_{min}) and maximum (h_{max}) layer thickness limits set by the user), making it particularly suited to long-term investigations, and requiring limited site-specific calibration (Patterson et al., 1984; Hamilton & Schladow, 1997; Bruce et

al., 2017). Layers each have a unique density computed based on the local salinity and temperature, and when sufficient energy becomes available to overcome density instabilities between adjacent layers, they will merge, thereby accounting for the process of mixing. For deeper systems, a stable vertical density gradient will form in response to periods of high solar radiation creating warm, less-dense conditions near the surface with cooler conditions deeper in the water, separated by a metalimnion region which includes the thermocline. The number of layers $N_{LEV}(t)$, is adjusted throughout the simulation to maintain homogenous properties within a layer. Initially, the layers are assumed to be of equal thickness, and the initial number of layers, $N_{LEV}(t = 0)$. As the model simulation progresses, density changes due to surface heating, vertical mixing, and inflows and outflows lead to dynamic changes in the layer structure, associated with layers amalgamating, expanding, contracting or splitting.

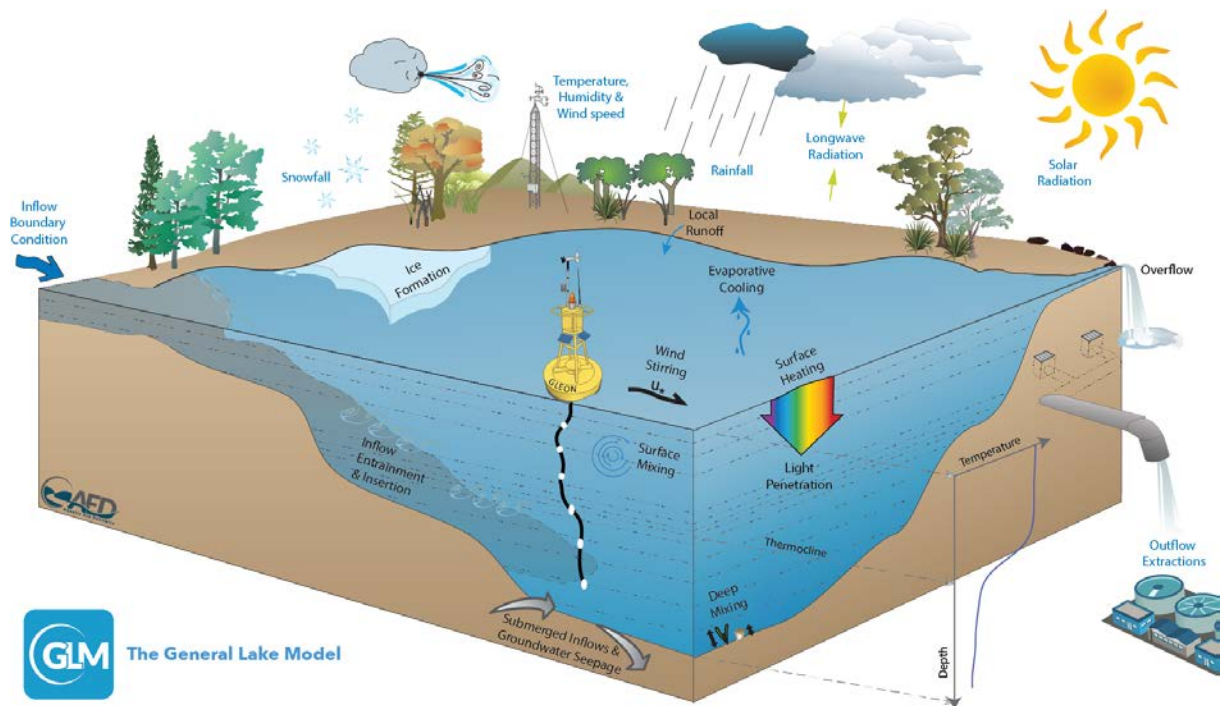


Fig. 2.1. Schematic of a GLM simulation domain, input information (blue text) and key simulated processes (black text).

Because this approach assumes layer properties are laterally averaged, the model is suitable for investigations where resolving the horizontal variability is not a requirement of the study. This is often the case for ecologists and biogeochemists studying natural lakes (e.g.,

Gal et al., 2009), managers simulating drinking water reservoirs (e.g., see Chapter 3 or Weber et al., 2017), or mining pit lakes (e.g., Salmon et al., 2017), or for analyses exploring the coupling between lakes and regional climate (e.g., Stepanenko et al., 2016). Further, whilst the model is able to resolve vertical stratification, it may also be used to simulate shallow lakes, wetlands, wastewater ponds and other small waterbodies that experience well-mixed conditions. In this case, the layer resolution, with upper and lower layer bounds specified by the user, will automatically simplify, and mass and energy will continue to be conserved.

2.2 Adaptive offtake dynamics

For reservoir applications, a special outflow option has been implemented to simulate an adaptive offtake or selective withdrawal. This approach is used for accommodating flexible reservoir withdrawal regimes and their effects on the thermal structure within a reservoir. For this option, a target temperature is specified by the user and GLM estimates the corresponding withdrawal height within a predefined (facility) range to meet this target temperature during the runtime of the simulation, i.e. the withdrawal height follows adaptively the thermal stratification in the reservoir. The target temperature can be defined as a constant temperature (e.g. 14 °C) or a time series like a measured water temperature from an upstream river (via a *.csv file). The height of the adaptive offtake is printed out in a *.txt file and may be used for reservoir operation. In addition to the basic adaptive offtake function, GLM can also simulate withdrawal mixing, i.e. water from the adaptive offtake is mixed with water from another predefined height (e.g. bottom outlet). For this option, the discharges at both locations need to be predefined by the user (via outflow *.csv file) and GLM chooses the adaptive withdrawal from a height, where the water temperature is such that the resulting mixing temperature meets the target temperature. This withdrawal mixing is a common strategy in reservoir operation where deep water withdrawal and temperature control is required at the same time.

An example of the adaptive offtake function (AOF) with and without withdrawal mixing, assuming a constant water temperature of 14 °C of the outflowing water, shows that GLM is able to deliver a constant outflow temperature of 14 °C during the stratified period (Figure 2.2). In winter, when the water column is cooler than 14 °C, the model withdraws surface water. The adaptive offtake functionality can be used in a stand-alone mode or coupled to the dissolved oxygen concentration (via water quality model AED2). In the latter case, the effect of the withdrawal regime on the oxygen dynamics in the hypolimnion can be

simulated (see Chapter 3 or Weber et al., 2017). In this setting, the simulated hypolimnetic dissolved oxygen concentration at a specified height is checked against a critical threshold. If the hypolimnetic oxygen falls below the critical threshold, the height of the adaptive offtake will be automatically switched to a defined height (usually deep outlets in order to get rid of the oxygen-depleted water) to withdraw water from this layer, until the oxygen concentrations have recovered. For a full description of the adaptive withdrawal functionality processes, readers are referred to Figure 2.3 and Online Resource ESM_3 in Chapter 3.

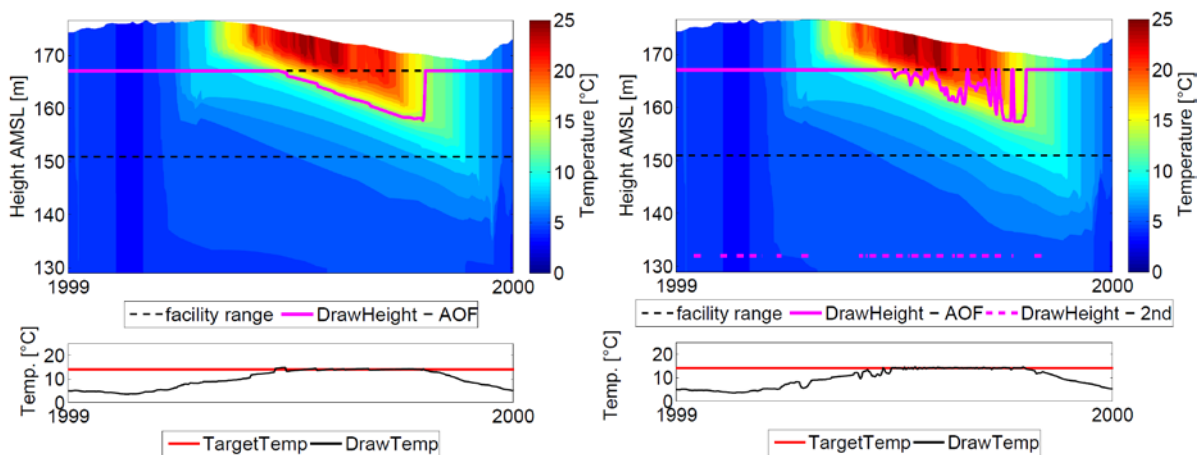


Fig. 2.2. Adaptive offtake function (AOF, selective withdrawal) reservoir simulation; simulated water temperatures of the adaptive offtake model assuming a constant temperature of 14 °C without (left) and with (right) mixing with bottom outlet withdrawal. The black dashed line represents the range of the variable withdrawal facility and the magenta lines the adaptive offtake and second withdrawal height (bottom outlet in this case).

2.3 Dynamic coupling with biogeochemical and ecological model libraries

Beyond modelling the water and heat balance of a lake, the model has been designed to couple with biogeochemical and ecological model libraries. Currently the model is distributed pre-linked with the Framework for Aquatic Biogeochemical Models (FABM; Bruggeman and Bolding, 2014) and the Aquatic Ecodynamics (AED2) Model Library (Hipsey et al., 2013) simulation library. Through connection with these libraries GLM can simulate the seasonal changes in vertical profiles of turbidity, oxygen, nutrients, phytoplankton, zooplankton, pathogens and other water quality variables of interest. For more information on the water quality model AED2, readers are referred to Hipsey et al. (2013).

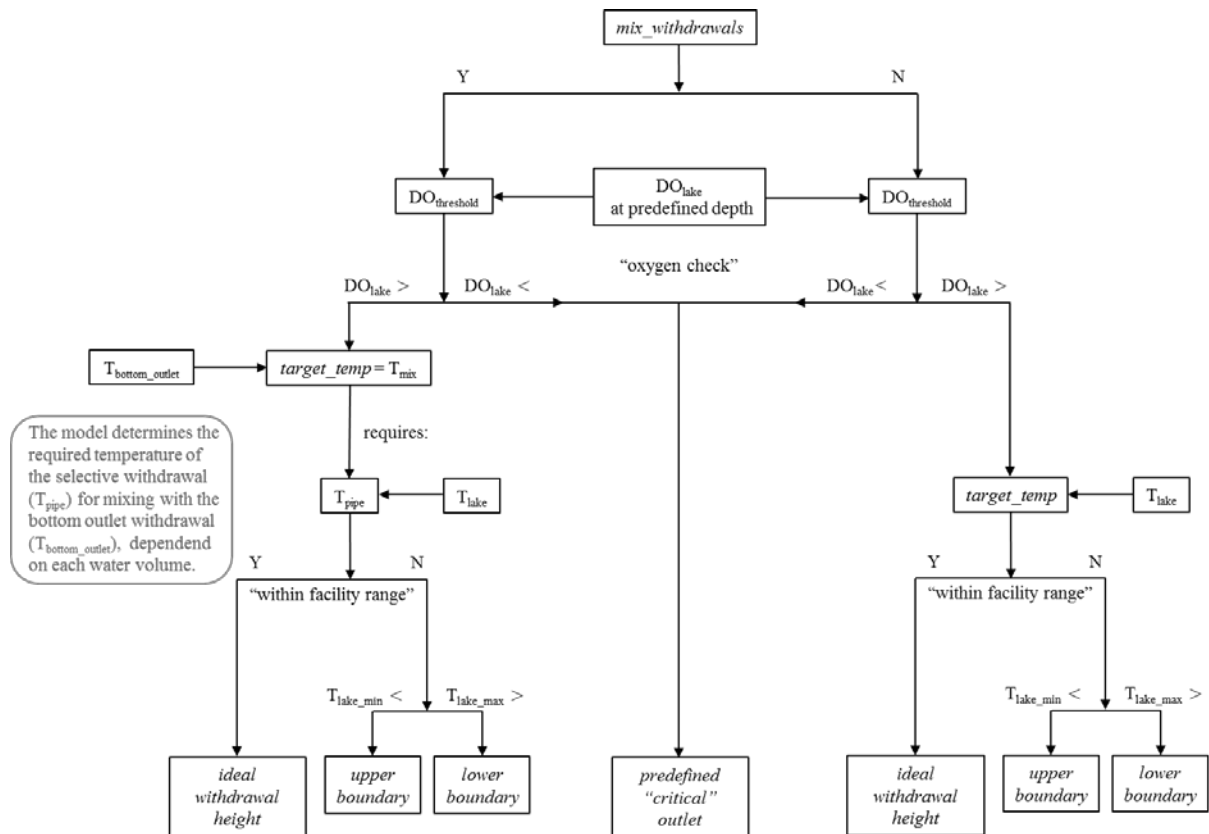


Fig. 2.3. Decision tree to estimate the withdrawal height depending on the thermal structure (T_{lake}) and the hypolimnetic dissolved oxygen (DO_{lake}) concentration in GLM-AED2.

Chapter 3: Optimizing withdrawal from drinking water reservoirs to reduce downstream temperature pollution and reservoir hypoxia

Note by the author

This chapter is based on a published paper in Journal of Environmental Management. Due to copyright issues, the text of the chapter was replaced by the reference information and its web link. The interested reader is kindly asked to access the published paper via the following reference:

Weber, M., Rinke, K., Hipsey, M.R., Boehrer, B., 2017. Optimizing withdrawal from drinking water reservoirs to reduce downstream temperature pollution and reservoir hypoxia. Journal of Environmental Management 197, 96-105. doi:10.1016/j.jenvman.2017.03.020

[Click here to see the published paper.](#)

Chapter 4: Minimizing environmental impact whilst securing drinking water quantity and quality demands from a reservoir

Abstract

Complying the demands of drinking water supply whilst minimizing environmental impact is a great challenge. This study investigates the potential of withdrawal management of drinking water reservoirs to alleviate the disruption of the river continuum by a reservoir dam with respect to temperature and discharge. The aim is the identification of an optimal withdrawal strategy to provide a near natural discharge temperature and flow for the downstream river without jeopardizing drinking water production. First, we identify the applicability of such a new withdrawal strategy regarding raw water sustainability and downstream river demands. Second, we search for an ideal withdrawal regime in scenario simulations with a calibrated and validated reservoir model (“General Lake Model” –GLM). The scenarios demonstrate that we are able to derive an optimal reservoir management for Grosse Dhuenn Reservoir. Implications of the results for reservoir management are discussed and the numerical model is provided for operators as a simple and efficient tool for optimizing the withdrawal strategy within reservoir management.

Keywords: reservoir operation, river management, modelling, selective withdrawal, hypolimnetic dissolved oxygen, thermal stratification

4.1 Introduction

Dam construction will globally be boosted in the next decades (Zarfl et al., 2015). The main purposes of these dams are electric power generation, drinking and irrigation water supply and flood protection (Kennedy, 1999). However, dams and reservoirs disrupt the river continuum and affect water temperature, flow discharge, sediment transport and nutrient concentration downstream (Nilsson et al., 2005). In times of global change and population growth, fresh water resources like rivers and reservoirs need protection (Brookes et al., 2014). Integration of reservoir operation into river management plans is mandatory. Therefore, the demands on water supply and downstream ecology should be balanced. Selective withdrawal structures like multi-level intakes or pivoted pipes provide new operational strategies to integrate reservoir storage in water quality management.

In fact, selective reservoir withdrawal can mitigate the disruption of temperature and flow discharge (Olden and Naiman, 2010). The withdrawal from the epilimnion or metalimnion facilitates a more natural temperature of the water discharged into the downstream river. However, as Weber et al. (2017) have shown, the predominant withdrawal from the upper, warm layers will strengthen the thermal stability and may harm reservoir water quality by low oxygen conditions in the hypolimnion at the end of the stratification period. In the simplest case, the withdrawal should then switch to the bottom outlet to withdraw cold and low-oxygenated hypolimnetic water. However, this would lead to an abrupt drop in discharge temperature (also called thermopeaking, Zolezzi et al., 2011). Then, the positive ecological effects of the restored, i.e. quasi-natural, temperature may be annulled by the thermopeaking in autumn. In general, the thermopeaking effect can be observed in many rivers downstream of drinking water reservoirs and hydropower dams worldwide and has a decisive impact on the biological communities (Gore et al., 1989; Carolli et al., 2012).

The use of a parallel and additional hypolimnetic withdrawal (e.g. through bottom outlet) will alleviate the thermopeaking effect or even prevent it. The export of nutrients and low-oxygenated water secures raw water quality in the reservoir and drinking water production. Nevertheless, hypolimnetic withdrawal also has some negative feedbacks. Besides the thermopeaking, hypolimnetic withdrawal will weaken stratification and increase hypolimnetic water temperatures (Gaugush, 1984). Additionally it discharges highly valuable cold water into the downstream river, which otherwise would be available for drinking water production. Balancing withdrawal of cold hypolimnetic water with selective withdrawal of warm epilimnetic or metalimnetic water will provide a simple but powerful tool to modify discharge temperatures and DO concentrations in the deepest reservoir layers. The current goals for optimizing reservoir operation are:

- restoring temperature and flow downstream with no thermopeaking,
- protecting reservoir water quality to guarantee a safe raw water supply,
- minimizing the loss of valuable hypolimnetic water.

All three goals are linked and, hence, could not be altered without a feedback on the others (Figure 4.1). Therefore, we need an integrated and smart multi-objective based management of reservoirs and rivers. With the help of a new class of reservoir models that can be applied in an operational mode, we are able to link water quantity management with

water quality and explicitly include operational rules into the source code of a numerical model.

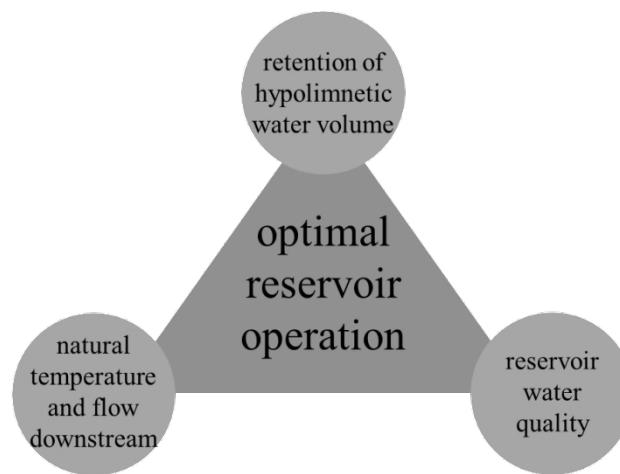


Fig. 4.1. Main goals in reservoir operation optimization in this study

Such optimization techniques in reservoir management have been applied to combine different demands for downstream river and raw water quality (Labadie, 2004; Kerachian and Karamouz, 2006; Castelletti et al., 2014). However, these powerful tools are complex and often difficult to apply in operational use. Consequently, we need a new class of reservoir models that balance efforts and effects associated with raw water availability and downstream river conditions.

The aim of this study is the improvement of the current withdrawal strategy to provide a near natural discharge temperature and flow for the downstream river without jeopardizing raw water supply for drinking water production. Therefore, we include operational reservoir management rules in the source code of a one-dimensional reservoir model for a realistic withdrawal management. Based on selective withdrawal and the development of stratification, the model autonomously determines the best withdrawal height according to the temperature and flow requirements of the downstream river over the simulated period. In scenario simulations, we search for an improved withdrawal strategy to avoid DO concentrations below a defined threshold while keeping discharge temperature natural. Here, we aim for a balance between parallel withdrawal of cold hypolimnetic water with warm epilimnetic or metalimnetic water. Our flexible and simple reservoir model together with the improved withdrawal strategy will then be integrated into the operational use. The reservoir model

source code is freely available for download from GitHub (<https://github.com/AquaticEcoDynamics>).

4.2 Methods

4.2.1 Study site

Our study site, Grosse Dhuenn Reservoir, is located in the western part of Germany east of Cologne (51.066 °N, 7.190 °E). It has a maximum volume of 81 million m³ and a maximum depth of 53 m and hence is one of the largest drinking water reservoirs in Germany. It supplies up to 42 million m³ per year of raw water for drinking purposes to 1 million inhabitants. The reservoir is also used for flood protection and maintaining an ecological minimum discharge in the downstream river Dhuenn (see also Weber et al. 2017). The reservoir has 2 large and 15 smaller dams above the main reservoir (pre-dams) to reduce nutrient and suspended solid inputs from the numerous tributaries. The reservoir is considered oligotrophic and monomictic. On average, the Grosse Dhuenn Reservoir is supplied with 36 million m³ of water per year from the two main inflows and with 23 million m³ from direct run-off and the overflow of the ungauged 15 smaller pre-dams. The mean outflow for raw water supply amount to 37 million m³ and downstream river discharge to 22 million m³, respectively. Therefore, the residence time of the main reservoir at maximum water level is 1.3 years (mean of 1996-2014).

Until 2013, the water for the downstream river Dhuenn was withdrawn exclusively from the bottom outlet and was therefore cold year-round. Additionally, the withdrawal was performed as a staircase like hydrograph (“old strategy”, see Figure 4.2) especially during higher flow discharges. In 2014, a pivoted pipe was installed at the withdrawal tower to selectively withdraw warm water from the upper water layers (epilimnion/metalimnion) to the downstream river. The aim was reducing the impact of the reservoir on the downstream river and restoring the natural temperature and discharge to allow the reestablishment of a natural fish community. With the new facility, water from that pivoted pipe could be withdrawn exclusively from the epi- or metalimnion in order to realize a given target temperature or it could be mixed with water from the bottom outlet. In this latter case, the withdrawn water must be warmer than the target temperature given the cold hypolimnion of 4-6°C. For a

scheme of the withdrawal structure at Grosse Dhuenn Reservoir, readers are referred to Weber et al. (2017).

4.2.2 Model description and source code modifications

To simulate reservoir management and its impact on the water body, we applied the 1D “General Lake Model” (GLM) coupled by the Aquatic EcoDynamics library (AED2) for capturing the thermal stratification and the dissolved oxygen (DO) dynamics in the hypolimnion. GLM is an open-source community model that simulates water balance, vertical stratification, mixing, heat exchange and the effect of inflows/outflows (Hipsey et al., 2014). The model has further been extended to accommodate a variety of lake and reservoir model applications. To capture the DO dynamics in the hypolimnion, we added a simple oxygen model with two temperature dependent depletion rates: the water column oxygen depletion rate J_V [$g\ m^{-3}yr^{-1}$] and the sediment-related (i.e. areal) oxygen depletion rate J_A [$g\ m^{-2}yr^{-1}$]. We neglected primary production because the management focus was on the oxygen status of the reservoir hypolimnion where no photosynthesis is taking place (for more details see Weber et al., 2017).

The new pivoted pipe at the withdrawal tower was included in the source code of GLM as a separate module with the purpose to withdraw water having a user-defined, time-dependent target temperature being defined on basis of the natural temperature regime in the downstream river. An automated algorithm determines the withdrawal height of the pivoted pipe in the model each day on basis of the current temperature stratification, the range of the pivoted pipe and the desired discharge temperature. We defined this target discharge temperature based on the inflow river temperature. Furthermore, if a certain withdrawal through the bottom outlet is mandatory, e.g. under flooding conditions or for maintaining a certain water renewal in the deep hypolimnion, a mixing temperature calculation is performed. In these cases, the withdrawal height of the pivoted pipe is calculated in such a way that the resulting temperature of the mixed water flows (outlet from pivoted pipe and from bottom outlet) meets the target temperatures for the downstream river (i.e. selecting a warmer temperature than in the case without bottom outlet).

4.2.3 Input data

Hydrological, meteorological and basic morphological data were provided by the reservoir authority Wupperverband. As a guideline for restoring the natural temperature in the downstream river Dhuenn, we used the inflow temperature of the largest upstream river (Grosse Dhuenn). Daily measurements of inflow temperatures for Grosse Dhuenn were available for the period 2011-2013. Inflow water temperatures of the whole simulation period from 1996-2013 were generated by the model tool “air2stream” (Toffolon and Piccolroaz, 2015). After 1000 iterations, the air2stream model of Grosse Dhuenn River reproduced measured daily inflow temperatures well over the period 2011-2013 (RMSE 1.3 °C). Hence, the inflow temperatures could be provided as desired target temperature in the downstream river over the entire period 1996-2013 (Figure 4.2).

Additionally, we aimed at restoring a natural and dynamic flow discharge in the downstream river as a new discharge strategy (see Figure 4.2). We postulated that the discharge was equal (1:1) to the inflow of upstream river Grosse Dhuenn. However, we retained a minimum discharge of 0.1 m³/s for ecological reasons, i.e. at times of very low inflow discharge the outflow was subsidized by water from the reservoir storage. Furthermore, the pivoted pipe was limited to a maximum discharge of 0.8 m³/s. During floods, (>0.8 m³/s) the bottom outlet was activated in order to reestablish the natural flow dynamics and withdrew water in parallel to the pivoted pipe.

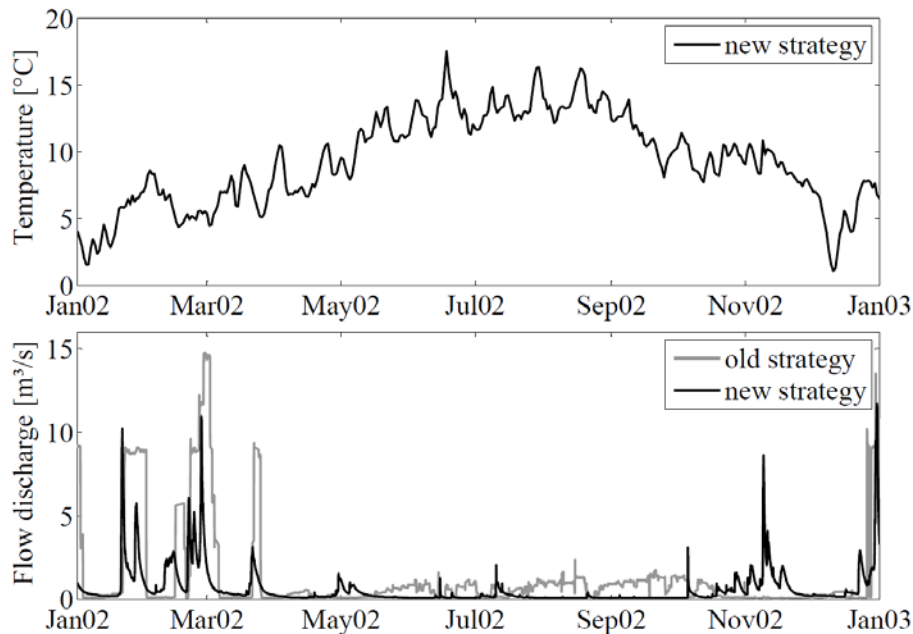


Fig. 4.2. Time series of downstream water temperature and flow discharge for the model of Grosse Dhuenn Reservoir assuming the new strategy for the example year 2002 (black solid lines); the grey solid line indicates the operated discharge into the downstream river according to the staircase like hydrograph (old strategy) before the installation of the pivoted pipe.

4.2.4 Scenario definitions

Initial scenario

As a reference, we simulated the withdrawal through the pivoted pipe (selective withdrawal) with an activation of the parallel bottom outlet withdrawal only during flooding conditions for the period of 1996-2013. The water temperature flow discharge for the downstream river was assumed to be natural (new strategy) as described in section 2.3. As also shown in Weber et al. (2017), low-oxygen conditions occurred when water was predominantly withdrawn from upper layers (epilimnion/metalimnion) due to minimal water renewal at the sediment-water interface. They suggested to activate the bottom outlet and to remove oxygen-depleted water from the deepest layers for a safe raw water supply. Therefore we defined a DO threshold of 4 mg/L (as in Weber et al., 2017) that DO should not fall considerably below to identify the need for action. This guideline is included to prevent hypoxia or even anoxia and water quality deteriorations from a release of heavy metals and nutrients from the sediment (Baden et al., 1995).

Management parameter improvement

In separate yearly simulation runs for the period of 1996-2013, we determined each day of year when the simulated DO concentration in the lower hypolimnion hit this threshold based on analyzing the initial scenario (predominant withdrawal through the pivoted pipe). In order to find alternative management strategies that prevent DO concentrations below the threshold of 4 mg/L, we tried different activation dates and discharge levels for the parallel bottom outlet withdrawal for each year. Therefore, we considered the following management parameters:

- DBT_{BO} , the number of days before reaching the threshold of 4 mg/L, and, hence,
- DOY_{BO} , the day of year when the additional parallel bottom outlet withdrawal was activated,
- DIS_{BO} , the constant flow discharge and
- $DAYS_{BO}$, the number of days the bottom withdrawal was activated.

We varied DBT_{BO} from 1 to 60 “Days Before Threshold” in 2 days steps and its discharge (DIS_{BO}) from 0.05 to 3 m³/s in 0.1 m³/s steps. This resulted in 900 scenario simulations and corresponding management parameter combinations for each year. The activation date of the bottom outlet DOY_{BO} was derived from DBT_{BO} . Once the (additional) parallel bottom outlet was activated, it withdrew bottom layer waters with a given discharge until autumn overturn (mixing) for a number of days $DAYS_{BO}$ resulting in a specific hypolimnetic water volume that is lost through the bottom outlet.

We searched for the ideal management parameter combination of DBT_{BO} and DIS_{BO} for each year between 1996-2013 fulfilling the following goals:

- avoidance of hypolimnetic DO concentrations below threshold of 4 mg/L,
- minimizing the yearly additional discharge volume from the hypolimnion through the bottom outlet and
- shifting the starting date DOY_{BO} towards the end of the stratification period (decrease DBT_{BO}).

By this method valuable hypolimnetic water for raw water supply should be saved during periods with a high raw water consumption, especially in summer.

4.3 Results

4.3.1 Initial scenario

Reservoir volume

In the initial scenario, we simulated the conditions from 1996-2013, as if all water was withdrawn through the pivoted pipe with an activation of the parallel bottom outlet withdrawal only during floods ($>0.8 \text{ m}^3/\text{s}$). Assuming the new discharge strategy with a downstream discharge equal to the discharge of the largest upstream (Grosse Dhuenn) with a minimum flow of $0.1 \text{ m}^3/\text{s}$ conserved valuable raw water for drinking water supply in wet years compared to the old withdrawal strategy (staircase like discharge, see period 1998-2008 in Figure 4.3). The maximum retention of additional 17 million m^3 valuable hypolimnetic waters for drinking water production corresponds to $\sim 22\%$ of the total volume of the main dam (in 2004). The main reasons for this large retention was that (i) the total inflow volume was higher than the total outflow volume and that we assumed (ii) low flow periods from spring to late summer and (iii) a natural discharge instead of a staircase like discharge during floods (see Figure 4.2).

On the contrary, in dry years, when all inflows from the catchment did not supply enough water, the above mentioned withdrawal strategy decreased the reservoir volume (see years 1996-1997 and 2009-2013 in Figure 4.3). The maximum loss of valuable hypolimnetic water was 4 million m^3 (in 1998, $\sim 5\%$ of the total volume of the main dam). In these dry years, the outflow volume was mostly higher than the inflow volume mainly because of the minimum discharge of 100 l/s for downstream river Dhuenn.

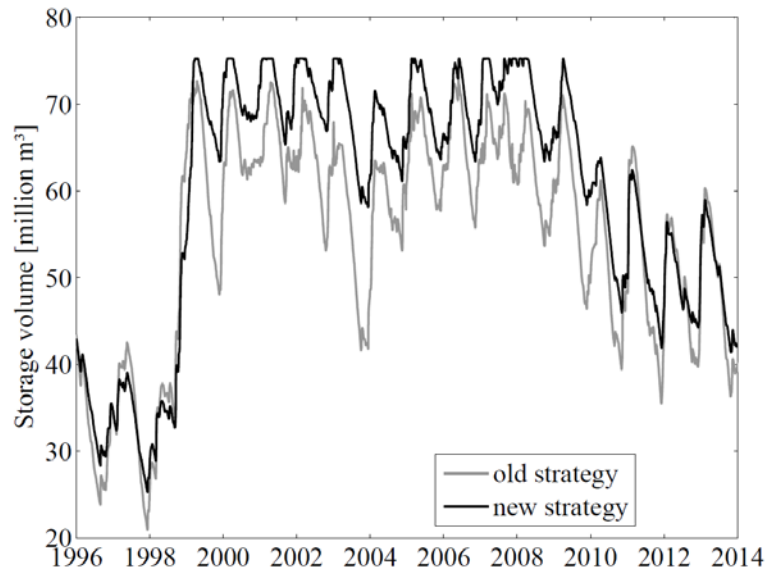


Fig. 4.3. Time series of water storage volumes of the Grosse Dhuenn Reservoir main dam for the models assuming the original staircase like discharge (old strategy) and a discharge 1:1 to upstream inflow with minimum discharge of 0.1 m³/s (new strategy) during 1996-2013.

Discharge temperature

According to the implemented operational rules (section 2.2), the model autonomously determined the best withdrawal height for the pivoted pipe on basis of:

- the development of stratification,
- the (target) upstream river temperature and flow discharge and
- the activation of the bottom outlet, when both withdrawals are mixed.

The discharge temperature followed the upstream river temperatures as closely as possible (RMSE of 1.6°C, see Figure 4.4b) for the summer period from April to September. In years of low water levels (1996-1998 and 2010-2013), discharge water temperatures were slightly higher, as the thermocline had been shifted beyond the lower reach of the pivoted pipe. In contrast, in years of high water levels (1999-2009), the temperatures were slightly below the target temperature, as the pivoted pipe could not reach high enough into the thermocline. However, compared to an exclusive withdrawal through the bottom outlet as operated during 1996-2013 (old strategy), with discharge temperatures between 4 and maximum 10 °C, the new withdrawal management would improve the temperature in the

downstream river Dhuenn by approximately 6.2 °C to an average temperature in the summer period (April-September) of 11.6 °C and supply a near natural temperature over the year.

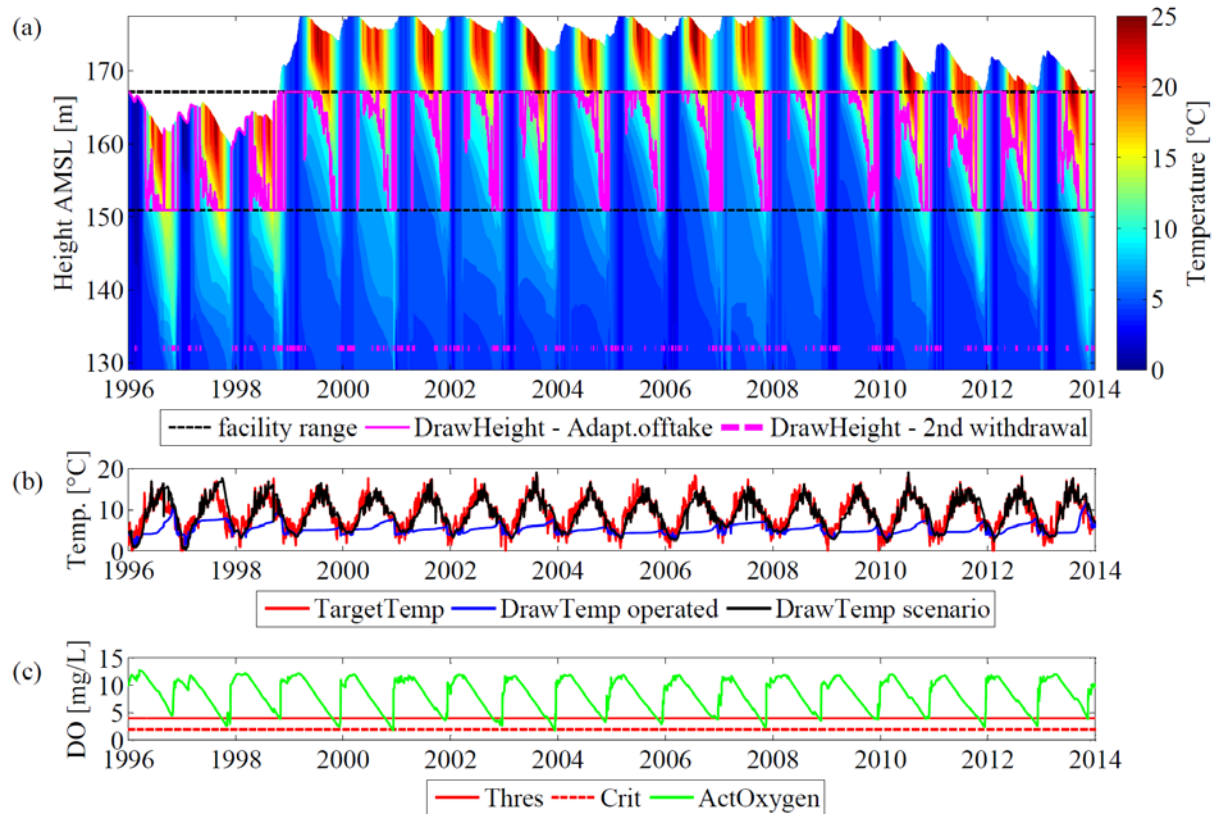


Fig. 4.4. (a) Contour plot of simulated water temperatures of the Grosse Dhuenn Reservoir model for the initial scenario over the period of 1996-2013; the solid magenta line indicates the autonomously determined withdrawal height for the pivoted pipe; the dashed magenta line indicates withdrawal through the bottom outlet, when activated during flooding events. (b) Upstream river temperature as target discharge temperature (red) versus original operated (blue) and initial scenario (black) discharge water temperature. (c) Dissolved oxygen concentrations in 5 m above bottom (green) of the initial scenario, the threshold for the model of 4 mg/L (solid red) and the critical concentration of 2 mg/L (dashed red).

Hypolimnetic DO

As a result of the summer stratification and the predominant selective withdrawal strategy by the pivoted pipe, DO concentrations in the deep hypolimnion decreased steadily during summer stratification periods (Figure 4.4c). In almost every year during the period of 1996-2013, the DO concentrations in the deep hypolimnion (i.e. 5 m above the reservoir

bottom close to the lowest raw water offtake) fell below the threshold of 4 mg/L. In 2000 and 2003, minimum DO concentrations even went down to 1.8 mg/L, where a release of manganese, iron and nutrients could set in.

4.3.2 Management parameter improvement

With an improved withdrawal management by parallel activation of the bottom outlet, we expected less alarming DO concentrations. Therefore, we simulated each separate year based on the initial scenario (see section 3.1) during 1996-2013. We found certain parameter combinations for each year trying to retain a minimum hypolimnetic DO concentration of 4 mg/L. The optimal parameter combination for each year was determined by (i) minimizing the parallel bottom outlet discharge DIS_{BO} and (ii) decreasing the “Days Before Threshold” DBT_{BO} that corresponds to a shorter duration of the parallel bottom outlet withdrawal. By this approach, the additional bottom outlet withdrawal volume and, hence, the loss of highly valuable raw water for drinking water production was minimized. As an example, the optimal parameter combination for the year 2004 out of 900 simulations/combinations was obtained to $DBT_{BO} = 23$ d, $DIS_{BO} = 0.25$ m³/s and $DAYS_{BO} = 66$ d (Figure 4.5a). This parameter combination corresponded to an additional bottom outlet discharge of 1.43 million m³. In contrast, the supposed best parameter combination to reach a DO concentration of 4 mg/L for the year 2002 was $DBT_{BO} = 17$ d, $DIS_{BO} = 2.05$ m³/s and $DAYS_{BO} = 73$ d (Figure 4.5b). This parameter combination corresponded to a net volume discharged through the bottom outlet of ~13 million m³.

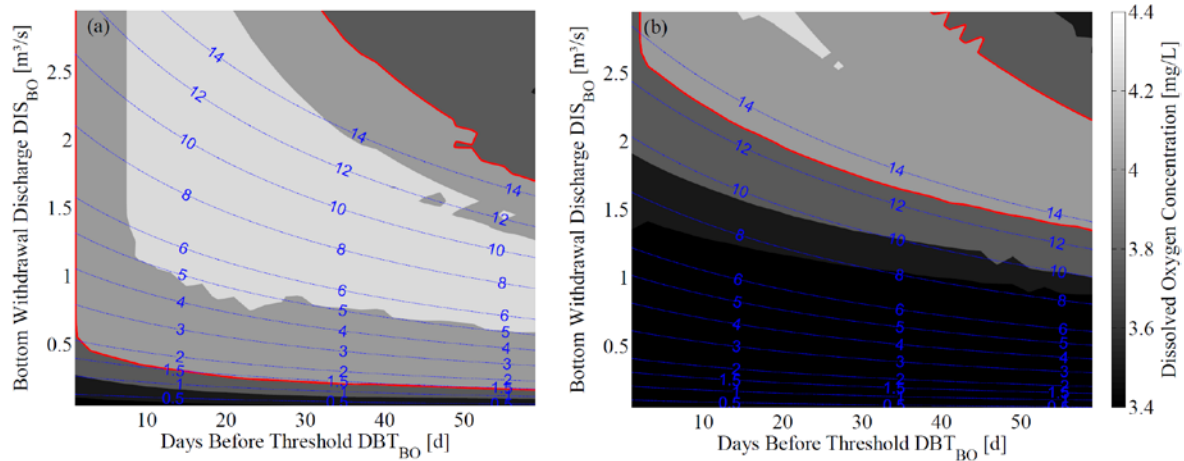


Fig. 4.5. Contour plots of simulated minimum dissolved oxygen (DO) concentrations (in grey) in the deep hypolimnion of Grosse Dhuenn Reservoir as a result of the variation of “Days Before Threshold” DBT_{BO} of 4 mg/L and the bottom outlet flow discharge DIS_{BO} for the year 2004 (a) and 2002 (b) ($n = 900$ runs); the activation date of the bottom outlet DOY_{BO} and the number of discharge days $DAYS_{BO}$ were derived from DBT_{BO} and the DOY of autumn overturn (mixing); the red solid line indicates 4 mg/L, whereas the fine blue lines indicate the net volume in million m^3 discharged through the bottom outlet.

In summary, the simulations showed that the improved management strategy for each individual year was able to retain DO concentrations of 4 mg/L in the deep hypolimnion in almost every year; exceptions were years 1997 and 2011, where minimum DO could only be raised to concentrations of 3.53 mg/L and 3.41 mg/L, respectively. However, in some years, the mean proposed additional discharge volume of 11.18 million m^3 was too high for a sustainable reservoir operation. Consequently, we determined the optimal management parameter combination for the additional bottom outlet withdrawal for simulating the entire period of 1996-2013 on basis of the remaining years (Table 4.1, $n = 8$ years). While DBT_{BO} , DOY_{BO} and $DAYS_{BO}$ are the mean values, DIS_{BO} represents the maximum flow discharge. The corresponding additional bottom outlet discharge volume was found to be 2.66 million m^3 .

4.3.3 Optimized reservoir management

Running the scenario for the whole period of 1996-2013 with the improved parameter combination (Table 4.1), the model showed that in almost all years, except 1996, 1998, 2010

and 2013, the additional bottom outlet withdrawal significantly improved the DO concentrations 5 m above ground up to 46% in 2003 (from 1.745 mg/L to 3.237 mg/L, mean: 25%, $n = 14$ years). In 7 out of 18 years, this improved management was able to increase the minimum DO concentrations from below 4 mg/L to above 4 mg/L (Figure 4.6). A moderate increase in DO from below 3 mg/L to 3-4 mg/L was achieved in 6 years. However, 6 out of 18 years showed an improvement of the hypolimnetic DO conditions of almost 1 mg/L. Averaged over all years, the optimized management improved the DO situation in the deepest layers of the reservoir by 19% (mean, $n = 18$ years) to a minimum of 2.9 mg/L (from originally <1.8 mg/L in 2000 and 2003, see Figure 4.6), suggesting that hypoxic conditions in the bottom layer are becoming successfully prevented.

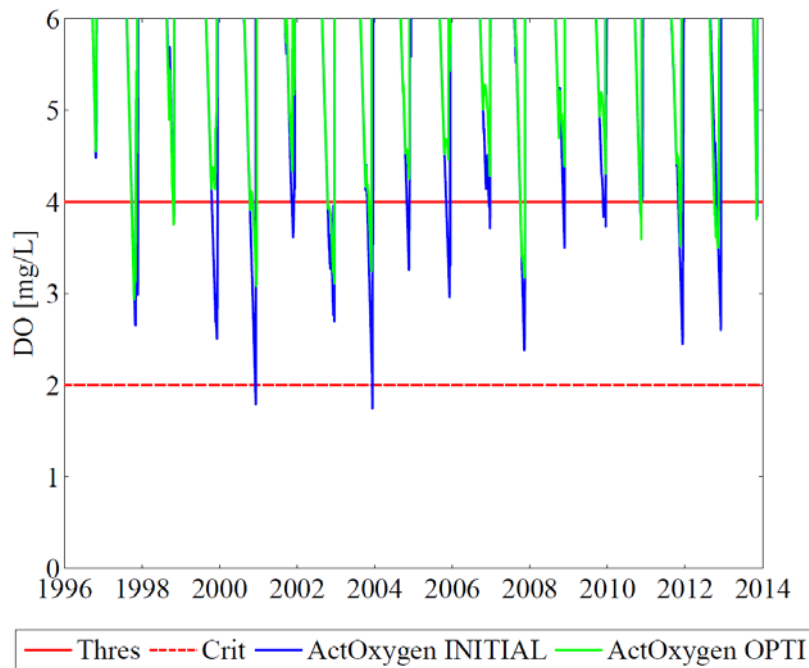


Fig. 4.6. Simulated dissolved oxygen concentrations of the Grosse Dhuenn Reservoir model during 1996-2013 in 5 m above bottom assuming selective withdrawal (pivoted pipe) with an activation of the parallel bottom outlet withdrawal only during flooding conditions (blue solid line, initial scenario) and parallel selective and bottom outlet withdrawal during flooding conditions with additional discharge due to optimized management (green solid line, optimized scenario); the red solid and dashed lines show the threshold of 4 mg/L and the critical concentration of 2 mg/L, respectively.

Besides the benefits of our improved withdrawal strategy, we found some limitations. In 1997, the optimal withdrawal strategy was not able to improve DO to above 2.9 mg/L. Additionally, in the years 1998, 2010 and 2013, the additional bottom outlet withdrawal of 2.66 million m³ of water per year even led to a decrease in hypolimnetic DO (maximum 0.28 mg/L). This effect was potentially induced by the modified stratification and is discussed below.

Table 4.1. Improved withdrawal management parameters for Grosse Dhuenn Reservoir for the period of 1996-2013; DBT_{BO} is the number of days before reaching the threshold of 4 mg/L, DOY_{BO} the day of year when the additional parallel bottom outlet withdrawal with the constant flow discharge DIS_{BO} should be activated for the number of days $DAYS_{BO}$.

DBT_{BO} [d]	DOY_{BO} [-]	DIS_{BO} [m ³ /s]	$DAYS_{BO}$ [d]
24	290	0.55	56

Our model was able to follow the predefined inflow temperature of the upstream river Grosse Dhuenn as a target temperature as closely as possible. The modelled temperature of the withdrawn water for downstream river Dhuenn deviated from the (target) inflow temperature of river Grosse Dhuenn by an RMSE of only 1.7 °C in the summer periods (April-September) of 1996-2013. Compared to the initial scenario, without an optimized management but with parallel bottom outlet withdrawal only during flooding conditions, the RMSE was slightly higher (+0.1 °C). For the same period, the average water temperature of the withdrawn water was 11.7 °C and, therefore, approximately 6.3 °C higher than with a withdrawal strategy using the bottom outlet withdrawal exclusively.

4.4 Discussion

Our numerical model of Grosse Dhuenn Reservoir was able to determine the ideal height for the selective withdrawal (pivoted pipe) autonomously on basis of:

- the upstream river water temperature and flow discharge,
- the prescribed hydrological boundary conditions,
- the modelled water quality parameters temperature and dissolved oxygen and

- the parallel activation of the bottom outlet, when both withdrawals are mixed.

We observed negative effects of a selective withdrawal from the epilimnion and metalimnion (see also Weber et al., 2017): a predominant withdrawal of water from the upper layers strengthened the thermal stability (Barbiero et al., 1997), supported the oxygen consumption in the deep hypolimnion and, hence, led to lower DO concentrations. Therefore, we provided an improved strategy to ensure a sustainable and safe raw water management by avoiding low oxygen conditions in the deep hypolimnion of the reservoir in combination to satisfy downstream river demands.

Our optimized withdrawal strategy was based on the smart mixing from both outlets: warm water from the pivoted pipe with cold water from the bottom outlet. While epilimnetic or metalimnetic withdrawal delivered warm water for the downstream river and conserved valuable cold water in the hypolimnion (Kennedy, 1999) for drinking water production, hypolimnetic withdrawal removed oxygen depleted water from the reservoir and as a consequence exported phosphorus and further reduced the release of nutrients and metals from the sediment (Olszewski, 1961; Nürnberg et al., 1987). With the help of our reservoir model and scenario simulations, we found a simple withdrawal strategy that:

- improved the temperature conditions of the withdrawn water for the downstream river,
- restored the natural and dynamic flow conditions downstream,
- kept hypolimnetic DO concentrations sufficiently high (3-4 mg/L) and, therefore,
- prevented a release of metals and nutrients from the sediment.

Furthermore, the new optimized withdrawal strategy, based on only four parameters (see section 3.2), could be easily integrated into operational use. First results from implementing optimal withdrawal at Grosse Dhuenn Reservoir confirmed this. The activation of the bottom outlet in parallel to the withdrawal of epilimnetic/ metalimnetic waters improved the DO conditions in the deep hypolimnion by 19% (n = 18 years). However, in three years during the simulation period (1996-2013), the additional parallel discharge of hypolimnetic waters led to a minor but not negligible decline in DO (-0.28 mg/L), primarily as a result of thermocline deepening (Gaugush, 1984) where higher water temperatures increased the sediment-related oxygen demand.

Our simulations of optimal reservoir management could avoid thermopeaking in most cases. We mostly observed relatively small differences to target discharge temperatures before and late after DOY_{BO} – the activation of the bottom outlet (see Figure 4.7). The differences in temperature are mainly caused, when the required water temperature was out of the reach for the pivoted pipe:

- In October 1996, the water temperatures in the facility range were too high due to the low water level (see Figure 4.7a and 4.7d). The abrupt decrease in discharge temperature was induced by the cooling of the epilimnion shortly before overturn. In this case, an earlier activation of the bottom outlet to decrease the mixing temperature should be considered to achieve the target temperature.
- In October 1999, the water temperatures in the facility range were too low due to the high water level (see Figure 4.7b and 4.7e). Some days after activating the parallel bottom outlet withdrawal, the water temperatures at the uppermost facility range were too low to achieve a sufficiently warm discharge temperature in times of increasing inflow temperatures (until the end of October, see Figure 4.7e).

Similarly, in 2001, we observed a sudden decrease in discharge water temperatures due to the low water temperatures in the facility range (see Figure 4.7c and 4.7f). The defined target temperature could not be reached although the pivoted pipe was withdrawing on the uppermost facility range. Here, a warm period in October lead to higher target inflow temperatures when cooling of the reservoir surface waters was dominating but heating of small streams by the remaining solar energy was sufficiently high enough.

However, in all years, we did not observe an abrupt drop of DO to hypoxic or even anoxic conditions (see Figure 4.7g-i). In conclusion, we propose that the defined optimal withdrawal strategy should be carefully adjusted with the help of weather prediction models in these weather periods. However, if we take into account that almost every reservoir is equipped with a stilling basin after the bottom outlet, a sudden drop in the withdrawn temperature and DO is smoothed by mixing and atmospheric exchange: When full, the stilling basin of Grosse Dhuenn Reservoir elongates in a 200x40 m wide and 0.5 m deep channel with approximately 4000 m³ of water. This amount of water has a large mixing efficiency so low-oxygenated discharge water should be reaerated quickly and cold discharge water should be gradually heated up slightly. In general, if the mixing efficiency of a stilling

basin is too low or a reservoir is not equipped with such a feature, a stepwise activation of the bottom outlet could be a chance to alleviate sudden drops in discharge temperature and DO. Further work on this is required to ensure a perfect balance between a save raw water supply and a reservoir discharge that complies with the downstream river demands.

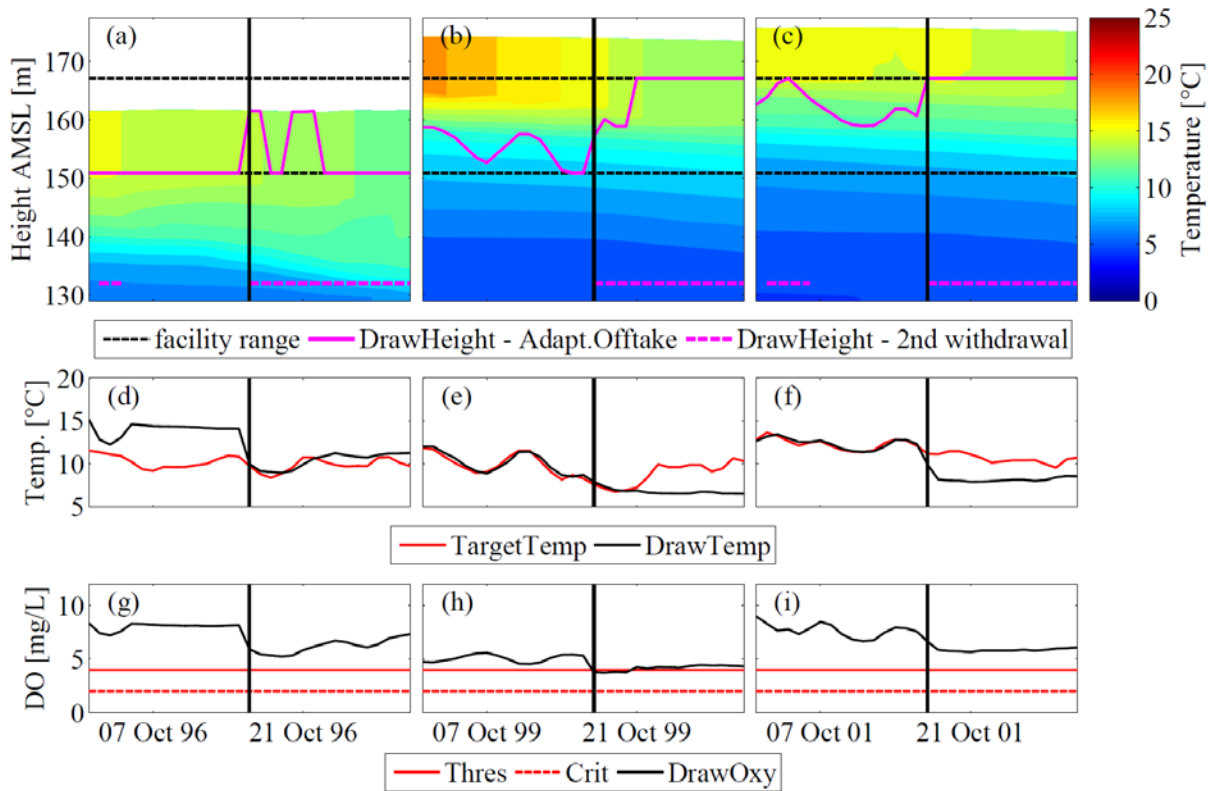


Fig. 4.7. Contour plots of simulated water temperatures of the Grosse Dhuenn Reservoir model for the “optimal” management in October 1996 (a), 1999 (b) and 2001 (c); the solid magenta line indicates the autonomously determined ideal withdrawal height for the selective withdrawal (pivoted pipe); the dashed magenta line indicates withdrawal through the bottom outlet. Target upstream river temperature (red) and discharge water temperature (black) for October 1996 (d), 1999 (e) and 2001 (f). Dissolved oxygen concentrations (black) and the threshold for the model of 4 mg/L (red) for October 1996 (g), 1999 (h) and 2001 (i); the three vertical black solid lines indicate the starting date DOY_{BO} of the parallel bottom outlet withdrawal.

In general, the alleviation the river continuum disruption is realised by reconstructing the natural downstream temperature and discharge (Olden and Naiman, 2010; Sherman et al., 2007). This improved the ecological river habitat conditions for the reestablishment of a more

natural fish and benthic community. As a consequence, pre-conditions for a good ecological status of rivers were achieved which could comply with regulations in water policy like the European Water Framework Directive. Fitting reservoirs with multi-level intakes or pivoted pipes and integrating reservoir operations into river basin management plans could mitigate the disruption of the river continuum (see also Nilsson et al., 2005) and alleviate a global pressing environmental problem.

4.5 Conclusion

A smart reservoir withdrawal management can alleviate the disruption of the river continuum in the focus of a natural temperature and (dynamic) discharge while keeping raw water quality safe. We used the open source hydrodynamic model GLM together with the water quality library AED2 to optimally control reservoir withdrawal regarding raw water safety and downstream river demands. This study indicated that:

- Our model was able to supply water for the downstream river close to a target temperature (upstream river) with a natural and dynamic discharge.
- Negative effects of selective withdrawal on water quality could quantitatively be simulated.
- An optimal withdrawal strategy by mixing selective withdrawal (warm water) with bottom outlet withdrawal (cold water) improved raw water and downstream river discharge water quality and avoided harmful water quality deteriorations.

Our flexible and simple reservoir model together with the proposed optimal withdrawal strategy can be integrated into operational use. Progressing hydrological and temperature changes due to climate change as well as the accelerating importance of dam operations worldwide (Zarfl et al., 2015) will further increase the demand for such tools.

Acknowledgements

This research was supported by District Council Cologne and Ministry of Environment North Rhine-Westphalia. We acknowledge the reservoir authority Wupperverband for providing data.

Chapter 5: Major findings and discussion

The present study identified the potential of reservoir withdrawal management to mitigate the river continuum disruption with respect to temperature and discharge while keeping raw water quality safe. The main focus of this modelling study was on drinking water reservoirs, however, the numerical tool and the results of this thesis are partly transferable to reservoirs for other purposes. With this study, we showed how reservoir operators can reconstruct the natural downstream temperature and discharge and, hence, improve the ecological river habitat conditions for the reestablishment of a more natural fish and benthic community. As presented in Chapter 1.5, there is still a need for numerical models as tools for a smart reservoir management and a comprehensive understanding how to improve withdrawal management to reach certain objectives. Therefore, we dealt with following research questions:

- Can we extend existing one-dimensional hydrodynamic models and integrate operational rules and management decisions into the simulation of reservoir water quality and stratification?
- Can we restore the quasi-natural temperature and flow conditions in downstream rivers by changing the current withdrawal strategy?
- What is the impact of a modified withdrawal strategy on stratification and water quality, especially hypolimnetic DO?
- Can we combine downstream river demands with a sustainable raw water supply by an optimal withdrawal strategy?

5.1 Numerical models in realistic reservoir simulations

In Chapter 2 and 3, we extended the existing one-dimensional hydrodynamic and water quality model GLM/AED2. This new model simulates the impact of a modified withdrawal strategy on water quality within the reservoir and realizes a quasi-natural downstream temperature regime by an adaptive selective withdrawal. In detail, we included an adaptive withdrawal functionality on basis of the real operational reservoir management, which adapts the withdrawal height during the runtime of the model. Furthermore, a simple oxygen module for oxygen depletion at the sediment surface and in lake water with two temperature dependent coefficients was integrated into the source code. To the author's knowledge, this adaptive withdrawal functionality was a novel tool in scientific reservoir modelling and an advancement compared to previous tools, where the withdrawal height had been fixed as a boundary condition before the simulation. The new tool enabled the user to link withdrawal operations with water quality for simulating realistic withdrawal management (Figure 5.1a and b). Based on a predefined daily target temperature for the downstream discharge, the model determined the ideal height for the selective withdrawal (pivoted pipe) autonomously considering stratification and the parallel activation of the bottom outlet.

After adding operational rules and the oxygen module to the source code, we set-up the model for Grosse Dhuenn Reservoir with hydrological, meteorological and morphological data. We calibrated and validated the model with measured temperature and dissolved oxygen concentration data for the period before the pivoted pipe was installed. The calibrated model for Grosse Dhuenn Reservoir showed a good agreement between the measured and simulated temperature and dissolved oxygen concentration profiles. The stratification patterns and the dissolved oxygen dynamics were reproduced well. In detail, the root mean square error (RMSE) of the modelled temperature (1.23 °C) and dissolved oxygen concentration (1.05 mg/L) was comparable to values from the literature (Table 5.1). Our results were in the range of the values produced by different models, independent of their type (3D/ 2D/ 1D/ empirical, see Table 5.1). This confirmed that a 1D numerical hydrodynamical and water quality model was sufficient for achieving our objectives. However, we expect some limitations applying the model tool in very long reservoirs with significant side arms. Here, strong longitudinal gradients in temperature and DO occur that could not sufficiently be reproduced in 1D or 2D models. Also upwelling events create spatial variations in

stratification (Bocaniov et al., 2014). In this case, the results for 1D and 2D should be carefully checked against the 3D model results.

Table 5.1. Root mean square error (RMSE) of various studies on simulating temperature and dissolved oxygen concentration in different lakes and reservoirs; ^a Weber et al. (2017), ^b Bocaniov and Scavia (2016), ^c Brett et al. (2016), ^d Schwefel et al. (2016), ^e Couture et al. (2015), ^f Moreno-Ostos et al. (2008), ^g Kerimoglu and Rinke (2013), ^h Bocaniov et al. (2014); p = profiles, h = hypolimnion, e = epilimnion.

Lake/Reservoir	T [°C]	DO [mg/L]	Model
Grosse Dhuenn Res., DE ^a	1.23 (p)	1.05 (h)	GLM/AED2 (1D)
Lake Erie, US ^b	1.47 - 1.96 (p)	1.16 (h)	ELCOM-CAEDYM (3D)
Lake Spokane, US ^c	1.30 (p)	1.20 (p)	CE-QUAL-W2 (2D)
Lake Geneva, FR/CH ^d	0.50 (h)	0.51 (h)	SIMSTRAT (1D)
Lake Langtjern, NO ^e	0.02 (e)	1.70 (e)	MyLake (1D)
Sau Res., ES ^f	1.43 (p)	-	Empirical
Bautzen Res., DE ^g	1.25 (e)	-	DYRESM (1D)
Rappbode Res., DE ^h	0.94 (p)	-	ELCOM (3D)

5.2 Temperature as a key factor in regulated rivers

Dam construction and operation led to downstream temperature pollution in regulated rivers worldwide. We explored the potential of selective withdrawal to mitigate downstream temperature pollution by a numerical model (Chapter 3). As proposed by Olden and Naiman (2010), temperature is a key factor in rivers worldwide. Therefore, the goal of a simplified scenario was to discharge a pre-described temperature into the downstream river. The desired discharge water temperature was specified to 14 °C from the operating company Wupperverband on the basis of mean summer river temperatures (2006-2013) of a small undammed stream of the Dhuenn river catchment. In this simplified test case, we focused on the potential of the selective withdrawal structure for increasing discharge water temperatures.

First, water for the downstream river was abstracted exclusively by selective withdrawal (pivoted pipe) from the epilimnion and metalimnion and not from the bottom outlet as the standard case. Selective withdrawal from the upper, warm layers is a common (theoretical) strategy to save cold hypolimnetic water on the one hand and to increase the discharge temperature on the other hand. We applied the numerical model for Grosse Dhuenn Reservoir to test if the reservoir operator was able to restore the quasi-natural temperature downstream by modifying the reservoir withdrawal strategy. Second, we investigated the effect of this modified withdrawal strategy on the in-reservoir water quality focusing on hypolimnetic dissolved oxygen concentration. According to the integrated operational rules and management decisions, the numerical model should then act as an autonomous decision-support-system.

The results on the in-reservoir processes showed that an exclusive epilimnetic/metalimnetic withdrawal strengthened the thermal stability (see also Casamitjana et al., 2003). Furthermore, it conserved up to 10 Million m³ of valuable raw water, which corresponded to ~14% of total water volume of the Grosse Dhuenn Reservoir. We also found, that our model was able to determine the best withdrawal height for the pivoted pipe to deliver a desirable discharge temperature (Figure 5.1b). Our study indicated a potential for increasing the average temperature in the river Dhuenn by 7.4 °C from 5.9 °C to 13.3 °C from April to September. This showed that selective withdrawal could mitigate the temperature disruption in downstream rivers and could even restore the natural temperature in the downstream river. Although the reestablishment of a natural fish community is a long term process (Vinson, 2001), we can make an important step towards ecological recovery of the riverine fish communities.

However, in Chapter 3 we did not consider three important parts of a desirable in-reservoir and quasi-natural downstream river water quality and quantity. Firstly, we included a constant discharge temperature of 14 °C instead of a natural temperature for model simplicity. Therefore, the transferability of the results in Chapter 3 to reservoir systems in other climate zones is limited. Secondly, we did not consider a natural and dynamic flow discharge to the downstream river. According to Poff et al. (1997) “The natural flow regime organizes and defines river ecosystems”. The benefit from temporally varying flow conditions like flooding or droughts help to keep diversity of aquatic and riparian species high. Therefore, further work was required to combine in-reservoir and downstream river

objectives. Thirdly, despite the advantages of the selective withdrawal strategy from the epilimnion and metalimnion for mitigating the temperature pollution, this study showed negative effects on the hypolimnetic oxygen content. The exclusive withdrawal from upper, warm layers severely decreased the hypolimnetic dissolved oxygen concentrations (see Figure 5.1b). Then, safeguarding the raw water quality in drinking water reservoirs receives priority.

5.3 Hypolimnetic oxygen as a key factor for in-reservoir water quality

Drinking water reservoirs have been built for storing high quality raw water. Operators have to guarantee an adequate supply of raw water for the drinking water treatment plant. The downstream withdrawal from the upper, warm layers is a common strategy to achieve a conservation of cold raw water. However, during stratified periods, oxygen is depleted in the deep hypolimnion. If there is no withdrawal of low-oxygenated water from the deepest layer (e.g. bottom outlet), the deepest layers can severely run into hypoxic (<2 mg/L) or even anoxic conditions. Then, a release of nutrients, manganese and iron from sediments can be induced (Davison, 1993). This leads to a deterioration and loss of raw water as well as increased treatment costs. Additionally, dissolved substances like nutrients that are released out of the sediments will accumulate in the hypolimnion during the stratified season. At times of intense mixing, these substances will become available for phytoplankton groups in the metalimnion and epilimnion, especially for cyanobacteria. Then, harmful algal blooms (Brookes and Carey, 2011) could be initiated. This demonstrates how closely biological processes and water quality are linked to reservoir management. Hypolimnetic DO is a key factor in water quality of many reservoirs worldwide and a major control variable for reservoir operation, especially drinking water reservoirs.

The thesis has shown that a complex management is needed to control DO and to keep raw water quality save in drinking water reservoirs if different goals/ objectives, like raw and discharge water quality, are pursued. Besides selective withdrawal, there are a few measures to control stratification and DO content in the hypolimnion such as artificial mixing (Sherman et al., 2010) and hypolimnetic oxygenation (Bryant et al., 2011; Chen et al., 2017). Artificial mixers like surface pumps and draft tube mixers destratify the water body of lakes and reservoirs and, thus, can increase the oxygen content in the hypolimnion. In contrast, hypolimnetic oxygenation does not reduce stratification and is primarily effective in the deep hypolimnion to prevent hypoxic/ anoxic conditions. Although such facilities are installed in

lakes and reservoirs around the world (e.g. UK, Australia) they are cost-intensive and efficiency is sometimes not guaranteed. In contrast, specialized infrastructures like multi-level intakes or pivoted pipes (Olden and Naiman, 2010) are the most effective and flexible measures to selectively withdraw water from a reservoir for controlling in-reservoir and discharge water quality. Selective withdrawal can help to remove water layers with high algal biomass or turbidity by epilimnetic or metalimnetic flushing (see also Moreno-Ostos et al., 2008). A withdrawal from epi-/ meta- and hypolimnion can control the DO concentrations in the hypolimnion and modify downstream water temperatures. As shown in Chapter 4, a smart mixing with the bottom outlet could be a viable strategy to restore the quasi-natural temperature and flow discharge downstream whilst securing raw water quality (Figure 5.1c).

5.4 Improved reservoir withdrawal strategy to mitigate the dam impact whilst securing raw water quality

In Chapter 4, we used a simple approach for improving a reservoir withdrawal strategy, consisting of a numerical model for hydrodynamics and water quality combined with basic reservoir operational rules. Our objective was the provision of a quasi-natural temperature and flow discharge to the downstream river without jeopardizing raw water quality. Therefore we activated the bottom outlet in parallel to the selective withdrawal by the pivoted pipe for a given period to prevent low-oxygen conditions in the deep hypolimnion (see Figure 5.1c). At these times, the model selected higher withdrawal heights (warmer temperatures) for the pivoted pipe to raise temperatures of the mixed water towards the target temperatures for the downstream river. Furthermore, we aimed at adapting the reservoir outflow towards the natural temperature and flow regime of the largest (unregulated) reservoir inflow. Compared to the mean desired grayling temperature regime of 12.4 °C during the period of April to September, the model was able to deliver water downstream with mean temperatures of 11.7 °C. The discharged water temperature was always in the range of the specified minimum and maximum temperatures for grayling and brown trout, although cold water from the bottom outlet was periodically released downstream (Figure 5.2). This demonstrated the accuracy and flexibility of the developed reservoir model and the proposed (improved) withdrawal strategy. The new tool was easily integrated into the existing reservoir operation and management.

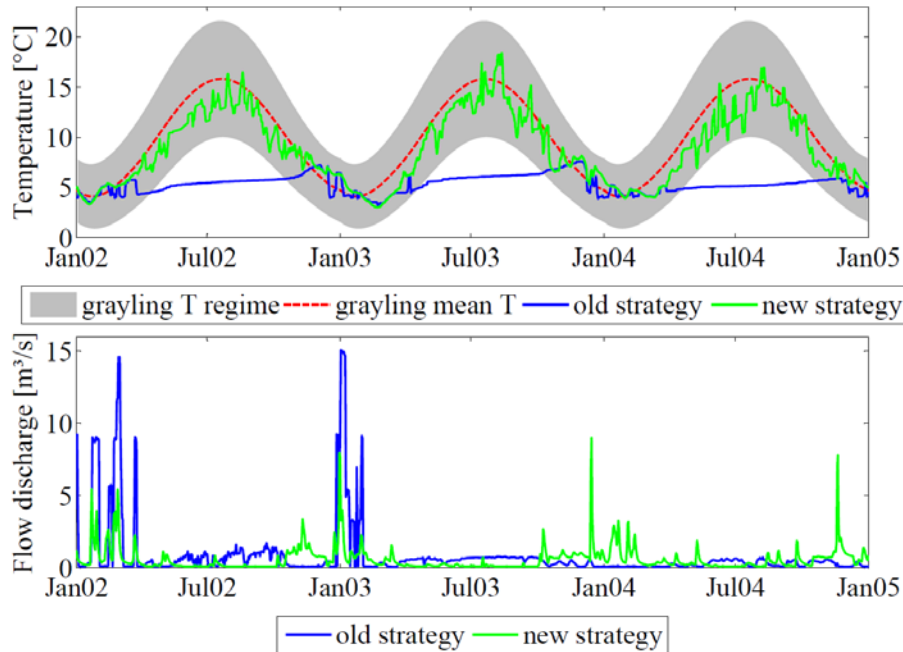


Fig. 5.2. Simulated and measured discharge water temperatures and flows for the (desired) discharged water at Grosse Dhuenn Reservoir. The grey shaded area and the dotted red line show the temperature range and the mean temperature for the grayling habitat (Hari and Guettinger, 2004); the modelled discharge water temperature and flows using an exclusive bottom outlet (blue, old strategy) and selective withdrawal from the bottom outlet and pivoted pipe (green, new strategy).

5.5 Implications for reservoir modelling

Drinking water reservoirs

The application of GLM/AED2 to Grosse Dhuenn Reservoir and its modelling results indicated that the model was ready to be implemented in the management of other deep oligotrophic drinking water reservoirs. A simple recalibration of the parameters wind factor and light extinction coefficient (GLM) as well as the water column and sediment area dependent oxygen depletion rate (AED2) would be needed. However, we recognized some limitations for combining downstream river demands and sustainable raw water management in reservoirs with a higher trophic level and/ or shallow reservoirs:

In mesotrophic or even eutrophic drinking water reservoirs, we primarily have to consider higher nutrient content and higher hypolimnetic oxygen depletion (Marcé et al., 2010). Then, the optimization approach is governed by tighter boundary conditions such as the (lower) oxygen content in the hypolimnion. However, we suggest three important methods

for improving the operation of meso-/ eutrophic reservoirs. First, the current goal of this thesis to preserve a concentration of 4 mg/L must be reconsidered for reservoirs with a higher trophic level. Here, the number of days with hypoxic or anoxic conditions in the hypolimnion or the “anoxic factor” (Nürnberg, 1995) could be an alternative to a concentration threshold. Second, the additional flushing of “undesirable” water layers can support operators of meso-/ eutrophic drinking water reservoirs. With this method, they can try to limit epi-/ metalimnetic algal blooms (Taylor et al., 1988) as well as the availability of hypolimnetic nutrients and metals. Third, the combination of real-time reservoir modelling and online measurement data would be a powerful tool for operators to respond fast to changing conditions. In conclusion, adjusting the optimization approach and using real-time modelling and monitoring improves the operation of drinking water reservoirs with a higher trophic level.

There are also two limitations for using our model in shallow reservoirs. First, the epilimnion-hypolimnion ratio determines the distance between epilimnetic and hypolimnetic extraction points and, hence, the water temperature range at the extraction points for mixing a desired water temperature and discharge could be limited. As a result, the combination of withdrawing a predefined water quality and guaranteeing a safe raw water quality is hampered. Second, the hypolimnetic discharge volume should be adjusted carefully to prevent a deepening of the thermocline and an acceleration of hypolimnetic oxygen depletion. The combination of reservoir shallowness and higher trophic level will further impede the combination of downstream river demands with a sustainable raw water supply. This will limit the ability to control the water quality in these reservoirs. Therefore, the decision-support of those model applications should be considered in the design and operation of future dams.

Reservoirs for hydro-power, irrigation and recreation

The new tool presented in this thesis can be also used for multi-objective modelling on reservoirs for hydro-power, irrigation and recreation. Then, other objectives like maintaining the head for electricity generation, preventing thermopeaking (see Chapter 4), flushing of deposited sediments (Espa et al., 2016) or turbid inflows, controlling discharge quality for irrigation (Kerachian and Karamouz, 2006; Kunz et al., 2013) and examining pathogen dynamics (Hipsey et al., 2004) play a role. Therefore, other existing water quality modules/

processes in AED2 e.g. for phytoplankton, suspended solids and pathogens (see Hipsey et al., 2013) must be included. This will make the model more complex, but the inclusion of additional processes is necessary for reservoir optimization.

5.6 Decision support for Integrated Water Resources Management

The combination of water quantity and quality is one of the most important challenges in water resources management. Focusing on reservoirs, their management is dependent on the type of reservoir and its multiple objectives. However, in some cases like extreme floods, long-lasting dry periods or even new international laws, operators have to prioritize one objective. Then, either reservoir water quality, discharge quality or flood protection should play the major role. In this case, reservoir models can help to (i) evaluate the scope for action, (ii) support the prioritization or even (iii) combine the prioritized objective with minor objectives. An example could be the provision of sufficient retention volume and a quasi-natural temperature and flow regime for the downstream river at high discharges before and during flooding conditions. The forecasting ability of reservoir models is very important in such situations. Their prediction can help to maintain a sufficiently large retention volume before and during floods while keeping discharge temperatures as natural as possible.

At a larger scale, the integrated management of reservoirs and rivers on basin scale is important to mitigate the global threat to water security and river biodiversity (Vörösmarty et al., 2010). Therefore, we urgently need to couple reservoir models with hydrological (catchment) models. Seibert et al. (2014) used a coupled hydrological-hydrodynamic model for flood mitigation at the Danube catchment in Bavaria, Germany. With their coupled model, they identified the retention potential of reservoirs within the catchment. Further work on adaptive water resources management by coupled hydrological-hydrodynamic models was done by Zhao et al. (2016). They aimed at decision support to reduce flood risk and enhance water supply in times of growing utilization pressure and environmental changes on Brazos River Basin in Texas. The impact of changes in reservoir management, land use and climate conditions on the in-reservoir water quality was studied by Nguyen et al. (2017). In scenario simulations they analyzed changes in chlorophyll-a concentrations as an important factor for eutrophication effects at Millbrook catchment in South Australia. All these studies demonstrated the importance of coupled hydrological-hydrodynamic models for integrated water resources management. Progressing hydrological, land use and climate changes as well

as the accelerating importance of dam operations worldwide (Zarfl et al., 2015) will further increase the demand for reservoir and basin scale model tools. In times of growing utilization pressure on freshwater systems like reservoirs and rivers, a smart catchment management will become mandatory.

Chapter 6: Conclusions

The present thesis extended the one-dimensional hydrodynamic model GLM together with the water quality library AED2 and integrated operational rules and management decisions. The model provided a valuable instrument for capturing stratification patterns and oxygen concentrations in a reservoir with selective withdrawal management. According to the implemented operational rules, it autonomously calculated the required height for the selective withdrawal on basis of:

- the upstream river water temperature and flow discharge,
- the prescribed hydrological boundary conditions,
- the modelled water quality parameters temperature and dissolved oxygen and
- the parallel activation of the bottom outlet, when both withdrawals are mixed.

The results show that the quasi-natural temperature and flow conditions in the downstream river can be restored by changing the current withdrawal strategy. The temperature of the discharged water matched the desired temperature range for grayling and brown trout. However, predominant withdrawal from the upper and warm layers had a large impact on stratification and water quality. It lowered the thermocline, strengthened the thermal structure and led to a stronger decrease of the hypolimnetic dissolved oxygen. As a result, a smart (optimized) reservoir withdrawal strategy was developed to combine downstream river demands with a sustainable raw water supply. Here, the mixing of selective withdrawal (warm water) with bottom outlet withdrawal (cold water) improved raw water and downstream river discharge water quality and avoided harmful water quality deterioration. Generally, this thesis indicated the potential of reservoir withdrawal and numerical models to alleviate the disruption of the river continuum by a reservoir dam with respect to temperature and discharge.

References

- Arismendi, I., Safeeq, M., Dunham, J.B., Johnson, S.L., 2014. Can air temperature be used to project influences of climate change on stream temperature? *Environ Res Lett* 9(8): 084015. doi:10.1088/1748-9326/9/8/084015
- Baden, S.P., Eriksson, S.P., Weeks, J.M., 1995. Uptake, accumulation and regulation of manganese during experimental hypoxia and normoxia by the decapod *Nephrops norvegicus* (L.). *Mar Pollut Bull* 31(1-3), 93-102. doi:10.1016/0025-326X(94)00257-A
- Barbiero, R.P., James, W.F., Barko, J.W., 1997. The effects of a change in withdrawal operations on phytoplankton and nutrient dynamics in Eau Galle Reservoir, Wisconsin (USA). *Int. Revue ges. Hydrobiol. Hydrogr.* 82(4), 531-543. doi:10.1002/iroh.19970820410
- Bartholow, J., Hanna, R.B., Saito, L., Lieberman, D., Horn, M., 2001. Simulated Limnological Effects of the Shasta Lake Temperature Control Device. *Environ Manage* 27(4), 609-626. doi:10.1007/s0026702324
- Bocaniov, S.A., Ullmann, C., Rinke, K., Lamb, K.G., Boehrer, B., 2014. Internal waves and mixing in a stratified reservoir: insights from three-dimensional modeling. *Limnologica* 49, 52-67. doi:10.1016/j.limno.2014.08.004
- Bocaniov, S. A., Scavia, D., 2016. Temporal and spatial dynamics of large lake hypoxia: Integrating statistical and three-dimensional dynamic models to enhance lake management criteria. *Water Resour Res* 52(6), 4247-4263. doi:10.1002/2015WR018170
- Brett M.T., Ahopelto, S.K., Brown, H.K., Brynestad, B.E., Butcher, T.W., Coba, E.E., Curtis, C.A., Dara, J.T., Doeden, K.B., Evans, K.R., et al., 2016. The modeled and observed response of Lake Spokane hypolimnetic dissolved oxygen concentrations to phosphorus inputs. *Lake Reserv Manage* 32(3), 246-258. doi:10.1080/10402381.2016.1170079
- Brookes, J.D., Carey, C.C., 2011. Resilience to blooms. *Science* 334, 46-47. doi:10.1126/science.1207349
- Brookes, J.D., Carey, C.C., Hamilton, D.P., Ho, L., van der Linden, L., Renner, R., Rigosi, A., 2014. Emerging Challenges for the Drinking Water Industry. *Environ Sci Technol* 48(4), 2099-2101. doi:10.1021/es405606t
- Brooks, N.H., Koh, R.C.Y., 1969. Selective withdrawal from density stratified reservoirs. *J Hydraul Div-ASCE* 95(HY4), 1369-1400.
- Bruce, L.C., Frassl, M.A., Arhonditsis, G.B., Gal, G., Hamilton, D.P., Hanson, P.C., et al., 2017. A multi-lake comparative analysis of the General Lake Model (GLM): Stress-testing

- across a global observatory network. *Environ Modell Softw*, accepted pending final revision.
- Bruggeman, J., Bolding, K., 2014. A general framework for aquatic biogeochemical models. *Environ Modell Softw* 61, 249-265. doi:10.1016/j.envsoft.2014.04.002
- Bruno, M.C., Siviglia, A., Carolli, M., Maiolini, B., 2013. Multiple drift responses of benthic invertebrates to interacting hydropeaking and thermopeaking waves. *Ecohydrol* 60(4), 511-522. doi: 10.1002/eco.1275
- Bryant, L. D., Hsu-Kim, H., Gantzer, P. A., Little, J. C., 2011. Solving the problem at the source: Controlling Mn release at the sediment-water interface via hypolimnetic oxygenation. *Water Res* 45(19), 6381-6392. doi:10.1016/j.watres.2011.09.030
- Çalışkan, A., Elçi, Ş., 2009. Effects of selective withdrawal on hydrodynamics of a stratified reservoir. *Water Resour Manage* 23(7), 1257-1273. doi:10.1007/s11269-008-9325-x
- Casamitjana, X., Serra, T., Colomer, J., Baserba, C., Pérez-Losada, J., 2003. Effects of the water withdrawal in the stratification patterns of a reservoir. *Hydrobiologia* 504(1-3), 21-28. doi:10.1023/B:HYDR.0000008504.61773.77
- Cassidy, R.A., 1989. Water temperature, dissolved oxygen, and turbidity control in reservoir releases, in: Gore, J.A., Petts, G.E. (Eds.), *Alternatives in regulated river management*. CRC Press, Boca Raton, Florida, pp 28-62.
- Carolli, M., Bruno, M. C., Siviglia, A., Maiolini, B., 2012. Responses of benthic invertebrates to abrupt changes of temperature in flume simulations. *River Res Applic* 28, 678-691. doi:10.1002/rra.1520
- Castelletti, A., Yajima, H., Giuliani, M., Soncini-Sessa, R., Weber, E., 2014. Planning the Optimal Operation of a Multioutlet Water Reservoir with Water Quality and Quantity Targets. *J Water Res Pl-ASCE* 140(4), 496-510. doi:10.1061/(ASCE)WR.1943-5452.0000348
- Chen, S., Lei, C., Carey, C.C., Gantzer, P.A., Little, J.C., 2017. A coupled three-dimensional hydrodynamic model for predicting hypolimnetic oxygenation and epilimnetic mixing in a shallow eutrophic reservoir. *Water Resour Res* 53, 470-484. doi:10.1002/2016WR019279
- Chung, E.G., Schladow, S.G., Perez-Losada, J., Robertson, D.M., 2008. A linked hydrodynamic and water quality model for the Salton Sea. *Hydrobiologia* 604:57-75.
- Couture, R.-M., de Wit, H. A., Tominaga, K., Kiuru, P., Markelov, I., 2015. Oxygen dynamics in a boreal lake responds to long-term changes in climate, ice phenology, and DOC inputs. *J Geophys Res Biogeosci* 120, 2441-2456. doi:10.1002/2015JG003065
- Davison, W., 1993. Iron and manganese in lakes. *Earth-Sci Rev* 34(2), 119-163. doi:10.1016/0012-8252(93)90029-7

- Espa, P., Brignoli, M.L., Crosa, G., Gentili, G., Quadroni, S., 2016. Controlled sediment flushing at the Cancano Reservoir (Italian Alps): Management of the operation and downstream environmental impact. *J Environ Manage* 182, 1-12. doi:10.1016/j.jenvman.2016.07.021
- Fontane, D.G., Labadie, J.W., Loftis, B.O., 1981. Optimal Control of Reservoir discharge quality through selective withdrawal. *Water Resour Res* 17(6), 1594-1604. doi:10.1029/WR017i006p01594
- Gal, G., Imberger, J., Zohary, T., Antenucci, J., Anis, A., Rosenberg, T., 2003. Simulating the thermal dynamics of Lake Kinneret. *Ecol Modell* 162, 69-86. doi: 10.1016/S0304-3800(02)00380-0
- Gal, G., Hipsey, M.R., Parparov, A., Wagner, U., Makler, V., Zohary, T., 2009. Implementation of ecological modeling as an effective management and investigation tool: Lake Kinneret as a case study. *Ecol Modell* 220(13), 1697-1718. doi:10.1016/j.ecolmodel.2009.04.010
- Gantzer, P.A., Bryant, L.D., Little, J.C., 2009. Controlling soluble iron and manganese in a water-supply reservoir using hypolimnetic oxygenation. *Water Res* 43(5), 1285-1294. doi:10.1016/j.watres.2008.12.019
- Gaugush, R.F., 1984. Mixing events in Eau Galle Lake. *Lake Reserv Manage* 1(1), 286-291. doi:10.1080/07438148409354526
- Giles, C.D., Isles, P.D.F., Manley, T., Xu, Y., Druschel, G.K., Schroth, A.W., 2016. The mobility of phosphorus, iron, and manganese through the sediment–water continuum of a shallow eutrophic freshwater lake under stratified and mixed water-column conditions. *Biogeochemistry* 127, 15-34. doi:10.1007/s10533-015-0144-x
- Gore J.A., Nestler J.M., Layzer, J.B., 1989. Instream flow predictions and management options for biota affected by peaking power hydroelectric operations. *Reg Rivers: Res Manage* 3, 35-48. doi:10.1002/rrr.3450030106.
- Goudsmit, G.H., Peeters, F., Gloor, M., Wüest, A., 1997. Boundary versus internal diapycnal mixing in stratified natural waters. *J Geophys Res* 102(C13), 27903-27914. doi:10.1029/97JC01861
- Gudasz, C., Bastviken, D., Steger, K., Premke, K., Sobek, S., Tranvik, L.J., 2010. Temperature-controlled organic carbon mineralization in lake sediments. *Nature* 466, 478-481. doi:10.1038/nature09186
- Hamilton, D.P., Schladow, S.G., 1997. Water quality in lakes and reservoirs. Part I Model description. *Ecol Modell* 96, 91-110. doi:10.1016/S0304-3800(96)00062-2

- Hari R.E., Guettinger, H., 2004. Temperaturparameter von 25 Flüssen in den 2 Perioden 1978-1987 und 1988-2002 und der Vergleich mit dem optimalen Temperaturband für Bachforellen. Fischnetz Schlussbericht, Eawag Duebendorf. 97pp.
- Hipsey, M.R., Antenucci, J.P., Brookes, J.D., Burch, M.D., Regel, R.H., Linden, L., 2004. A three-dimensional model of *Cryptosporidium* dynamics in lakes and reservoirs: a new tool for risk management. *Intl. J. River Basin Manage* 2, 181-197. doi:10.1080/15715124.2004.9635231
- Hipsey, M.R., Bruce, L.C., Hamilton, D.P., 2013. Aquatic Ecodynamics (AED) Model Library, Science Manual, The University of Western Australia, Perth, Australia. 34pp.
- Hipsey, M.R., Bruce, L.C., Hamilton, D.P., 2014. GLM - General Lake Model: Model Overview and User Information. AED Report #26, The University of Western Australia, Perth, Australia. 42pp.
- Hocking, G.C., Patterson, J.C., 1991. Quasi-two-dimensional reservoir simulation model. *J Environ Eng* 117, 595-613.
- Imberger, J., Patterson, J., Hebbert, B., Loh, I., 1978. Dynamics of reservoir of medium size. *J Hydraul Div-ASCE* 104, 725-743.
- Imberger, J., Patterson, J.C., 1981. A dynamic reservoir simulation model-DYRESM: 5, in: Fischer, H.B. (Ed.) *Transport models for inland and coastal waters*. Academic Press, New York, pp 310-361.
- International Commission on Large Dams (2011) *World Register of Dams*. <http://www.icold-cigb.org>. Accessed 30 May 2017
- Kasten, F., Czeplak, G., 1980. Solar and terrestrial-radiation dependent on the amount and type of cloud. *Sol Energy* 24(2), 177-189. doi:10.1016/0038-092x(80)90391-6
- Kennedy, R.H., 1999. Reservoir design and operation: limnological implications and management opportunities, in: Tundisi, J.G., Straskraba, M. (Eds.), *Theoretical reservoir ecology and its applications*. Backhuys, Leiden, pp 1-28.
- Kerachian, R., Karamouz, M., 2006. Optimal reservoir operation considering the water quality issues: A stochastic conflict resolution approach. *Water Resour Res* 42(12), W12401. doi:10.1029/2005WR004575
- Kerimoglu, O., Rinke, K., 2013. Stratification dynamics in a shallow reservoir under different hydro-meteorological scenarios and operational strategies. *Water Resour Res* 49(11), 7518-7527. doi:10.1002/2013WR013520
- Koenings, J.P., Edmundson, J.A., 1991. Secchi disk and photometer estimates of light regimes in Alaskan lakes: Effects of yellow color and turbidity. *Limnol Oceanogr* 36, 91-105. doi:10.4319/lo.1991.36.1.0091

- Kunz, M.J., Senn, D.B., Wehrli, B., Mwelwa, E.M., Wüest, A., 2013. Optimizing turbine withdrawal from a tropical reservoir for improved water quality in downstream wetlands. *Water Resour Res* 49(9), 5570-5584. doi:10.1002/wrcr.20358
- Labadie, J., 2004. Optimal operation of multireservoir systems: State-of-the-art review. *J Water Res Pl-ASCE* 130(2), 93-111. doi:10.1061/(ASCE)0733-9496(2004)130:2(93).
- Livingstone, D.M., Imboden, D.M., 1996. The prediction of hypolimnetic oxygen profiles: a plea for a deductive approach. *Can J Fish Aquat Sci* 53(4), 924-932. doi:10.1139/f96-301
- Marcé, R., Moreno-Ostos, E., García-Barcina, J.M., Armengol, J., 2010. Tailoring dam structures to water quality predictions in new reservoir projects: Assisting decision-making using numerical modelling. *J Environ Manage* 91(6), 1255-1267. doi:10.1016/j.jenvman.2010.01.014
- McCord, S.A., Schladow, S.G., 1998. Numerical simulations of degassing scenarios for CO₂-rich Lake Nyos, Cameroon. *J Geophys Res: Solid Earth* 103(B6), 12355-12364.
- Moreno-Ostos, E., Marcé, R., Ordóñez, J., Dolz, J., Armengol, J., 2008. Hydraulic Management Drives Heat Budgets and Temperature Trends in a Mediterranean Reservoir. *Int Rev Hydrobiol* 93(2), 131-147. doi:10.1002/iroh.200710965
- Nguyen, H.H., Recknagel, F., Meyer, W., Frizenschaf, J., Shrestha, M.K., 2017. Modelling the impacts of altered management practices, land use and climate changes on the water quality of the Millbrook catchment-reservoir system in South Australia. *J Environ Manage* 202, 1-11. doi:10.1016/j.jenvman.2017.07.014
- Nilsson, C., Reidy, C.A., Dynesius, M., Revenga, C., 2005. Fragmentation and flow regulation of the World's large river systems. *Science* 308(5720), 405-408. doi:10.1126/science.1107887
- North, R.P., 2012. The influence of climate change on the occurrence of hypoxia in Swiss lakes. Dissertation 20802, ETH Zürich, Switzerland, 81 pp. doi:10.3929/ethz-a-009756882
- Nürnberg, G.K., 1987. Hypolimnetic withdrawal as lake restoration technique. *J Environ Eng-ASCE* 113(5), 1006-1017. doi:10.1061/(ASCE)0733-9372(1987)113:5(1006)
- Nürnberg, G.K., Hartley, R., Davis, E., 1987. Hypolimnetic withdrawal in two north American lakes with anoxic phosphorus release from the sediment. *Water Res* 21(8), 923-928. doi:10.1016/S0043-1354(87)80009-X
- Nürnberg, G.K., 1995. Quantifying anoxia in lakes. *Limnol. Oceanogr.* 40,1100-1111. doi:10.4319/lo.1995.40.6.1100
- Olden, J.D., Naiman, R.J., 2010. Incorporating thermal regimes into environmental flows assessments: modifying dam operations to restore freshwater ecosystem integrity. *Freshwater Biol* 55, 86-107. doi:10.1111/j.1365-2427.2009.02179.x

- Olszewski, P., 1961. Versuch einer Ableitung des hypolimnischen Wassers aus einem See. *Verh Internat Verein Theor Angew Limnol* 14, 855-861.
- Patterson, J.C., Hamblin, P.F., Imberger, J. 1984. Classification and dynamics simulation of the vertical density structure of lakes. *Limnol Oceanogr* 29, 845-861.
- Piccolroaz, S., Calamita, E., Majone, B., Gallice, A., Siviglia, A., Toffolon, M., 2016. Prediction of river water temperature: a comparison between a new family of hybrid models and statistical approaches. *Hydrol. Process.* 30(21), 3901-3917. doi: 10.1002/hyp.10913
- Poff, N. L., Allan, J. D., Bain, M. B., Karr, J. R., Prestegard, K. L., Richter, B. D., Sparks, R.E., Stromberg, J. C., 1997. The natural flow regime: A paradigm for river conservation and restoration. *BioScience* 47(11), 769-784. doi:10.2307/1313099
- Preece, R.M., 2004. Cold Water Pollution Below Dams in New South Wales: A Desktop Assessment. NSW Department of Infrastructure, Planning and Natural Resources, Sydney, NSW
- Read, J.S., Winslow, L.A., Hansen, G.J.A., Van Den Hoek, J., Hanson, P.C., Bruce, L.C., Markfort, C.D., 2014. Simulating 2368 temperate lakes reveals weak coherence in stratification phenology. *Ecol Model* 291, 142-150. doi:10.1016/j.ecolmodel.2014.07.029
- Rippey, B., McSorley, C., 2009. Oxygen depletion in lake hypolimnia. *Limnol Oceanogr* 54(3), 905-916. doi:10.4319/lo.2009.54.3.0905
- Salmon, S.U., Hipsey, M.R., Wake, G.W., Ivey, G.N., Oldham, C.E., 2017. Quantifying Lake Water Quality Evolution: Coupled Geochemistry, Hydrodynamics, and Aquatic Ecology in an Acidic Pit Lake. *Environ Sci Technol* 51(17), 9864-9875. doi:10.1021/acs.est.7b01432
- Schwefel, R., Gaudard, A., Wüest, A., Bouffard, D., 2016. Effects of climate change on deepwater oxygen and winter mixing in a deep lake (Lake Geneva): Comparing observational findings and modeling. *Water Resour Res* 52, 8811-8826. doi:10.1002/2016WR019194
- Seibert, S.P., Skublics, D., Ehret, U., 2014. The potential of coordinated reservoir operation for flood mitigation in large basins - A case study on the Bavarian Danube using coupled hydrological-hydrodynamic models. *J Hydrol* 517, 1128-1144. doi:10.1016/j.jhydrol.2014.06.048
- Sherman, B., Todd, C.R., Koehn, J.D., Ryan, T., 2007. Modelling the impact and potential mitigation of cold water pollution on Murray cod populations downstream of Hume Dam, Australia. *River Res Appl* 23, 377-389. doi:10.1002/rra.994
- Sherman, B.S., Lemckert, C., Zhang, H., 2010. The Impact of Artificial Destratification on Reservoir Evaporation. Urban Water Security Research Alliance Technical Report No. 35. 25pp.

- Stepanenko, V., Mammarella, I., Ojala, A., Miettinen, H., Lykosov, V., Vesala, T., 2016. LAKE 2.0: a model for temperature, methane, carbon dioxide and oxygen dynamics in lakes. *Geosci Model Dev* 9(5), 1977-2006. doi:10.5194/gmd-9-1977-2016
- Stevens, L.E., Shannon, J., Blinn, D.W., 1997. Colorado River Benthic Ecology in Grand Canyon, Arizona, USA: Dam, tributary and geomorphological influences. *Regul. Rivers: Res. Manage*, 13: 129–149. doi:10.1002/(SICI)1099-1646(199703)13:2<129::AID-RRR431>3.0.CO;2-S
- Taylor, W.D., Barko, J.W., James, W.F., 1988. Contrasting diel patterns of vertical migration in the dinoflagellate *Ceratium hirundinella* in relation to phosphorus supply in a north temperate reservoir. *Can J Fish Aquat Sci* 45(6), 1093-1098. doi:10.1139/f88-133
- Toffolon, M., Piccolroaz, S., 2015. A hybrid model for river water temperature as a function of air temperature and discharge. *Environ. Res. Lett.*, 10(11): 114011. doi:10.1088/1748-9326/10/11/114011
- Vinson, M.R., 2001. Long-term dynamics of an invertebrate assemblage downstream from a large dam. *Ecol Appl* 11(3), 711-730.
- von Rohden, C., Ilmberger, J., 2001. Tracer experiment with sulfur hexafluoride to quantify the vertical transport in a meromictic pit lake. *Aquat Sci* 63, 417-431.
- Vörösmarty, C.J., McIntyre, P.B., Gessner, M.O., Dudgeon, D., Prusevich, A., Green, P., Glidden, S., Bunn, S.E., Sullivan, C.A., Reidy Liermann, C., Davies, P.M., 2010. Global threats to human water security and river biodiversity. *Nature* 467, 555-561. doi:10.1038/nature09440
- Weber, M., Rinke, K., Hipsey, M.R., Bohrer, B., 2017. Optimizing withdrawal from drinking water reservoirs to reduce downstream temperature pollution and reservoir hypoxia. *J Environ Manage* 197, 96-105. doi:10.1016/j.jenvman.2017.03.020
- Wilmsen, B., 2016. After the Deluge: A longitudinal study of resettlement at the Three Gorges Dam, China. *World Development* 84, 41-54. doi:10.1016/j.worlddev.2016.04.003
- Wupperverband, 2008. Handbuch der Dhünn, Grundlagen zur Gewässer- und Raumentwicklung. [http://www.wupperverband.de/internet/mediendb.nsf/gfx/med_IWER-8P2LQU_57A08B/\\$file/1_2008_brosch_dhuenn_2.pdf](http://www.wupperverband.de/internet/mediendb.nsf/gfx/med_IWER-8P2LQU_57A08B/$file/1_2008_brosch_dhuenn_2.pdf). Accessed 26 July 2016.
- Yeates, P.S., Imberger, J., 2003. Pseudo two-dimensional simulations of internal and boundary fluxes in stratified lakes and reservoirs. *Int J River Basin Manage*, 1(4) 297- 319. doi:10.1080/15715124.2003.9635214
- Zarfl, C., Lumsdon, A.E., Berlekamp, J., Tydecks, L., Tockner, K., 2015. A global boom in hydropower dam construction. *Aquat Sci* 77(1), 161-170. doi:10.1007/s00027-014-0377-0

- Zhang, M., Lin, Q.Q., Xiao, L.J., Wang, S., Qian, X., Han, B.P., 2013. Effect of intensive epilimnetic withdrawal on the phytoplankton in a (sub)tropical deep reservoir. *J Limnol* 72(3), 430-439. doi:10.4081/jlimnol.2013.e35
- Zhao, G., Gao, H., Naz, B.S., Kao, S.-C., Voisin, N., 2016. Integrating a reservoir regulation scheme into a spatially distributed hydrological model, *Adv Water Resour* 98, 16-31. doi:10.1016/j.advwatres.2016.10.014
- Zolezzi, G., Siviglia, A., Toffolon, M., Maiolini, B., 2011. Thermopeakings in Alpine streams: event characterization and time scales. *Ecohydrol* 4, 564-576. doi:10.1002/eco.132

Author contributions

This dissertation is based on three research articles. I was the leading author of two articles (Article 1 and 2).

Article 1: Weber, M. (MW), Rinke, K. (KR), Hipsey, M.R.(MRH), Boehrer, B. (BB), 2017. Optimizing withdrawal from drinking water reservoirs to reduce downstream temperature pollution and reservoir hypoxia. *Journal of Environmental Management* 197, 96-105. doi:10.1016/j.jenvman.2017.03.020 (Chapter 3)

Conception and design: MW, KR, BB
 Source code add-ons and modifications: MW, MRH
 Data acquisition: MW
 Data analysis: MW, BB
 Interpretation of results: MW, BB, KR
 Writing the manuscript: MW
 Editorial support: BB, KR

Article 2: Weber, M. (MW), Boehrer, B. (BB), Rinke, K. (KR), in review since July 2017. Minimizing environmental impact whilst securing drinking water quantity and quality demands from a reservoir. *River Research and Applications* (Chapter 4)

Conception and design: MW, KR, BB
 Source code add-ons and modifications: MW
 Data acquisition: MW
 Data analysis: MW, BB, KR
 Interpretation of results: MW, BB, KR
 Writing the manuscript: MW
 Editorial support: BB, KR

Article 3: Hipsey, M.R. (MRH), Weber, M. (MW), et al., in review since November 2017. A General Lake Model (GLM 2.4) for linking with high-frequency sensor data from the Global Lake Ecological Observatory Network (GLEON). *Geoscientific Model Development* (Chapter 2)

Conception and design: MRH, MW and others
 Source code add-ons and modifications: MRH, MW and others
 Data acquisition: MRH, MW and others
 Data analysis: MRH, MW and others
 Writing the manuscript: MRH, MW and others
 Editorial support: MRH, MW and others

My task in this multi-author article was predominantly modifying the source code (e.g. adaptive withdrawal functionality, deep mixing module), finding and fixing bugs in the code for the newest release v2.4, running simulations, analyzing data and writing parts of or whole subchapters 2.5.2, 2.6.1 and 2.6.4 in Appendix 1. I was also contributing in other chapters and giving a lot of editorial support.

Other contributions

Bruce, L.C., Frassl, M.A., Arhonditsis, G.B., Gal, G., Hamilton, D.P., Hanson, P.C., **Weber, M.**, et al., 2018. A multi-lake comparative analysis of the General Lake Model (GLM): Stress-testing across a global observatory network. *Environ Modell Softw*, 102: 274-291. doi:10.1016/j.envsoft.2017.11.016

Giling, D.P., Staehr, P.A., Grossart, H.P., Andersen, M.R., Boehrer, B., Escot-Muñoz, C., Evrendilek, F., Gener, L.G., Honti, M., Jones, I.D., Karakaya, N., Laas, A., Moreno, Q., Rinke, K., Scharfenberger, U., Schmidt, S.R., **Weber, M.**, Woolway, R.I., Zwart, J., Obrador, B., 2017. Delving deeper: Metabolic processes in the metalimnion of stratified lakes. *Limnol. Oceanogr.*, 62, 1288-1306. doi:10.1002/lno.10504

Schultze, M., Sudbrack, R., Neumann, V., Frassl, M., Willmitzer, H., Möller, M., Scharf, W., **Weber, M.**, Boehrer, B., Rinke, K., 2016. Unterwasserabgabe nicht aus dem Grundablass - Motive und Folgen alternativer Ausleittiefen. Discharge not from the bottom - motivations and consequences of alternative discharge depths. *Wasserwirtschaft* 106 (6), 82-85.

Declaration

I hereby declare, that the thesis entitled “Optimizing withdrawal from drinking water reservoirs to combine downstream river demands with a sustainable raw water management” is the result of my own work except where otherwise indicated.

I hereby also declare, that my thesis has not been submitted for another examination, assignment, dissertation or any other degree to another university or scientific institution.

Leipzig, 22 December 2017



Michael Weber

Curriculum Vitae



Michael Weber

Date of birth	02 October 1983
Place of birth	Räckelwitz
Nationality	German
E-mail	michael.weber@ufz.de

Background

Since 06 2014	PhD student at the Helmholtz Centre for Environmental Research (UFZ), Department of Lake Research <i>“Optimizing withdrawal from drinking water reservoirs to combine downstream river demands with a sustainable raw water management”</i>
12 2011 – 11 2013	Research assistant at the Limnological Institute of the University of Constance, Department of Environmental Physics <i>„The role of littoral zones as source of methane in lakes: Dynamics, distribution patterns and emissions“</i>
12 2009 – 11 2011	Research assistant at the Institute for Lake Research Langenargen, Department of Sedimentology and Lake Physics <i>„Erosion and monument protection at Lake Constance and Lake Zurich. Measuring and modelling of hydrodynamic and morphodynamic processes“</i>
01 2009 – 07 2009	Diploma thesis at the Institute for Lake Research Langenargen <i>„Hydrodynamic modelling of flow and transport in an artificial stagnant water body (Schwarzenbachtalsperre, Forbach). Preparation of different scenarios and their impact on the turbulent mixing of the reservoir“</i>
10 2003 – 07 2009	Study of Hydrology at Dresden University of Technology

Danksagung

Ein herzliches Dankeschön geht an meine Familie für ihre Unterstützung während der gesamten Doktorarbeit. Ohne den Rückhalt meiner Frau und meiner zwei Söhne, wäre diese Arbeit wohl nicht zustande gekommen. Eure Liebe, Zuversicht, Geduld, Kraft und euer Verständnis haben mich immer gestärkt. Ich danke auch sehr meinen Eltern für all ihre Mühe, Nerven und Energie, die sie all die Jahre seit meiner Geburt für mich aufgewendet haben. Ohne euch alle wäre ich nicht da, wo ich jetzt stehe. Ich danke euch allen, dass ihr diese stressige Zeit mitgemacht habt und mich immer noch liebt.

Ich danke Bertram Boehrer für die exzellente Betreuung - einen besseren Mentor gibt es nicht. Wirklich. Er erfüllt alle Kriterien für einen „Perfekten Betreuer“. Ich habe überaus viel von ihm gelernt und bin ihm für die Unmengen an Zeit für wissenschaftliche und private Gespräche sehr dankbar. Er hat meine junge wissenschaftliche Laufbahn stark positiv geprägt. Ich wünsche jedem Doktoranden einen Betreuer wie ihn.

Außerdem danke ich Karsten Rinke für all die Möglichkeiten für meine wissenschaftliche Weiterentwicklung. Dies spiegelt sich nicht nur im Forschungsaufenthalt in Australien und den unzähligen Workshops/Tagungen, sondern auch in meinen vier Koautorenschaften wider. Zusätzlich hat sein Blick für die Biologie und das Talsperrenmanagement meiner Arbeit unheimlich gut getan.

Ich danke meinem Universitätsbetreuer Andreas Lorke für seine Mühe und Zeit, die er in mich als externen Doktoranden und meine Arbeit gesteckt hat. Ich bin immer noch verblüfft, wie schnell er sich in komplexe Dinge hineinversetzen kann, um dann an den richtigen Stellen kritische Fragen zu stellen, beziehungsweise passende Antworten zu geben. Sein konstruktives Feedback hat die Qualität dieser Arbeit deutlich verbessert.

Ein Dankeschön geht an alle Mitarbeiter im Department Seenforschung bzw. am UFZ-Standort Magdeburg für die tollen dreieinhalb Jahre. Ich habe mich stets wohl gefühlt und werde euch sehr vermissen. Allen voran meine Kollegen Marieke, Valerie, Karoline, Claudia, Chenxi, Martin, Matthias, Katrin, Andreas, Micha, Frau Klapputh und Frau Bibiko.

Außerdem danke ich Karsten Rahn und Martin Wieprecht für Ihre Bemühungen sowie Hilfe beim Monitoring der Talsperre Große Dhünn. Die Ausfahrten wurden stets perfekt organisiert und durchgeführt. Es hat sehr viel Spaß mit euch gemacht.

Ein besonderer Dank geht an das Team der Talsperre Große Dhünn, allen voran Marco Solmecke, Uwe Wolter, Jürgen Bohring und Thorsten Luckner für all ihre Mühe und Herzlichkeit. Ein großes Dankeschön geht an Wilfried Scharf vom Wupperverband für die freundlichen und konstruktiven Gespräche sowie die Unmengen an essentiellen Daten.

Ein weiteres Dankeschön geht an Matt Hipse, Casper Boon und Louise Bruce im 14.000 km entfernten Perth. Eure Hilfe beim Coding in Fortran und C sowie die konstruktiven

Gespräche haben mir sehr geholfen. Vor allem eure Gastfreundschaft hat diesen Forschungsaufenthalt unvergesslich gemacht.

Ich danke auch allen hier nicht erwähnten Personen, die mich, meine wissenschaftliche Weiterentwicklung oder meine Arbeit unterstützt haben. Vielen Dank!

Der Wupperverband und das Land Nordrhein-Westfalen (Zuwendungsbescheid der BR Köln/MUNLV NRW vom 30.06.2009) haben diese Arbeit im Rahmen des Teilprojektes “Thermorüssel - Monitoring zur Erfolgskontrolle und Modellierung des Wasserkörpers der Talsperre Große Dhünn“ finanziert.

Appendix 1

The original description paper:

Hipsey, M.R., Weber, M., et al., in review since November 2017. A General Lake Model (GLM 2.4) for linking with high-frequency sensor data from the Global Lake Ecological Observatory Network (GLEON). Geoscientific Model Development.

A General Lake Model (GLM 2.4) for linking with high-frequency sensor data from the Global Lake Ecological Observatory Network (GLEON)

Matthew R Hipsey^{1,*}, Louise C Bruce¹, Casper Boon¹, Brendan Busch¹, Cayelan C. Carey², David P Hamilton³, Paul C. Hanson⁴, Jordan S. Read⁵, Eduardo de Sousa¹, Michael Weber⁶, Luke A. Winslow⁷

¹ UWA School of Agriculture & Environment, The University of Western Australia, Crawley WA, 6009, Australia

² Department of Biological Sciences, Virginia Tech, Blacksburg VA, USA

³ Australian Rivers Institute, Griffith University, Nathan QLD, 4111, Australia

⁴ Center for Limnology, University of Wisconsin - Madison, Madison WI, USA

⁵ Center for Integrated Data Analytics, U.S. Geological Survey, Middleton WI, USA

⁶ Department of Lake Research, Helmholtz Centre for Environmental Research - UFZ, Magdeburg, Germany

⁷ Department of Biological Sciences, Rensselaer Polytechnic Institute, Troy NY, USA

* *Correspondence to:* Matthew R. Hipsey (matt.hipsey@uwa.edu.au)

Keywords: lake, stratification, mixing, water balance climate change, water quality, observatory network,

Word count: 12,000 words (text); 18,000 words (text+references+figures&tables+appendix)

Abstract. The General Lake Model (GLM) is a one-dimensional open-source model code designed to simulate the hydrodynamics of lakes, reservoirs and wetlands. GLM was developed to support the science needs of the Global Lake Ecological Observatory Network (GLEON), a network of lake sensors and researchers attempting to understand lake functioning and address questions about how lakes around the world vary in response to climate and land-use change. The scale and diversity of lake types, locations and sizes, as well as the observational data within GLEON, created the need for a robust community model of lake dynamics with sufficient flexibility to accommodate a range of scientific and management needs of the GLEON community. This paper summarises the scientific basis and

numerical implementation of the model algorithms, including details of sub-models that simulate surface heat exchange and ice-cover dynamics, vertical mixing and inflow/outflow dynamics. A summary of typical parameter values for lakes and reservoirs collated from a range of sources is included. GLM supports a dynamic coupling with biogeochemical and ecological modelling libraries for integrated simulations of water quality and ecosystem health. An overview of approaches for integration with other models, and utilities for the analysis of model outputs and for undertaking sensitivity and uncertainty assessments is also provided. Finally, we discuss application of the model within a distributed cloud-computing environment, and as a tool to support learning of network participants.

1 Introduction

Lakes and other lentic (standing) waters support extensive ecosystem services such as water supply, flood mitigation, hydropower, aesthetic and cultural benefits, as well as fisheries and biodiversity (Mueller et al., 2016). Lakes are often considered to be “*sentinels of change*”, providing a window into the sustainability of activities in their associated river basins (Williamson et al., 2009). They are also particularly susceptible to impacts from invasive species and land use development, which often lead to water quality deterioration and loss of ecosystem integrity. Recent estimates have demonstrated their significance in the earth system, contributing to heterogeneity in land surface properties and feedbacks to regional and global climate through energy, water and biogeochemical transfers (Martynov et al., 2012, Cole et al., 2007). For example, Tranvik et al. (2009) suggested carbon burial in lakes and reservoirs is substantial on the global scale, on the order of 0.6 Pg yr^{-1} , or four times the oceanic burial rate.

Given the diversity of lakes among continents, region-specific pressures and local management approaches, the Global Lake Ecological Observatory Network (GLEON: gleon.org) was initiated in 2004 as a grass-roots science community with a vision to observe, understand and predict freshwater systems at a global scale (Hanson et al., 2016). In doing so, GLEON has been a leading example of collaborative research within the hydrological and ecological science disciplines. GLEON aims to bring together environmental sensor networks, numerical models, and information technology to explore ecosystem dynamics across a vast range of scales - from an individual lake or reservoir (Hamilton et al., 2015) to regional (Read et al., 2014; Klug et al., 2012), and even global trends (Rigosi et al., 2015; O'Reilly et al., 2015). Ultimately, it is the aim of the network to facilitate primary discovery and synthesis to provide an improved scientific basis for sustainable freshwater resource management.

Environmental modelling forms a critical component of observing systems, as a way to make sense of the “data deluge” (Porter et al., 2012), allowing users to build virtual domains to support knowledge discovery at the system-scale (Ticehurst et al., 2007; Hipsey et al., 2015). In lake ecosystems the tight coupling between physical processes and water quality and ecological dynamics has long been recognised, and models have capitalized on comprehensive understanding of physical processes (e.g., Imberger and Patterson, 1990; Imboden and Wüest, 1995) to use hydrodynamic models as an underpinning basis for coupling to ecological models that have contributed to our understanding of lake dynamics, including aspects such as mixing regimes, eutrophication dynamics (Matzinger et al., 2007), harmful algal bloom dynamics (Chung et al., 2014), and fisheries (Makler-Pick et al., 2009).

In recent decades a range of 1, 2, and 3-dimensional hydrodynamic models has emerged for lake simulation across a diverse range of time scales. Depending on the dimensionality, the horizontal resolution of these models may vary from metres to tens of kilometres, and the spatial resolution from sub-metre to several metres. As in all modelling disciplines, identifying the most parsimonious model structure and degree of complexity and resolution is challenging, and users in the lake modelling community often tend to rely on heuristic rules or practical reasons for model choice (Mooij et al., 2010). High-resolution models are suited to studying events that occur at the time-scale of flow dynamics, but are not always desirable for ecological studies over longer time scales due to their computational demands and level of over-parameterisation. On the other hand, simple models may be more agile for a particular application, and more suited to parameter identification and scenario testing workflows, but are often less applicable across a wide variety of domains, making them less generalizable.

The lake modelling community has often relied on 1-dimensional (1D) models, which originated to capture lake water balance and thermal stratification dynamics (e.g., Imberger and Patterson, 1981; Peeters et al., 2007; Saloranta and Andersen, 2007; Perroud et al., 2009; Kirillin et al., 2011; Stepanko et al., 2013). Their use is justified given the dominant role of seasonal changes in vertical stratification on lake dynamics, including oxygen dynamics, nutrient and metal cycling and plankton dynamics (Hamilton and Schladow, 1997; Gal et al., 2009). Despite advances in computing power and more readily available 3D hydrodynamic drivers, they continue to remain attractive as they are easily linked with biogeochemical and ecological modelling libraries for complex ecosystem simulations, allowing them to be used to capture the long-term trajectory and resilience of lakes and reservoirs in response to climate change, hydrologic change and land use change; for example, changes to oxygen and nutrient cycles and the increasing risk of algal blooms (e.g., Hu et al., 2016; Snorheim et al., 2017). Furthermore, their low computational requirements relative to 3D models allow for their use in parameter identification routines, making them an attractive balance between process complexity and computational intensity. Nonetheless, there has been a continuing proliferation in the diversity of lake models (Mooij et al., 2010; Janssen et al., 2015), with no

clear packages that are suited to the broad range of geographic contexts, time-scales, and science questions and management issues being addressed by the network participants. In acknowledging that there is no single model suitable for all lake applications, a range of open-source community models and tools can enhance scientific capabilities and foster scientific collaboration and combined efforts (Read et al., 2016). To improve scientific collaboration within the limnological modelling community, however, there is an increasing need for a flexible, open-source community model that limnologists can apply to their own lakes (Trolle et al., 2012), as has been common in oceanography, hydrology and climate modelling communities.

In response to this need, the General Lake Model (GLM), a one-dimensional hydrodynamic model for enclosed aquatic ecosystems was developed. The model emerged as a new code from GLEON activities in 2012, and computes the lake water and energy balance by adopting a variable layer structure, allowing for simulation of vertical profiles of temperature, salinity and density, and considering the potential effects of inflows and outflows, surface heating and cooling, mixing and the effect of ice cover on heating and mixing of the lake. GLM is itself a hydrodynamic model, but has dynamic links to biogeochemical models, allowing for exploration of stratification and vertical mixing on the dynamics of biogeochemical cycles, water quality attributes, and lake ecology. The scope and capability of the model has since developed rapidly with application to numerous lakes within the GLEON network and beyond (e.g., Read et al., 2014; Bueche et al., 2017; Snorheim et al., 2017; Weber et al., 2017; Menció et al., 2017; Bruce et al., 2017). GLM has been designed to be an open-source community model suited to modelling studies across a broad spectrum of lakes, reservoirs and wetlands. It balances complexity of dimensional representation, applicability to a wide range of standing waters, and availability to a broad community (e.g., GLEON). Given that individual applications of the model are not able to describe the full array of features and details of the model structure, the aim of this paper is to present a complete description of GLM, including the scientific background (Section 2), model code organization (Section 3), approach to coupling with biogeochemical models (Section 4), and to overview use of the model within the context of GLEON specific requirements for model analysis, integration and education (Section 5-6).

2 Model Overview

2.1 Background and layer structure

GLM adopts a 1D approach for simulating lake mixing processes by resolving a vertical series of layers that describe the variation in water column properties. Users may configure any number of inflows and outflows, and more advanced options exist for simulating aspects

of the water and heat balance. Depending on the context of the simulation, either daily or hourly meteorological time-series data for surface forcing is required, and daily time-series of volumetric inflow and outflow rates can also be supplied. The model is suitable for operation in a wide range of climate conditions and is able to simulate ice formation, as well as accommodating a range of atmospheric forcing conditions.

Although GLM is a new model code written in the C programming language, the core layer structure and mixing algorithms is founded on principles and experience from model platforms including the Dynamic Reservoir Simulation Model (DYRESM; Imberger and Patterson, 1981; Hamilton and Schladow, 1997) and the Dynamic Lake Model (DLM; Chung et al., 2008). Other variations have been introduced to extend this underlying approach through applications to a variety of lake and reservoir environments, to which the reader is also referred (e.g., Hocking & Patterson, 1991; McCord & Schladow, 1998; Gal et al., 2003; Yeates and Imberger, 2003). The layer structure is numbered from the lake bottom to the surface, and adopts the flexible Lagrangian layer scheme first introduced by Imberger et al. (1978) and Imberger & Patterson (1981). The approach defines each layer as a ‘control volume’ that can change thickness by contracting and expanding in response to inflows, outflows, mixing with adjacent layers, and surface mass fluxes. Layer thickness limits are enforced to adequately resolve the vertical density gradient with fine resolution occurring in the metalimnion and thicker cells where mixing is occurring, as depicted schematically in Figure 1. Unlike fixed-grid (Eulerian) design of most 1D lake and ocean models, it has been reported that numerical diffusion at the thermocline can be restricted by this approach (depending on the user-defined minimum (h_{min}) and maximum (h_{max}) layer thickness limits set by the user), making it particularly suited to long-term investigations, and requiring limited site-specific calibration (Patterson et al., 1984; Hamilton & Schladow, 1997; Bruce et al., 2017). Layers each have a unique density computed based on the local salinity and temperature, and when sufficient energy becomes available to overcome density instabilities between adjacent layers, they will merge, thereby accounting for the process of mixing. For deeper systems, a stable vertical density gradient will form in response to periods of high solar radiation creating warm, less-dense conditions near the surface with cooler conditions deeper in the water, separated by a metalimnion region which includes the thermocline. The number of layers, $N_{LEV}(t)$, is adjusted throughout the simulation to maintain homogenous properties within a layer. Initially, the layers are assumed to be of equal thickness, and the initial number of layers, $N_{LEV}(t = 0)$. As the model simulation progresses, density changes due to surface heating, vertical mixing, and inflows and outflows lead to dynamic changes in the layer structure, associated with layers amalgamating, expanding, contracting or splitting.

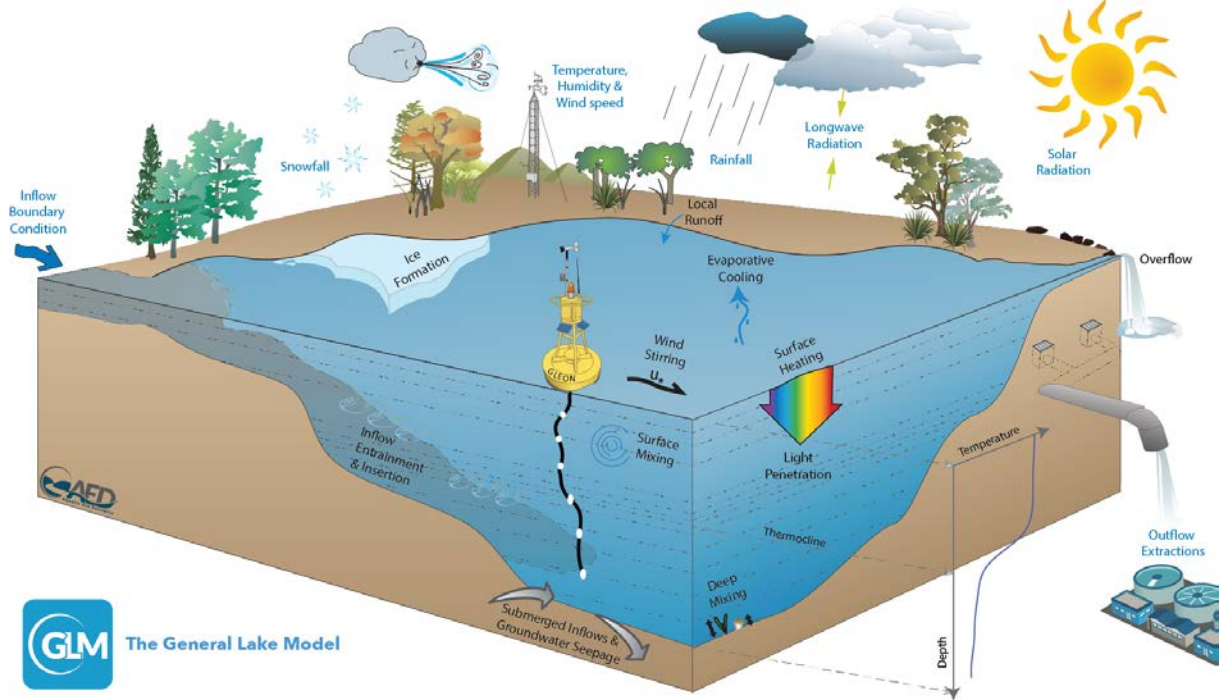


Figure 1: Schematic of a GLM simulation domain, input information (blue text) and key simulated processes (black text).

As layers change, their volumes change based on the site-specific hypsographic curve, whereby the overall lake volume is defined as $\int A(h)dh$, and the elevation (h), and area (A) relationship must be provided as a series of points based on bathymetric data. Layer volumes are determined by interpolating layer area at the appropriate height in the lake basin, whereby $A_i = f(h_i)$, and i is the layer number. This computation requires the user provides a number N_{BSN} of depths with corresponding areas, and the volumes are estimated as:

$$V_b = V_{b-1} + [A_{b-1} + 0.5(A_b - A_{b-1})](h_b - h_{b-1}) \quad (1)$$

where $1 < b \leq N_{BSN}$. Using the raw hypsographic data, a refined depth-area-volume relationship is internally computed using finer depth increments (e.g., ~ 0.1 m), giving N_{MORPH} levels that are used for subsequent calculations. The area and volume at the depth of each increment, h_z is interpolated from the supplied information as:

$$V_z = V_{b-1} \left(\frac{h_z}{h_{b-1}} \right)^{\alpha_b} \quad \text{and} \quad A_z = A_{b-1} \left(\frac{h_z}{h_{b-1}} \right)^{\beta_b} \quad (2)$$

where V_z and A_z are the volume and area at each of the elevations of the refined depth vector, and V_z refers to the nearest b level below h_z such that $h_{b-1} < h_z$. The interpolation coefficients are computed as:

$$\alpha_b = \left[\frac{\log_{10}\left(\frac{V_{b+1}}{V_b}\right)}{\log_{10}\left(\frac{h_{b+1}}{h_b}\right)} \right] \quad \text{and} \quad \beta_b = \left[\frac{\log_{10}\left(\frac{A_{b+1}}{A_b}\right)}{\log_{10}\left(\frac{h_{b+1}}{h_b}\right)} \right]. \quad (3)$$

The density in each layer i is computed based on the temperature, T , and salinity, S , at any given time according to the UNESCO (1981) equation of state whereby $\rho_i = \rho(T_i, S_i)$. Density calculations can also be customised as required.

Because this approach assumes layer properties are laterally averaged, the model is suitable for investigations where resolving the horizontal variability is not a requirement of the study. This is often the case for ecologists and biogeochemists studying natural lakes (e.g., Gal et al., 2009), managers simulating drinking water reservoirs (e.g., Weber et al., 2017), or mining pit lakes (e.g., Salmon et al., 2017), or for analyses exploring the coupling between lakes and regional climate (e.g., Stepanenko et al., 2016). Further, whilst the model is able to resolve vertical stratification, it may also be used to simulate shallow lakes, wetlands, wastewater ponds and other small waterbodies that experience well-mixed conditions. In this case, the layer resolution, with upper and lower layer bounds specified by the user, will automatically simplify, and mass and energy will continue to be conserved.

2.2 Water balance

The model solves the water balance of the lake domain by including several user-configurable water fluxes. The components include surface mass fluxes (evaporation, rainfall and snowfall), inflows (surface inflows, submerged inflows and local runoff from the surrounding exposed lake bed area) and outflows (withdrawals, overflow and seepage). The dynamics of inflows and outflows modify the overall lake water balance on a daily time-step, and may impact upon the layer structure by adding, merging or removing layers (described in Sect. 2.6). In addition, the mass balance the surface layer is computed at each model time step (usually hourly), by modifying the surface layer height according to:

$$\frac{dh_S}{dt} = E + S + f_R R + Q_R / A_S \quad (4)$$

where h_S is the top height of the surface layer (m), t is the time (days), E is the evaporation mass flux computed from the heat flux ϕ_E (W m^{-2}) described below, R is rainfall and S is snowfall (m day^{-1}), and f_R is a user-definable scaling factor that may be applied to increase or reduce the rainfall data (default = 1). Q_R is an optional term to account for runoff to the lake from the exposed banks, which may be important in reservoirs with a large drawdown range, or wetlands where periodic drying of the lake may occur. The runoff volume generated is averaged across the current lake area (A_S), and the amount is calculated using a simple model based on exceedance of a threshold rainfall intensity, R_L (m day^{-1}), and runoff coefficient:

$$Q_R = f_{ro}(f_R R - R_L)(A_{max} - A_s) \quad (5)$$

where f_{ro} is the runoff coefficient, defined as the fraction of rainfall that is converted to runoff at the lake's edge, and A_{max} is the maximum possible area of inundation of the lake (as defined by the area provided by the user at N_{BSN} area value).

Note mixing dynamics (i.e. the merging or splitting of layers to enforce the layer thickness limits), will impact the thickness of the surface mixed layer, z_{SML} , but not change the overall lake height. However, in addition to the terms in Eq. 4, h_s will also be modified as a result of ice formation/melt, and river inflows, withdrawals, seepage or overflows impacting upon the surface layer, which are described in subsequent sections; these are in addition to the above described terms.

2.3 Surface energy balance

A balance of shortwave and longwave radiation fluxes, and sensible and evaporative heat fluxes determine the net cooling and heating for GLM. The general heat budget equation is described as:

$$\left[\frac{c_p}{A_s z_{sml}} \right] \frac{dT_s}{dt} = \phi_{SW_s} - \phi_E + \phi_H + \phi_{LWin} - \phi_{LWout} \quad (6)$$

where c_p is the specific heat capacity of water ($4186 \text{ J kg}^{-1} \text{ }^\circ\text{C}^{-1}$), T_s is the surface temperature of the surface mixed layer and z_{sml} is the depth of the surface mixed layer. The RHS heat flux terms, including several options for customizing the individual surface heat flux components, are expanded upon individually below.

2.3.1 Solar heating and light penetration

Solar radiation is the key driver of the lake thermodynamics, however, data may not always be available from a nearby pyranometer. Users may choose to either have GLM compute surface irradiance from a theoretical approximation based on the Bird Clear Sky insolation model (BCSM) (Bird, 1984), modified for cloud cover and latitude, or alternatively, hourly or daily solar radiation intensity data may be specified directly. If the BCSM is used, then $\hat{\phi}_{SW}$ is calculated from (Bird, 1984; Luo et al., 2010):

$$\hat{\phi}_{SW} = \frac{\hat{\phi}_{DB} + \hat{\phi}_{AS}}{1 - (\alpha_{SW} \alpha_{SKY})} f(C) \quad (7)$$

where the model computes total irradiance, $\hat{\phi}_{SW}$ (W m^{-2}) from direct beam $\hat{\phi}_{DB}$, and atmospheric scattering $\hat{\phi}_{AS}$ components (refer to Appendix A for a detailed outline of the BCSM equations and parameters). In GLM, the clear sky value is reduced according to the cloud cover, C , according to:

$$f(C) = 0.66182 C^2 - 1.5236 C + 0.98475 \quad (8)$$

which is based on a polynomial regression of cloud data from Perth Airport, Australia, compared against nearby sensor data ($R^2 = 0.952$; see also Luo et al., 2010).

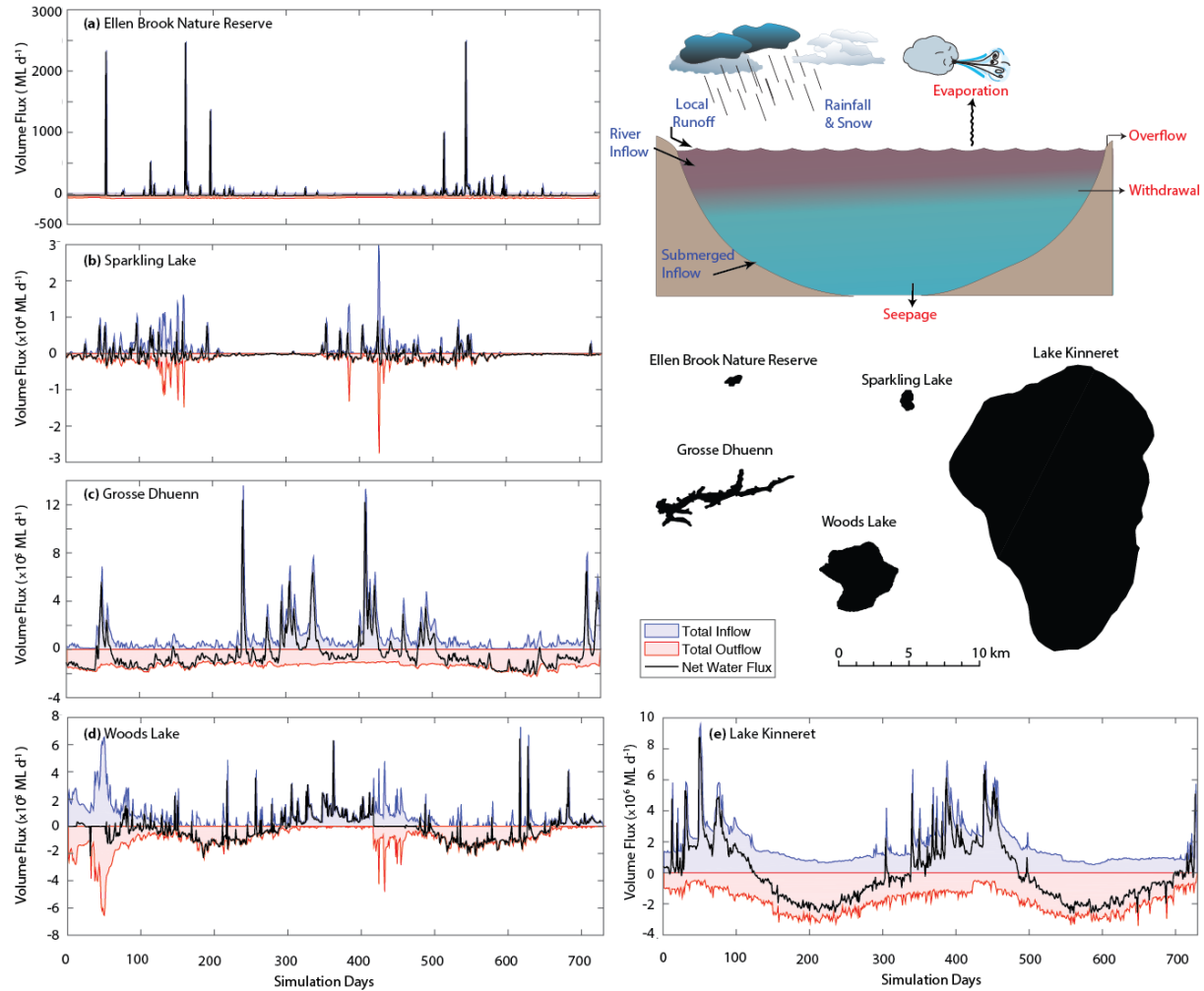


Figure 2: A two-year times-series of the simulated daily water balance for five example lakes, a-e, that range in size and hydrology. The water balance components summarised are depicted schematically in the inset. For more information about each lake and the simulation configuration refer to the Data availability section.

The albedo, α_{SW} , is the reflected fraction of $\hat{\phi}_{SW}$, with several computation options based on the angle of incident radiation, selected via the radmode option in the model configuration file:

Option 1 : Daily approximation, Hamilton & Schladow (1997)

$$\alpha_{SW} = \begin{cases} 0.08 + 0.02 \sin \left[\frac{2\pi}{365} d - \frac{\pi}{2} \right] & \text{:northern hemisphere} \\ 0.08 & \text{:equator} \\ 0.08 - 0.02 \sin \left[\frac{2\pi}{365} d - \frac{\pi}{2} \right] & \text{:southern hemisphere} \end{cases} \quad (9a)$$

Option 2 : Briegleb et al. (1986)

$$\alpha_{SW} = \frac{1}{100} \left(\frac{2.6}{1.1 \cos(\Phi_{zen})^{1.7} + 0.065} + 15 [\cos(\Phi_{zen}) - 0.1] [\cos(\Phi_{zen}) - 0.5] [\cos(\Phi_{zen}) - 1] \right) \quad (9b)$$

Option 3 : Yajima and Yamamoto (2014)

$$\alpha_{SW} = 0.001 RH [\cos(\Phi_{zen})]^{0.33} - 0.001 U_x [\cos(\Phi_{zen})]^{-0.57} - 0.001 \zeta [\cos(\Phi_{zen})]^{0.829}$$

where d is the day of the year, and Φ_{zen} is the solar zenith angle (radians) as outlined in Appendix A, RH is the relative humidity, ζ is the atmospheric diffuse radiation, d is the day of year, and U_x is wind speed. The second (oceanic) and third (lacustrine) options allow for diel and seasonal variation of albedo from approximately 0.01 to 0.4 depending on the sun-angle (Figure 3).

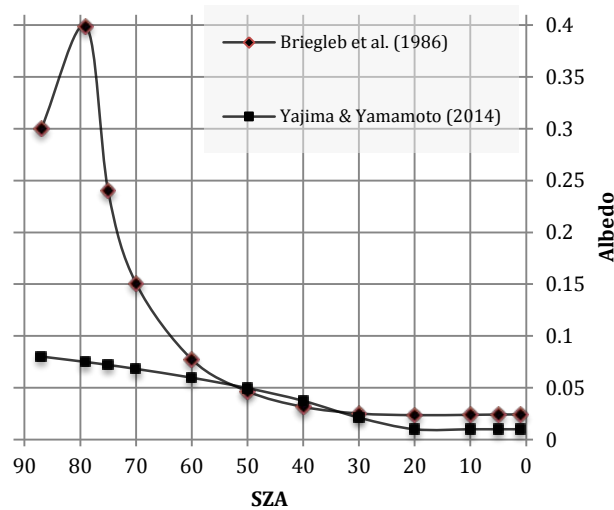


Figure 3: Variation of albedo (α_{SW}) with solar zenith angle ($SZA = 2\pi \Phi_{zen}/180$, degrees) for radmode 2 and 3.

Shortwave radiation penetration into the lake and through the layers is modelled according to the Beer-Lambert Law:

$$\phi_{SW}(z) = (1 - \alpha_{SW}) f_{SW} f_{PAR} \hat{\phi}_{SW} \exp[-K_w z] \quad (10)$$

where z is the depth of the layer from the surface, f_{SW} is a scaling factor that may be applied and adjusted as part of the calibration process, and K_w is the light extinction coefficient (m^{-1}). K_w may be set by the user as constant or linked to the water quality model (e.g. FABM or AED2, see Sect 4) in which case the extinction coefficient will change as a function of depth and time according to the concentration of dissolved and particulate constituents. Beer's Law is only applied for the photosynthetically active fraction (PAR) component, f_{PAR} , which is set as 45% of the incident light. The amount of light heating the surface layer, ϕ_{SW_S} , is therefore the above photosynthetically average fraction that is attenuated across z_{SML} , plus the remaining $(1 - f_{PAR})$ fraction which accounts for near infra-red and ultraviolet bandwidths of the incident shortwave radiation with significantly higher attenuation coefficients (Kirk, 1994).

In some applications, the extent to which the benthos has a suitable light climate is a good indicator of benthic productivity, and a proxy for the type of benthic habitat that might emerge. In addition to the light profiles, GLM predicts the benthic area of the lake where light intensity exceeds a user defined value (Figure 4), $\phi_{BEN_{crit}}$.

$$A_{BEN} = A_s - A(h_{BEN}) \quad (11)$$

where $h_{BEN} = h_{SURF} - z_{BEN}$, and z_{BEN} is calculated from Beer's law:

$$z_{BEN} = \ln \left[\frac{\phi_{BEN_{crit}}}{\phi_{SW_S}} \right] \frac{-1}{K_w} \quad (12)$$

The daily average benthic area above the threshold is reported in the lake.csv summary file as a percentage (A_{BEN}/A_s).

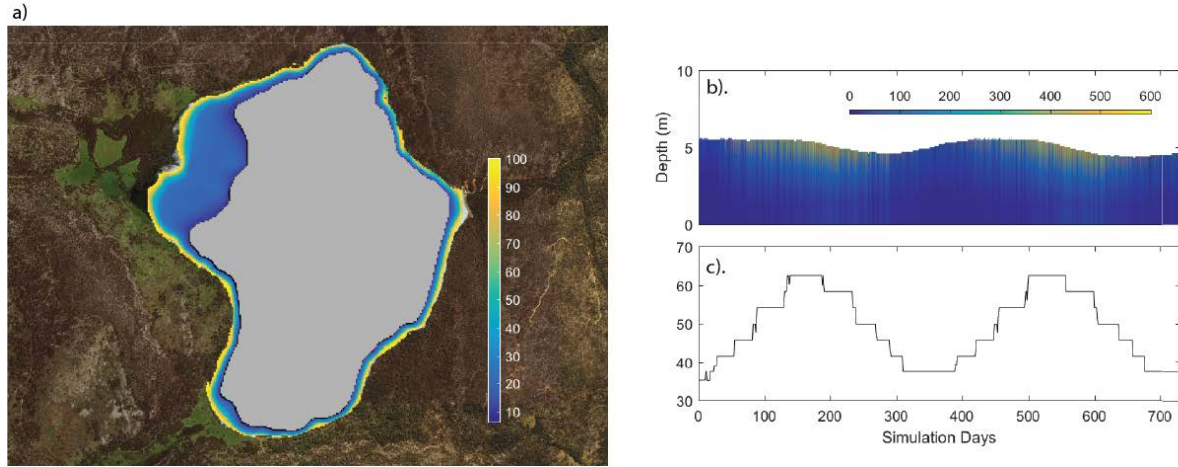


Figure 4: Example light data outputs from a GLM application to Woods Lake, Australia, showing a) the ratio of benthic to surface light, $\phi_{SW_{BEN}}/\phi_{SW_S}$ (%), overlain on the lake map based on the bathymetry, b) a time-series of the depth variation in light ($W\ m^{-2}$), and c) a time-series of A_{BEN}/A_S (%).

2.3.2 Longwave radiation

Longwave radiation can either be specified as net flux, incoming flux or, if there is no radiation data from which longwave radiation can be computed, then it may be calculated by the model internally based on the cloud cover fraction and air temperature. Net longwave radiation is described as:

$$\phi_{LW_{net}} = \phi_{LW_{in}} - \phi_{LW_{out}} \quad (13)$$

where

$$\phi_{LW_{out}} = \varepsilon_w \sigma [T_s + 273.15]^4 \quad (14)$$

and σ is the Stefan-Boltzman constant and ε_w the emissivity of the water surface, assumed to be 0.985. If the net or incoming longwave flux is not provided, the model will compute the incoming flux from:

$$\phi_{LW_{in}} = (1 - \alpha_{LW}) \varepsilon_a^* \sigma [T_a + 273.15]^4 \quad (15)$$

where α_{LW} is the longwave albedo (0.03), and the emissivity of the atmosphere is computed considering emissivity of cloud-free conditions (ε_a), based on air temperature (T_a) and vapour pressure, extended to account for reflection from clouds, such that $\varepsilon_a^* = f(T_a, C)$ calculated from (Henderson-Sellers, 1986):

$$\varepsilon_a^* = \begin{cases} (1 + 0.275C)(1 - 0.261 \exp[-0.000777 T_a^2]) & \text{Option 1: Idso and Jackson (1969)} \\ (1 + 0.17 C^2) (9.365 \times 10^{-6} [T_a + 273.15]^2) & \text{Option 2: Swinbank (1963)} \\ (1 + 0.275 C) 0.642 \left(\frac{e_a}{T_a}\right)^{\frac{1}{7}} & \text{Option 3: Brutseart (1975)} \\ \left[(1 - C^{2.796}) 1.24 \left(\frac{e_a}{T_a}\right)^{\frac{1}{7}} + 0.955 C^{2.796} \right] & \text{Option 4: Yajima and Yamamoto (2014)} \end{cases} \quad (16a-d)$$

where, C is the cloud cover fraction (0-1), e_a the air vapour pressure calculated from relative humidity, and options 1-4 are chosen via the cloudmode variable. Note that cloud cover is typically reported in octals (1-8) with each value depicting a fraction of 8. So a value of 1 would correspond to a fraction of 0.125. Some data may also include cloud type and their respective heights. If this is the case, good results have been reported by averaging the octal values for all cloud types to get an average value of cloud cover

If longwave radiation data does not exist and cloud data is also not available, but solar irradiance is measured, then it is possible to get GLM to compare the measured and theoretical (BCSM) solar irradiance to approximate the cloud cover fraction. This option utilises the above relation in Eq. 7 to compute $\hat{\phi}_{SW}$, and clouds are approximated by assuming that $\hat{\phi}_{SW_{OBS}}/\hat{\phi}_{SW_{BCSM}} = f(C)$. Note that if neither shortwave or longwave radiation are provided, then the model will use the BCSM to compute incoming solar irradiance and cloud cover will be assumed to be 0.

2.3.3 Sensible and latent heat transfer

The model accounts for the surface fluxes of sensible heat and latent heat using commonly adopted bulk aerodynamic formulae. For sensible heat:

$$\phi_H = -\rho_a c_p C_H U_x (T_s - T_a) \quad (17)$$

where c_p is the specific heat capacity of air ($1005 \text{ J kg}^{-1} \text{ }^\circ\text{C}^{-1}$), C_H is the bulk aerodynamic coefficient for sensible heat transfer ($\sim 1.3 \times 10^{-3}$), T_a the air temperature ($^\circ\text{C}$) and T_s the temperature of the surface layer ($^\circ\text{C}$). The air density is in kg m^{-3} and computed from $\rho_a = 0.348 (1 + r)/(1 + 1.61r) p/T_a$, where p is air pressure (hPa) and r is the mixing ratio, which is used to compute the gas constant.

For latent heat:

$$\phi_E = -\rho_a C_E \lambda U_x \frac{\kappa}{p} (e_s[T_s] - e_a[T_a]) \quad (18)$$

where C_E is the bulk aerodynamic coefficient for latent heat transfer, e_a the air vapour pressure, e_s the saturation vapour pressure (hPa) at the surface layer temperature ($^\circ\text{C}$), κ is the

ratio of molecular weight of water to molecular weight of air ($= 0.622$) and λ is the latent heat of vaporisation. The vapour pressure can be calculated by the following formulae:

$$e_s[T_s] = \exp \left[2.3026 \left(7.5 \frac{T_s}{T_s + 237.3} \right) + 0.7858 \right] \quad \text{Option 1 : TVA (1972) - (19a)}$$

$$\text{Magnus-Tetens} \quad (19b)$$

$$e_s[T_s] = \exp \left[6.1094 \left(\frac{17.625 T_s}{T_s + 243.04} \right) \right] \quad \text{Option 2 : August-Roche-Magnus} \quad (19c)$$

$$e_s[T_s] = 10^{\left(9.28603523 \frac{2322.37885 T_s}{T_s + 273.15} \right)} \quad \text{Option 3 : Tabata (1973) - Linear}$$

$$e_a[T_a] = \frac{RH}{100} e_s[T_a] \quad (20)$$

Correction for non-neutral atmospheric stability : For long-time integrations (i.e., seasonal), the bulk-transfer coefficients for momentum, C_D , sensible heat, C_H , and latent heat, C_E , can be assumed approximately constant because of the negative feedback between surface forcing and the temperature response of the water body (e.g. Strub and Powell, 1987). At finer timescales (hours to weeks), the thermal inertia of the water body is too great and so the transfer coefficients must be specified as a function of the degree of atmospheric stratification experienced in the internal boundary layer that develops over the water (Woolway et al. 2017). Monin and Obukhov (1954) parameterised the stratification in the air column using the now well-known stability parameter, z/L , which is used to define corrections to the bulk aerodynamic coefficients C_H and C_E , using the numerical scheme presented in Appendix B. The corrections may be applied as options in the model, and requires that the measurement of wind speed, air temperature and relative humidity within the internal boundary layer over the lake surface are supplied at an hourly resolution.

Still-air limit : The above formulations only apply when sufficient wind exists to create a defined boundary layer over the surface of the water. As the wind tends to zero (the ‘still-air limit’), Eqs. 16-17 are no longer appropriate as they do not account for free convection directly from the water surface. This is a relatively important phenomenon for small lakes, cooling ponds and wetlands since they tend to have small fetches that limit the build-up of wind speed. These water bodies are often sheltered from the wind and will develop surface temperatures warmer than the atmosphere for considerable periods. Therefore, we optionally augment Eqs. 16-17 with calculations under low wind-speed conditions by calculating the evaporative and sensible heat flux values for both the given U_x and for an assumed $U_x = 0$. The chosen value is found by taking the maximum value of the two calculations:

$$\phi_{H,E}^* = \max(\phi_{E,H}, \phi_{E,H_0}) \quad (21)$$

where ϕ_0 is the zero-wind flux, given below, and applies for both evaporative and sensible heat fluxes, and $\phi_{E,H}$ is calculated from Eqs. 16-17. The two zero-wind speed heat flux equations are taken from TVA (1972), but modified slightly to return energy flux in SI units (W m^{-2}):

$$\phi_{E_0} = \rho_s \lambda \alpha_e (C_0 - C_a) \quad (22)$$

$$\phi_{H_0} = \alpha_h (T_s - T_a)$$

$$\alpha_e = 2.283 \times 10^{-3} \xi \frac{\nu}{c_p \rho_s} \left[g \frac{|\rho_a - \rho_o|}{\rho_a \nu a} \right]^{1/3} \quad (23)$$

$$\alpha_h = 2.283 \times 10^{-3} \xi \nu \left[g \frac{|\rho_a - \rho_o|}{\rho_a \nu a} \right]^{1/3}$$

where $C = \kappa e/p$, with the appropriate vapour pressure values, e , for both surface and ambient atmospheric values. Here, ν is the molecular heat conductivity of air ($0.1 \text{ kJ m}^{-1} \text{ h}^{-1} \text{ K}^{-1}$), ν is the kinematic viscosity of the air ($0.0548 \text{ m}^2 \text{ h}^{-1}$), ρ_o is the density of the saturated air at the water surface temperature, ρ_s is the density of the surface water, ξ is a roughness correction coefficient for the lake surface (0.5) and a is the molecular heat diffusivity of air ($0.077 \text{ m}^2 \text{ h}^{-1}$). Note that the impact of low wind speeds on the drag coefficient is captured by the modified Charnock relation (Eq. A24), which includes an additional term for the smooth flow transition (see also Figure A1).

Wind sheltering: Wind-sheltering maybe parameterised according to several methods based on the context of the simulation and data available. Hipsey et al. (2003) presented a simple adjustment to the bulk transfer equation to account for the effect of wind-sheltering in small reservoirs. The method employs the use of a shelter index by accounting for the length scale associated with the vertical obstacle relative to the horizontal length scale associated with the water body itself. Within

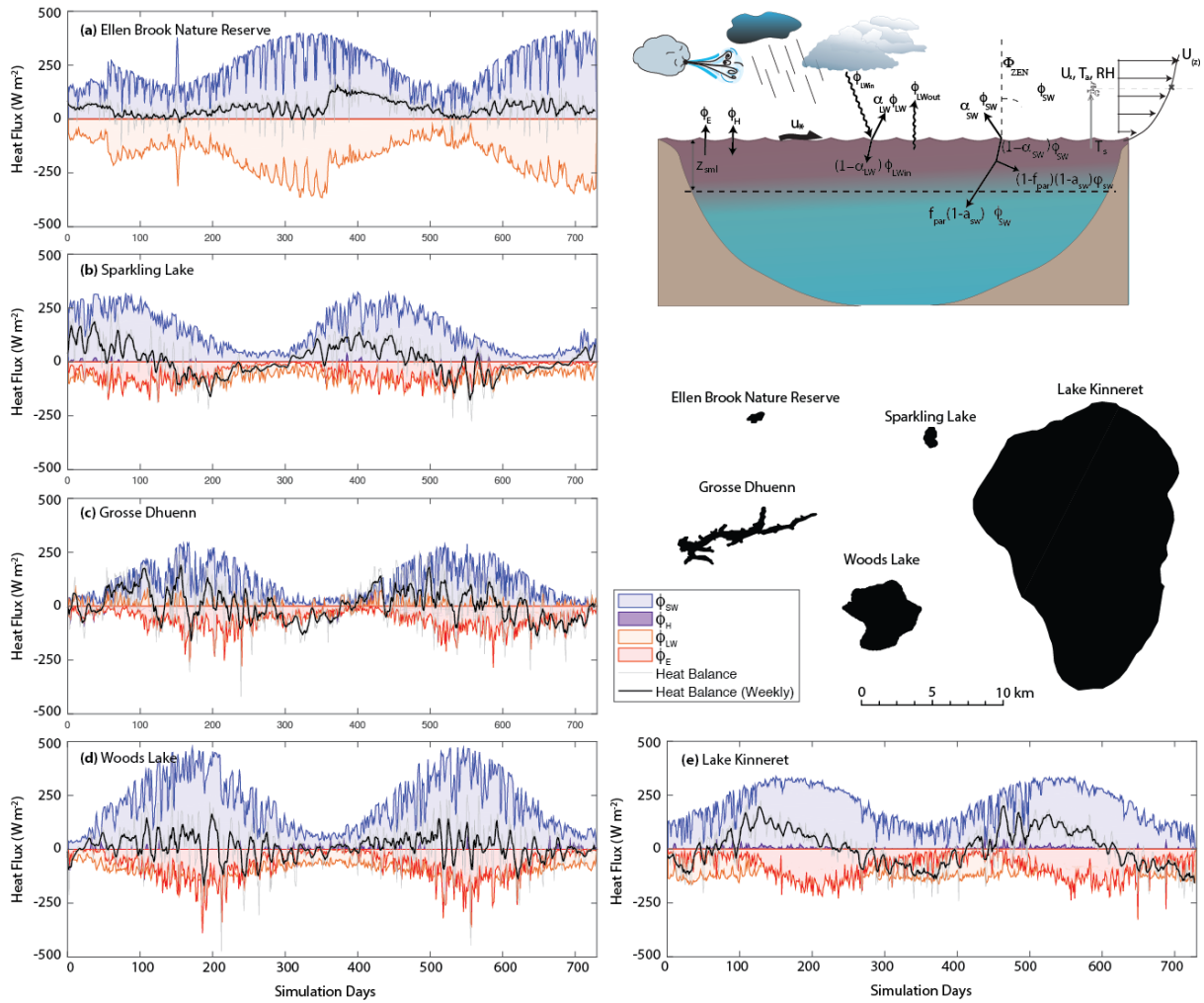


Figure 5: A two-year times-series of the simulated daily heat fluxes for five example lakes, a-e, that were depicted in Figure 2. The heat balance components summarised are depicted schematically in the inset, as described in Sect. 2.3.

GLM, users may specify the degree of sheltering or fetch limitation by optionally supplying the model with the wind direction, and a table linking direction and a wind scaling factor. Alternatively, if the direction-specific data is not available, an effective wind-sheltering coefficient has been implemented that reduces the effective surface area for heat and momentum fluxes:

$$A_E = \begin{cases} A_S \tanh\left(\frac{A_S}{A_C}\right) & \text{Yeates \& Imberger (2003)} & (24a) \\ \frac{D^2}{2} \cos^{-1}\left(\frac{x_\tau}{D}\right) - \frac{x_\tau}{D} \sqrt{D^2 - x_\tau^2} & \text{Markfort et al. (2009)} & (24b) \end{cases}$$

where A_C is the critical area. In GLM, the ratio of the effective area to the total area of the lake A_E/A_S is then used to scale U_x as a means of capturing the average wind speed over the entire lake surface.

2.4 Snow and ice dynamics

The algorithms for GLM ice and snow dynamics are based on previous ice modelling studies (Patterson and Hamblin, 1988; Gu and Stefan, 1993; Rogers et al., 1995; Vavrus et al., 1996; Launiainen and Cheng, 1998; Magee et al., 2016). To solve the heat transfer equation, the ice model uses a quasi-steady assumption that the time scale for heat conduction through the ice is short relative to the time scale of meteorological forcing (Patterson and Hamblin, 1988; Rogers et al., 1995). The steady-state conduction equations, which allocate shortwave radiation into two components, a visible ($A_1=70\%$) and an infra-red ($A_2=30\%$) spectral band, are used with a three-component ice model that includes blue ice (or black ice), white ice (or snow ice) and snow (see Eq. 1 and Fig. 5 of Rogers et al., 1995). White ice is generated in response to flooding, when the mass of snow that can be supported by the buoyancy of the ice cover is exceeded (see Eq. 13 of Rogers et al., 1995). By assigning appropriate boundary conditions to the interfaces and solving the quasi-steady state of heat transfer numerically, the model computes the upward conductive heat flux from the ice or snow cover to the atmosphere, ϕ_0 . The estimation of ϕ_0 involves the application of an empirical equation (Ashton, 1986) to estimate snow conductivity (K_s) from its density (Figure 6).

At the ice (or snow) surface, a heat flux balance is employed to provide the condition for surface melting:

$$\begin{aligned} \phi_0(T_0) + \phi_{net}(T_0) &= 0 & T_0 < T_m \\ \phi_{net}(T_0) &= -\rho L \frac{dh_i}{dt} & T_0 = T_m \end{aligned} \quad (25)$$

where L is the latent heat of fusion (see physical constants, Table 1), h_i is the height of the upper snow or ice layer, t is time, ρ is the density of the snow or ice, determined from the surface medium properties, T_0 is the temperature at the solid surface, T_m is the melt-water temperature (0°C) and $\phi_{net}(T_0)$ is the net incoming heat flux, at the solid surface:

$$\phi_{net}(T_0) = \phi_{LWin} - \phi_{LWout}(T_0) + \phi_H(T_0) + \phi_E(T_0) + \phi_R(T_0) \quad (26)$$

where ϕ_{LWin} and ϕ_{LWout} are incoming and outgoing longwave radiation, ϕ_H and ϕ_E are sensible and evaporative heat fluxes between the solid boundary and the atmosphere, and ϕ_R is the heat flux due to rainfall. These heat fluxes are calculated as above with modification for determination of vapor pressure over ice or snow (Gill, 1982) and the addition of the rainfall heat flux (Rogers et al., 1995). T_0 is determined using a bilinear iteration until surface heat

fluxes are balanced (i.e. $\phi_0(T_0) = -\phi_{net}(T_0)$) and T_0 is stable ($\pm 0.001^\circ\text{C}$). In the presence of ice (or snow) cover, surface temperature $T_0 > T_m$ indicates that energy is available for melting. The amount of energy for melting is calculated by setting $T_0 = T_m$ to determine the reduced thickness of snow or ice (as shown in Eq. 25).

Accretion or ablation of ice is determined through the heat flux at the ice-water interface, q_f . Solving for heat conduction through ice yields:

$$q_f = q_0 - A_1 \hat{\phi}_{SW} (1 - \exp[-K_{s1} h_{snow} - K_{w1} h_{white} - K_{b1} h_{blue}]) - A_2 \hat{\phi}_{SW} (1 - \exp[-K_{s2} h_{snow} - K h_{white} - K_{b2} h_{blue}]) - Q_{white} h_{snow} \quad (27)$$

where $\hat{\phi}_{SW}$ is the shortwave radiation penetrating the surface, K refers to the light attenuation coefficient of the ice and snow components designated with subscripts s , w and e for snow, blue ice and snow ice respectively, and h refers to the thickness of snow, white ice (snow ice) and blue ice. Q_{white} is a volumetric heat flux for formation of snow ice, which is given in Eq. 14 of Rogers et al. (1995). Ice and snow light attenuation coefficients in GLM are fixed to the same values as those given by Rogers et al. (1995). Shortwave albedo for the ice or snow surface is a function of surface medium (snow or ice), surface temperature and ice or snow thickness (see Table 2, Vavrus et al., 1996). Values of albedo derived from these functions vary from 0.08 to 0.6 for ice and from 0.08 to 0.7 for snow.

The imbalance between q_f and the heat flux from the water to the ice, q_w , gives the rate of change of ice thickness at the interface with water:

$$\frac{dh_{blue}}{dt} = \frac{q_f - q_w}{\rho_{blue} L} \quad (28)$$

where ρ_{blue} is the density of blue ice and q_w is given by a finite difference approximation of the conductive heat flux from water to ice:

$$q_w = -K_m \frac{\Delta T}{\Delta z}, \quad (29)$$

where K_m is molecular conductivity and ΔT is the temperature difference between the surface water and the bottom of the ice, which occurs across an assigned depth Δz . A value for Δz of 0.5 m is usual, based on the reasoning given in Rogers *et al.* (1995) and the typical vertical water layer resolution of a model simulation (0.125 – 1.5 m). Note that a wide variation in techniques and values is used to determine the basal heat flux immediately beneath the ice pack (*e.g.*, Harvey, 1990).

Figure 6 summarizes the algorithm to update ice cover, snow cover and water depth. The ice cover equations are applied when water temperature first drops below 0 °C. The ice thickness is set to its minimum value of 0.05 m, which is suggested by Patterson and Hamblin (1988) and Vavrus et al. (1996). The need for a minimum ice thickness relates primarily to horizontal variability of ice cover during the formation and closure periods. The ice cover equations are discontinued and open water conditions are restored in the model when the thermodynamic balance first produces ice thickness < 0.05 m.

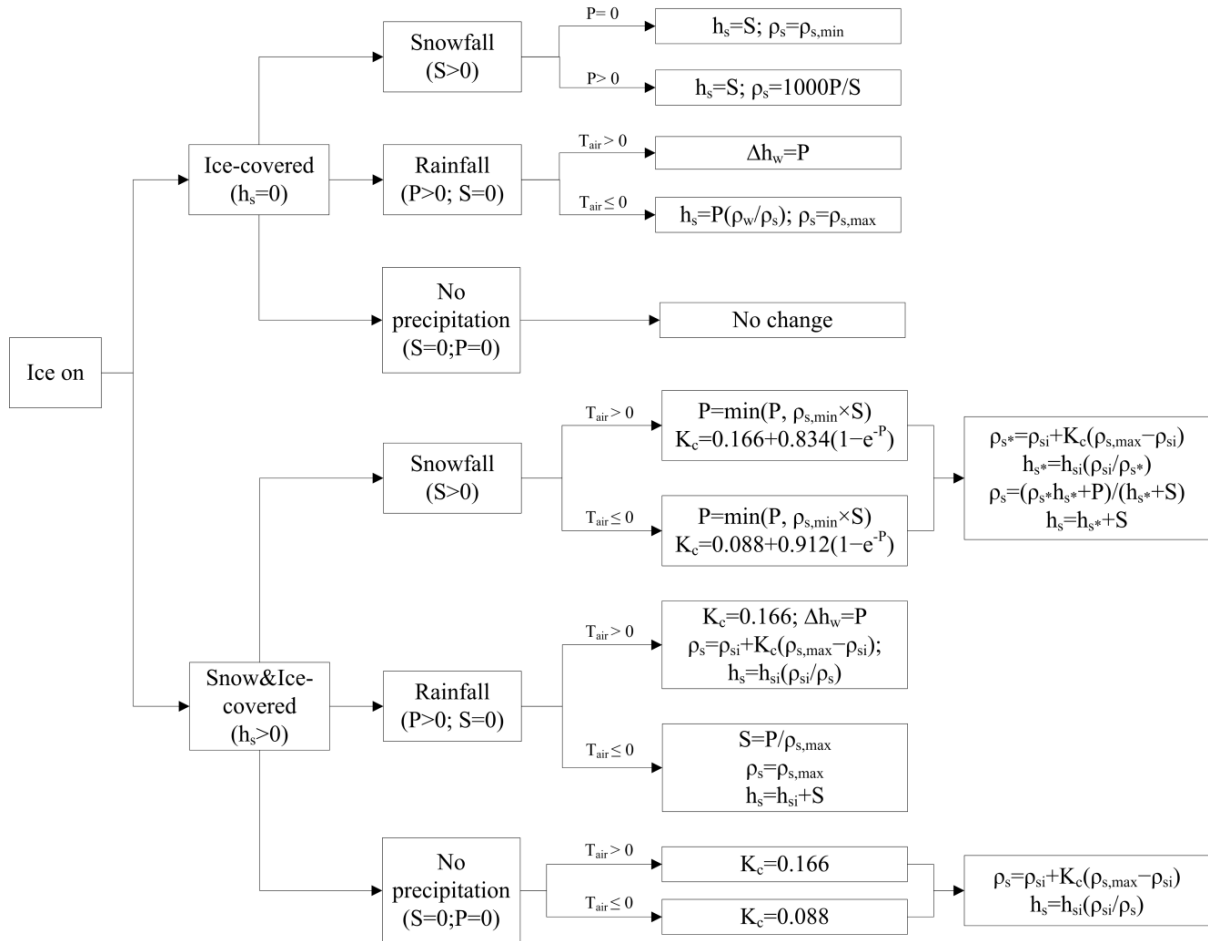


Figure 6: Decision tree to update ice cover, snow cover and water depth according to snow compaction, rainfall (P) and snowfall (S) on each day, and depth of snow cover (h_{si}) and snow density (ρ_{si}) for the previous day. Refer to Table 1 for definitions of other variables.

After the change in ice thickness due to heat exchange is calculated, the effects of snowfall, rainfall, and compaction of snow are calculated through appropriate choice of one of several options, depending on the air temperature and whether ice or snow is the upper solid boundary (Figure 6). Density of fresh snowfall is determined as the ratio of measured snowfall height to water-equivalent height, with any values exceeding the assigned maximum or minimum snow density (defaults: $\rho_{s,max} = 300 \text{ kg m}^{-3}$, $\rho_{s,min} = 50 \text{ kg m}^{-3}$) truncated to the appropriate limit. The snow compaction model is based on the exponential decay formula of

McKay (1968), with selection of snow compaction parameters based on air temperature (Rogers et al., 1995) as well as on rainfall or snowfall. The approach of snow compaction used by Rogers et al. (1995) is to set the residual snow density to its maximum value when there is fresh snowfall. This method is found to produce increases in snow density that are too rapid when there is only light snowfall. As a result, GLM uses a gradual approach where the new snowfall and the existing snow is used to form a layer with a combined mass and average density. Example outputs are shown in Figure 7, and see also Yao et al. (2014).

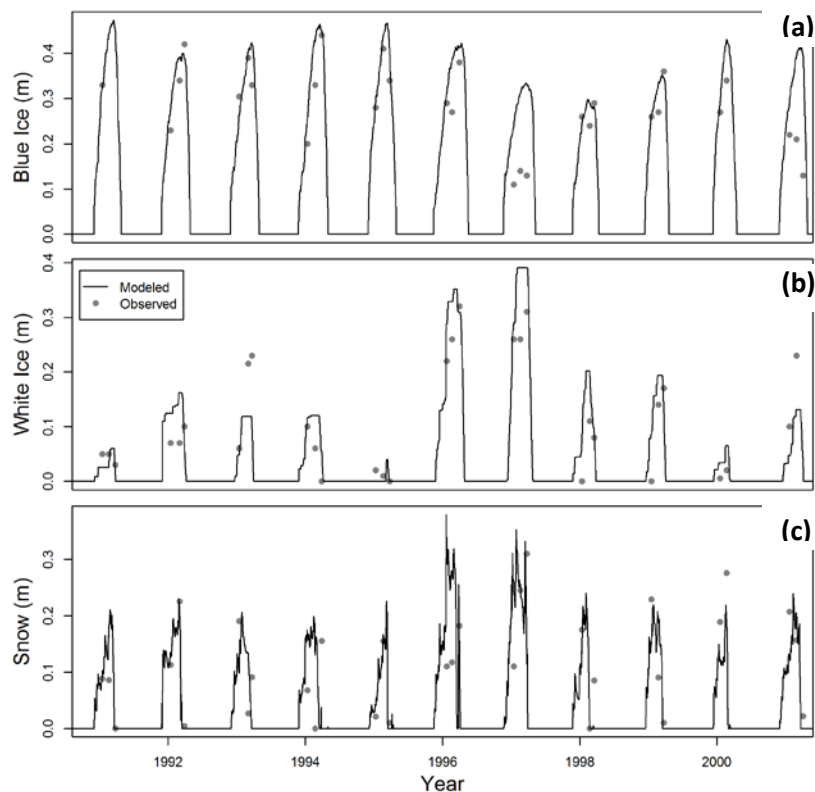


Figure 7: Example of modelled and observed blue ice (a), white ice (b) and snow (c) thickness for Sparkling Lake, Wisconsin. Lines are modelled thickness and points are average observed thicknesses.

2.5 Stratification and vertical mixing

2.5.1 Surface mixed layer

GLM works on the premise that the balance between the available energy, E_{TKE} , and the energy required for mixing to occur, E_{PE} , provides for the surface mixed layer (SML) deepening rate dz_{SML}/dt . For an overview of the dynamics readers are referred to early works on bulk mixed layer depth models by Kraus and Turner (1967) and Kim (1976), which were subsequently extended by Imberger and Patterson (1981) as a basis for hydrodynamic model design. In this model, the available kinetic energy is calculated due to contributions from

wind stirring, shear production between layers, convective overturn, and Kelvin-Helmholtz (K-H) billowing. They may be combined and summarised for E_{TKE} as (Hamilton and Schladow, 1997):

$$E_{TKE} = \underbrace{0.5C_K(w_*^3) \Delta t}_{\text{convective overturn}} + \underbrace{0.5C_K(C_W u_*^3) \Delta t}_{\text{wind stirring}} + \underbrace{0.5 C_S \left[u_b^2 + \frac{u_b^2}{6} \frac{d\xi}{dz_{sml}} + \frac{u_b \xi}{3} \frac{du_b}{dz_{sml}} \right]}_{\substack{\text{shear production} \\ \text{K-H production}}} \Delta z_{k-1} \quad (30)$$

where ξ is the K-H billow length scale (described below), u_b is the shear velocity at the interface of the mixed layer, and C_K , C_W , and C_S are mixing efficiency constants. For mixing to occur, the energy must be sufficient to lift up water at the bottom of the mixed layer, denoted here as the layer $k - 1$, with thickness Δh_{k-1} , and accelerate it to the mixed layer velocity. This also accounts for energy consumption associated with K-H production and expressed as, E_{PE} :

$$E_{PE} = \left[\underbrace{0.5C_T(w_*^3 + C_W u_*^3)^{2/3}}_{\text{acceleration}} + \underbrace{\frac{\Delta \rho}{\rho_o} g z_{SML}}_{\text{lifting}} + \underbrace{\frac{g\xi^2}{24\rho_o} \frac{d(\Delta\rho)}{dz_{sml}} + \frac{g\xi\Delta\rho}{12\rho_o} \frac{d\xi}{dz_{sml}}}_{\text{K-H consumption}} \right] \Delta z_{k-1} \quad (31)$$

where z_{SML} is the thickness of the surface mixed layer. To numerically resolve the above equations we sequentially compute the different components of the above expressions in light of the layer structure. Here GLM follows the algorithm outlined in Imberger and Patterson (1981) whereby cooling is computed so that layers are combined due to convection, then stirring, and then shear and K-H mixing are computed.

To compute mixing due to convective cooling, the value for w_* is calculated, which is the turbulent velocity scale associated with convection. The model adopts the algorithm used in Imberger and Patterson (1981), whereby the potential energy that is released by mixed layer deepening is computed by looking at the moments of the different layers in the surface mixed layer (from layers K to N_{LEV}):

$$w_*^3 = \frac{g}{\rho_{SML} \Delta t} \left(\sum_{k=K}^{N_{LEV}} [\rho_k \Delta z_k \widetilde{h}_k] - \widetilde{h}_{SML} \sum_{k=K}^{N_{LEV}} [\rho_k \Delta z_k] \right) \quad (32)$$

where ρ_{SML} is the mean density of the mixed layer including the combined layer, ρ_k is the density of the k^{th} layer, Δz_k is the height difference between two consecutive layers within the loop ($\Delta z_k = h_k - h_{k-1}$), \widetilde{h}_k is the mean height of layers to be mixed ($\widetilde{h}_k = 0.5[h_k + h_{k-1}]$), and \widetilde{h}_{SML} is the epilimnion (surface mixed layer) mid height, calculated from: $\widetilde{h}_{SML} = 0.5[h_{SURF} + h_{K-1}]$.

The velocity scale u_* is associated with wind stress and calculated according to the wind strength:

$$u_*^2 = C_D U_x^2 \quad (33)$$

where C_D is the drag coefficient for momentum. The model first has a check to see if the stirring energy can overcome the energy required to mix the k-1 layer, *i.e.*, mixing occurs if:

$$C_K(w_*^3 + C_W u_*^3) \Delta t \geq (g'_k z_{SML} + C_T(w_*^3 + C_W u_*^3)^{2/3}) \Delta z_{k-1} \quad (34)$$

and $g'_k = \frac{\Delta \rho}{\rho_o}$ is the reduced gravity between the mixed layer and k-1 layer. If the condition is not met the energy is stored for the next time-step.

Once stirring is completed, mixing due to velocity shear is applied. Velocity shear at the interface is approximated from:

$$u_b = \frac{u_*^2 t}{z_{sml}} + u_o \quad (35)$$

where t is characteristic time scale over which the shear has been operating, considered relative to t_{shear} , which is the time beyond which there is no shear production (*i.e.*, $u_b = 0$ if the time exceeds t_{shear}). This cut-off time assumes use of only the energy produced by shear at the interface during a period equivalent to half the basin-scale seiche duration, T_i , and modified to account for damping:

$$t_{shear} = T_i \left(1 + 0.59 \left[1 - \cosh \left(\frac{T_d}{T_i} - 1 \right) \right]^{-1} \right) \quad (36)$$

where T_d is the time-scale of damping (see Spigel, 1978). The wave period is approximated based on the stratification as $T_i = L_{META}/2c$, where L_{META} is the length of the basin at the thermocline and c is the internal wave speed. Once the velocity is computed, the energy for mixing from velocity shear is compared to that required for lifting and accelerating the next layer down, and layers are combined if there is sufficient energy:

$$0.5 C_S \left[\frac{u_b^2 (\widetilde{z_{SML}} + \Delta \xi)}{6} + \frac{u_b \xi \Delta u_b}{3} \right] + \left[g'_k \xi \left(\frac{\xi \Delta z_{k-1}}{24 z_{SML}} - \frac{\Delta \xi}{12} \right) \right] \geq (g'_k z_{SML} + C_T(w_*^3 + C_W u_*^3)^{2/3}) \Delta z_{k-1} \quad (37)$$

where the K-H length scale is $\xi = C_{KH} u_b^2 / g'_{EH}$ and $\Delta \xi = 2 C_{KH} u_b \Delta u_b / g'_{EH}$; in this case the reduced gravity is computed from the difference between the epilimnion and hypolimnion, and C_{KH} is a measure of the billow mixing efficiency.

Once shear mixing is done, the model checks the resultant density interface to see if it is unstable to shear (*i.e.*, K-H billows would be expected to form). This occurs if the gradient is

less than the K-H length scale. If K-H mixing is required, layers are further split and subject to mixing using an algorithm similar to above.

2.5.2 Deep mixing

Mixing below the SML in lakes, in the deeper stratified regions of the water column, is modelled using a characteristic vertical diffusivity, $K_Z = K_\varepsilon + K_m$, where K_m is the fixed molecular diffusivity of scalars. Three hypolimnetic mixing options are possible in GLM including: (i) no diffusivity (ii) a constant vertical diffusivity K_Z over the water depth below the thermocline or (iii) a derivation by Weinstock (1981), which is described as being suitable for regions displaying weak or strong stratification, whereby diffusivity increases with dissipation and decreases with heightened stratification.

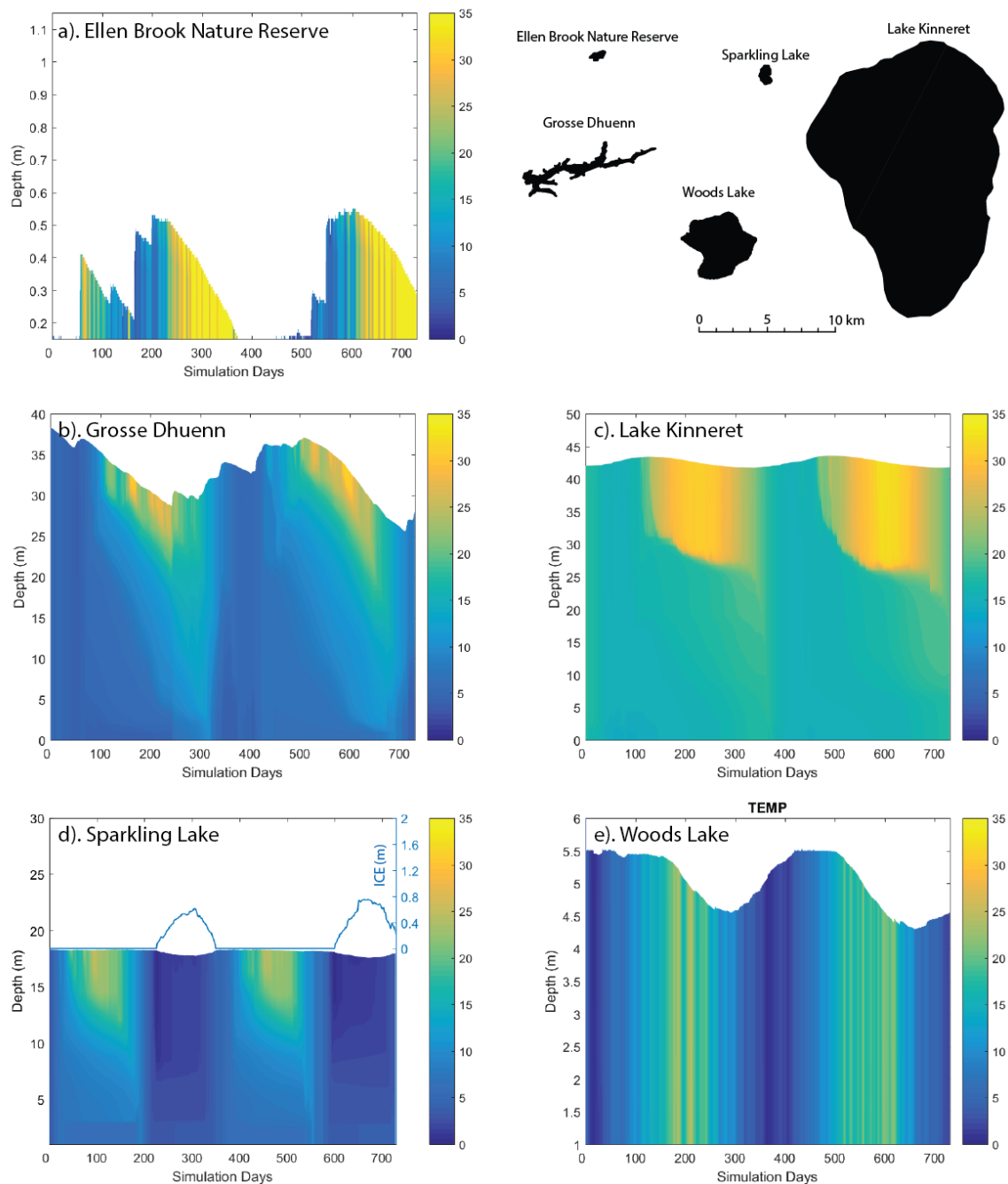


Figure 8: A two-year times-series of the simulated temperature profiles for five example lakes, a-e, that range in size and hydrology. For more information about each lake and the simulation configuration refer to the Data availability section (refer also to Fig. 2 and 5). Sparkling Lake (d) also indicates the simulated depth of ice.

For the constant vertical diffusivity option, the coefficient α_{TKE} is interpreted as a vertical diffusivity (m^2/s). For the Weinstock (1981) model, the diffusivity is computed according to:

$$K_z = \frac{\alpha_{TKE} \varepsilon_{TKE}}{N^2 + 0.6 k_{TKE}^2 u_*^2} \quad (38)$$

where α_{TKE} is the mixing efficiency of hypolimnetic TKE (~ 0.8 in Weinstock, 1981) and k_{TKE} is the turbulence wavenumber:

$$k_{TKE} = \frac{12.4 A_{top}}{\tilde{V} \Delta z_{top} 10^3} \quad (39)$$

and $u_* = \sqrt{1.612 \times 10^{-6} U_x^2}$. The term N^2 is the Brunt–Väisälä (buoyancy) frequency defined as:

$$N^2 = \frac{g \Delta \rho}{\rho \Delta z} \approx \left[\frac{g(\rho_{i+2} - \rho_{i-2})}{\rho_{ref}(h_{i+2} - h_{i-2})} \right] \quad (40)$$

Estimating the turbulent dissipation rate can be complex and GLM adopts a simple approach as described in Fischer et al. (1980) where a “net dissipation” is approximated by assuming dissipation is in equilibrium with energy inputs from external drivers:

$$\varepsilon_{TKE} \approx \overline{\varepsilon_{TKE}} = E_{WIND} + E_{INFLOW} \quad (41)$$

which is expanded and calculated per unit volume as:

$$\varepsilon_{TKE} = \underbrace{\frac{1}{(\tilde{V} \bar{\rho}) 10^3} \frac{m C_D \rho_a f_S U_x^3 A_l}{10^6}}_{\text{rate of working by wind}} + \underbrace{\frac{1}{(V_{mix} \bar{\rho}) 10^3} \sum_i^{N_{INF}} g \Delta \rho_i Q_i (h_{top} - h_i)}_{\text{rate of work done by inflows}} \quad (42)$$

The diffusivity is calculated according to Eq. 42, but since the dissipation is assumed to concentrate close to the level of strongest stratification, the “mean” diffusivity is modified to decay exponentially with distance from the thermocline:

$$K_{z_l} = \begin{cases} 0 & h_l \geq (h_{top} - z_{mix}) \\ K_z \exp\left[\frac{-(h_{top} - z_{mix} - h_l)^2}{\sigma}\right] & h_l < (h_{top} - z_{mix}) \end{cases} \quad (43)$$

where σ is the variance the N^2 distribution below h_{mix} and scales with the depth over which mixing decays.

Once the diffusivity is approximated (for either model 1 or 2 in Eq. 43), the diffusion of any scalar, C , between two layers is numerically accounted for by the following mass transfer expressions:

$$C_{i+1} = \bar{C} + \frac{\exp(-f) \Delta z_i \Delta C}{(\Delta z_{i+1} + \Delta z_i)} \quad (44)$$

$$C_i = \bar{C} - \frac{\exp(-f)\Delta z_{i+1}\Delta C}{(\Delta z_{i+1} + \Delta z_i)}$$

where \bar{C} is the weighted mean concentration of C for the two layers, and ΔC is the concentration difference between them. f is related to the diffusivity according to:

$$f = \frac{K_{z_{i+1}} + K_{z_i}}{(\Delta z_{i+1} + \Delta z_i)^2} \Delta t \quad (45)$$

The above diffusion algorithm is run once up the water column and once down the water column as a simple explicit method for capturing diffusion to both the upper and lower layers.

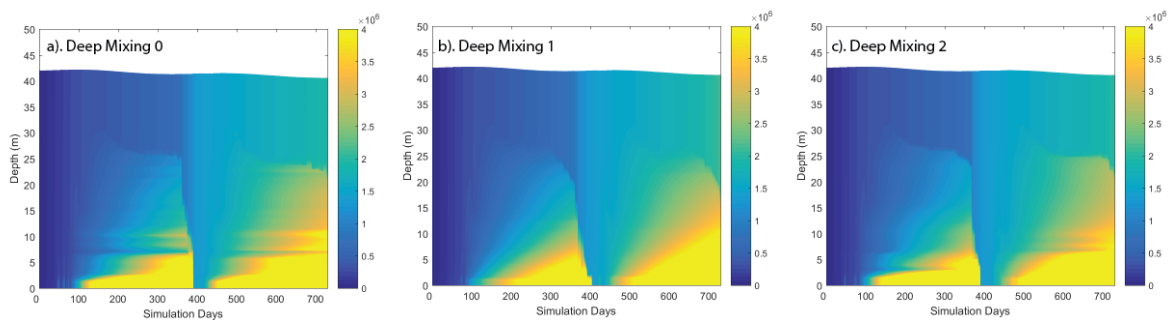


Figure 9: Simulations for Lake Kinneret showing hypolimnetic concentration of a passive tracer released from the bottom sediment at a constant rate for the case a) without deep mixing, b) constant vertical diffusivity, and c) calculated vertical diffusivity (Eq. 38). For thermal structure of this case refer to Figure 8c.

2.6 Inflows and outflows

Inflows can be specified as local runoff from the surrounding (dry) lake domain (Q_R described above, Eq. 5), rivers entering at the surface of the lake that will be buoyant or plunge depending on their momentum and density (Sect 2.6.1), or submerged inflows including groundwater (Sect 2.6.2). Any number of inflows to the lake body can be specified and these are applied daily. Four options for outflows are included in GLM, including withdrawals from a specified depth (Sect 2.6.3), adaptive offtake (Sect 2.6.4), vertical groundwater seepage (Sect 2.6.5).

2.6.1 River inflows

For river inflows, depending on the density of the river water, the inflow will form a positively or negatively buoyant intrusion that will enter the lake and insert at a depth of neutral buoyancy. As the inflow inserts it will entrains water depending on the rate of mixing created by the inflowing water. In GLM, as the inflow crosses layers it will entrain water from

each, until it reaches a level of neutral buoyancy and undergoes insertion. Therefore, when it reaches its point of neutral buoyancy a new layer of thickness dependent on the inflow volume at that time (including additions from entrainment) is created. Following insertion, the inflow layer may then amalgamate with adjacent layers depending on numerical criteria within the model for combining or splitting layers.

The rate of entrainment of the intrusion, E , can be calculated in a number of ways. For simplicity, in GLM the rate has been adapted from the first approximation given in Fischer et al. (1979):

$$E = 1.6 \frac{C_{D_i}^{3/2}}{Ri} \quad (46)$$

where C_{D_i} is the user specified drag coefficient for the inflow. The Richardson's number is adapted from Fischer et al. (1979) as:

$$Ri = \frac{C_{D_i} (1 + 0.21 \sqrt{C_{D_i}} \sin \alpha_{inf})}{\sin \alpha_{inf} \tan \phi_{inf}} \quad (47)$$

where α_{inf} is the stream half angle and ϕ_{inf} is the slope of the inflow at the point where it meets the water body (Figure 10).

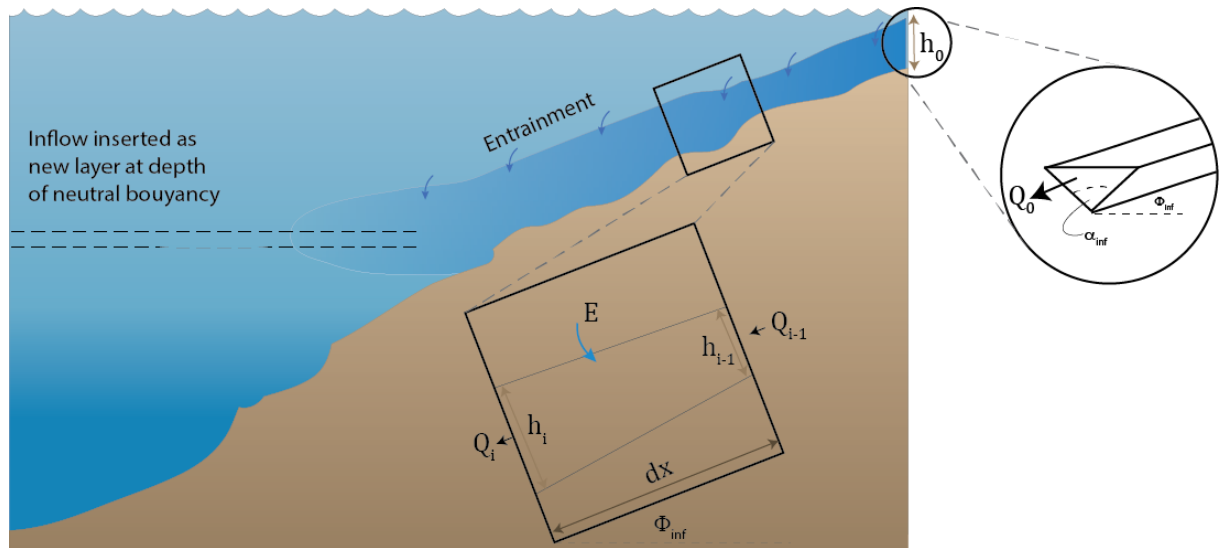


Figure 10: Schematic showing inflow insertion height, entrainment, E , slope, ϕ_{inf} and half angle, α_{inf} of an inflowing river entering with a user prescribed flow of Q_0 , and estimated starting height of h_0 .

As the inflow parcel travels through the layers, the increase in inflow thickness due to entrainment is estimated as:

$$h_i = 1.2Edx + h_{i-1} \quad (48)$$

where h_i is the inflow thickness, E is the entrainment rate and dx is the distance travelled by the inflowing water, calculated from the flow rate and inflow thickness. The initial estimate of the intrusion height is computed from Imberger and Patterson (1981) and Antenucci et al. (2005):

$$h_0 = \left(2Q_{inf}^2 \frac{Ri}{g'_{inf}} \tan^2 \phi_{inf} \right)^{1/5} \quad (49)$$

where Q_{inf} is the inflow discharge provided as a boundary condition and g' is the reduced gravity of the inflow given as:

$$g'_{inf} = g \frac{(\rho_{inf} - \rho_s)}{\rho_s} \quad (50)$$

where ρ_{inf} is the density of the inflow and ρ_s the density of the surface layer. The distance travelled by the inflow aliquot, dx , is estimated as the distance travelled in the vertical and the slope of the inflow river, ϕ_{inf} and given by:

$$dx = \frac{dz}{\sin \phi_{inf}} \quad (51)$$

where dz is the distance travelled in the vertical. The velocity of the inflow aliquot for that day is then calculated as:

$$u = h_i^2 \frac{Q_{inf}}{\tan \alpha} \quad (52)$$

Following conservation of mass, the flow is estimated to increase according to Imberger and Patterson (1981) and Antenucci et al. (2005):

$$Q_i = Q_{i-1} \left[\left(\frac{h_i}{h_{i-1}} \right)^{5/3} - 1 \right] \quad (53)$$

The above entrainment and insertion algorithm is repeated for each inflow. Aside from importing mass into the lake, river inflows also contribute turbulent kinetic energy to the hypolimnion, as discussed in the Sect 2.5.2 (e.g., see Eq. 42), and contribute to the scalar transport in the water column (Figure 11a).

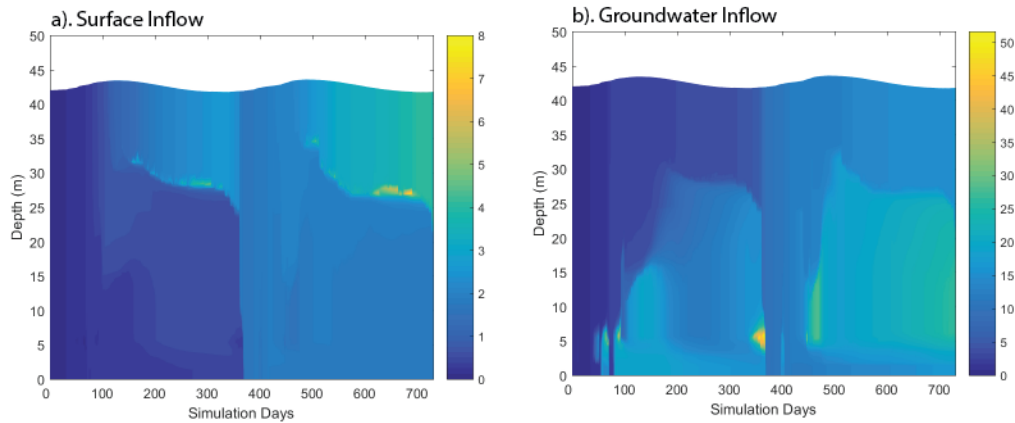


Figure 11: Simulation showing inflow tracer insertion example for the case where a) the inflow was set as a surface river inflow, and b) the inflow was set as a submerged inflow at a specified height ($h=5\text{m}$). After input the tracer is subject to mixing during inflow entrainment and by surface and deep mixing once inserted.

2.6.2 Submerged inflows

Submerged inflows are inserted at the user-specified depth with zero entrainment. The submerged inflow layer is created and then mixed with adjacent layers above or below depending on the density difference, until neutral buoyancy is attained (Figure 11b). This option can be used across one or more layers to account for groundwater inputs, or for capturing a piped inflow, for example.

2.6.3 Withdrawals

Outflows from a specific depth can be accommodated such as is required to simulate outlets from a dam wall offtake, or other piped withdrawal, or for removing water that may be lost during to groundwater discharge. The water will be removed from the layer corresponding to the specified depth, as well as layers above or below depending on the strength of discharge and stability of the water column. The thickness of the withdrawal layer is dependent on the internal Froude (Fr) and Grashof (Gr) numbers and the parameter, R (Fischer et al., 1979):

$$Fr = \frac{Q_{outf}}{N_{outf}^2 W_{outf} L_{outf}^2} \quad (54)$$

$$Gr = \frac{N_{outf}^2 A_{outf}^2}{v_{outf}^2} \quad (55)$$

$$R = Fr Gr^{1/3} \quad (56)$$

where W_{outf} , L_{outf} and A_{outf} are the width, length and area of the lake at the outlet elevation, and v_{outf}^2 is the vertical diffusivity of momentum averaged over the withdrawal layer. The Brunt- Väisälä frequency averaged over the thickness of the withdrawal layer, N_{outf}^2 , is calculated as:

$$N_{outf}^2 = \frac{g}{dz} \frac{\rho_{outf} - \rho_i}{\rho_{outf}} \quad (57)$$

where dz is the thickness of the withdrawal layer, ρ_{outf} is the density of the lake at the height of withdrawal and ρ_i is the density of the lake at the edge of the withdrawal layer. The thickness of the withdrawal layer is then calculated as follows (Fischer et al. 1978):

$$\delta_{outf} = 2L_{outf}Gr^{-1/6} \quad (58)$$

$$\delta_{outf} = 2L_{outf}Fr^{1/2}$$

The proportion of fluid withdrawn from each layer either above or below the layer of the outlet elevation is determined using a curve that fits the region of fluid drawn in a given time. To calculate the width and length of the lake at the height of outflow it is assumed, firstly, that the lake shape can be approximated as an ellipse, and secondly, that the ratio of length to width at the height of the outflow is the same as that at the lake crest. The length of the lake at the outflow height, L_{outf} and the lake width, W_{outf} are given by:

$$L_{outf} = \sqrt{A_{outf} \frac{4 L_{crest}}{\pi W_{crest}}} \quad (59a)$$

$$W_{outf} = L_{outf} \frac{W_{crest}}{L_{crest}} \quad (59b)$$

where A_{outf} is the area of the lake at the outflow height, L_{crest} is the length and W_{crest} the width of the lake at the crest height. Depending on the layer(s) the water is withdrawn from, the water taken will have the associated scalar concentrations.

2.6.4 Adaptive offtake dynamics

For reservoir applications, a special outflow option has been implemented that extends the dynamics in Sect. 2.6.3 to simulate an adaptive offtake or selective withdrawal. This approach is used for accommodating flexible reservoir withdrawal regimes and their effects on the thermal structure within a reservoir. For this option, a target temperature is specified by the user and GLM estimates the corresponding withdrawal height within a predefined (facility) range to meet this target temperature during the runtime of the simulation, i.e., the withdrawal

height adaptively follows the thermal stratification in the reservoir. The target temperature can be defined as a constant temperature (e.g., 14 °C) or a time-series such as a measured water temperature from an upstream river (via a *.csv file). The height of the adaptive offtake is printed out in a *.txt file and may be used for reservoir operation. In addition to the basic adaptive offtake function, GLM can also simulate withdrawal mixing, i.e., water from the adaptive offtake is mixed with water from another predefined height (e.g., the bottom outlet). For this option, the discharges at both locations need to be predefined by the user (via outflow *.csv file) and GLM chooses the adaptive withdrawal from a height, where the water temperature is such that the resulting mixing temperature meets the target temperature. This withdrawal mixing is a common strategy in reservoir operation where deep water withdrawal and temperature control are required simultaneously.

An example of the adaptive offtake function with and without withdrawal mixing, assuming a constant water temperature of 14 °C for the outflow water, shows that GLM is able to deliver a constant outflow temperature of 14 °C during the stratified period (Figure 12). In winter, when the water column is cooler than 14 °C, the model withdraws surface water. The adaptive offtake functionality can be used in a stand-alone mode or coupled to the dissolved oxygen concentration (via the water quality model AED2). In the latter case, the effect of the withdrawal regime on the oxygen dynamics in the hypolimnion can be simulated (see Weber et al., 2017). In this setting, the simulated hypolimnetic dissolved oxygen concentration at a specified height is checked against a critical threshold. If the hypolimnetic oxygen falls below the critical threshold, the height of the adaptive offtake will be automatically switched to a defined height (usually deep outlets in order to get rid of the oxygen-depleted water) to withdraw water from this layer, until the oxygen concentrations have recovered.

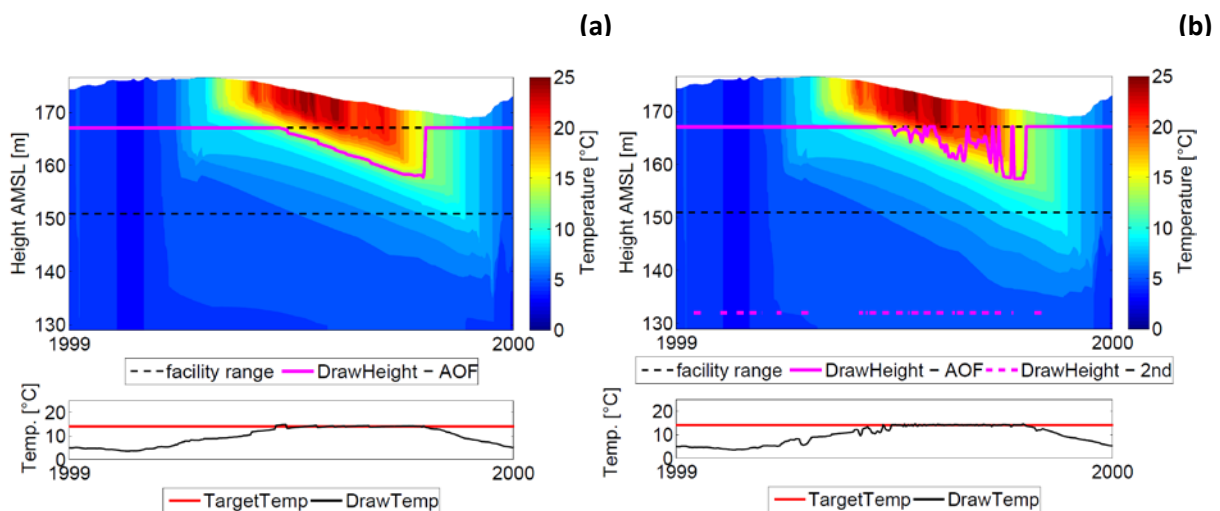


Figure 12: Adaptive offtake reservoir simulation; water temperatures of the adaptive offtake model assuming a constant temperature of 14 °C without (a) and with (b) mixing with bottom outlet withdrawal. The black dashed line represents the range of the variable withdrawal facility and the magenta lines the adaptive offtake and second withdrawal height.

2.6.5 Seepage

Seepage of water from the bottom layer is also configurable within the model, for example, as might be required in a wetland simulation or for small reservoirs perched above the water table that experience leakage to the soil below. Seepage is configured to leave the lake at a constant rate:

$$\frac{dh_B}{dt} = -G \quad (60)$$

where h_B is the depth of the bottom-most layer at any time, and G is the seepage rate (m day⁻¹). G is constrained within the model to ensure no more than 50% of the layer can be reduced in any one time-step. Note that in shallow-lake or wetland simulations, the layer structure may simplify to a single layer, in which case the surface and bottom layer are the same, and Eqs. 4 and 60 are effectively combined.

2.7 Wave height and bottom stress

Wind-induced resuspension of sediment from the bed of shallow lakes is sporadic and occurs as the waves created at the water surface create oscillatory currents that propagate down to the lake-bed. GLM does not predict resuspension and sediment concentration directly, but computes the bottom shear stress for later use by sediment and water quality modules. Nonetheless, even without this explicit formulation, the model can identify the areal extent and potential for bed-sediment resuspension by computing the area of the lake over which the bed shear stress exceeds some critical value required for resuspension to occur.

To compute the stress at the lake bottom we estimate the surface wave conditions using a simple, fetch-based, steady state wave model (Laenen and LeTourneau, 1996; Ji 2008). The wave geometry (wave period, significant wave height and wave length), is predicted based on the wind speed and fetch over which the waves develop (Figure 13), calculated as:

$$F = 2 \sqrt{A_s / \pi} \quad (61)$$

Using this model, the wave period, T , is calculated from fetch as:

$$T = 7.54 \left(\frac{U_x}{g} \right) \tanh(\xi) \tanh \left(\frac{0.0379 \left[\frac{gF}{U_x^2} \right]^{0.333}}{\tanh(\xi)} \right) \quad (62)$$

where:

$$\xi = 0.833 \left[\frac{g d_{avg}}{U_x^2} \right]^{0.375} \quad (63)$$

and h_{avg} is the average lake depth. Wave length is then estimated from:

$$L = \left[\frac{g T^2}{2\pi} \right] \tanh \left(\frac{2\pi d_{avg}}{\left[\frac{g T^2}{2\pi} \right]} \right) \quad (64)$$

and wave height from:

$$H_s = 0.283 \left(\frac{U_x^2}{g} \right) \tanh(\zeta) \tanh \left(\frac{0.00565 \left[\frac{g F}{U_x^2} \right]^{0.5}}{\tanh(\zeta)} \right) \quad (65)$$

where

$$\zeta = 0.53 \left[\frac{g d_{avg}}{U_x^2} \right]^{0.75} \quad (66)$$

Based on these properties the orbital wave velocity at depth (in the i^{th} layer) is calculated as:

$$U_{orb_i} = \frac{\pi H_s}{T \sinh \left[\frac{2\pi d_i}{L} \right]} \quad (67)$$

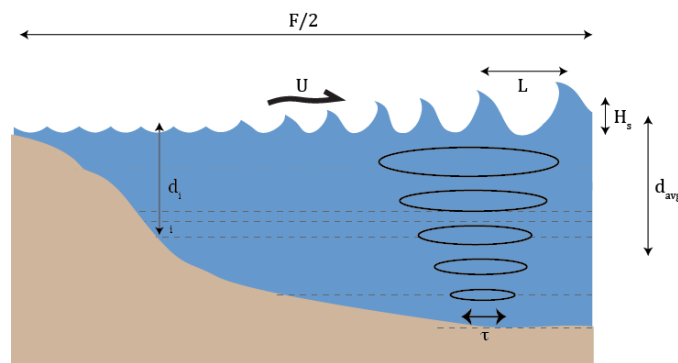


Figure 13: Schematic of the wave estimation approach depicting the lake fetch, surface wind speed, wave height and wavelength, and bottom stress created by the orbital velocity.

The total shear stress at the lake bed is calculated as:

$$\tau_i = \frac{1}{2} \rho_w [f_w U_{orb_i}^2 + f_c U_{m_i}^2] \quad (68)$$

where U_m is the mean velocity of the layer, computed during the mixing calculations (Eq. 33). The friction factors use D (a typical particle diameter). For the current stress we compute $f_w = 0.24/\log(12d_{avg}/2.5D)$ and for waves:

$$f_w = \exp \left[-5.977 + 5.213 \left(\frac{a}{2.5D} \right)^{-0.19} \right] \quad \text{Option 1 : Laenen and LeTourneau, 1996} \quad (69)$$

$$f_w = 0.00251 \exp \left[5.213 \left(\frac{U_{orb} T}{4\pi D} \right)^{-0.19} \right] \quad \text{Option 3 : Kleinhans & Grasmeyer (2006)}$$

$$f_w = \frac{2\beta g \rho_D D}{U^2 \rho_w} \quad \text{Option 3 : Le Roux (2007)}$$

Figure 14 demonstrates wave-related outputs from a shallow lake.

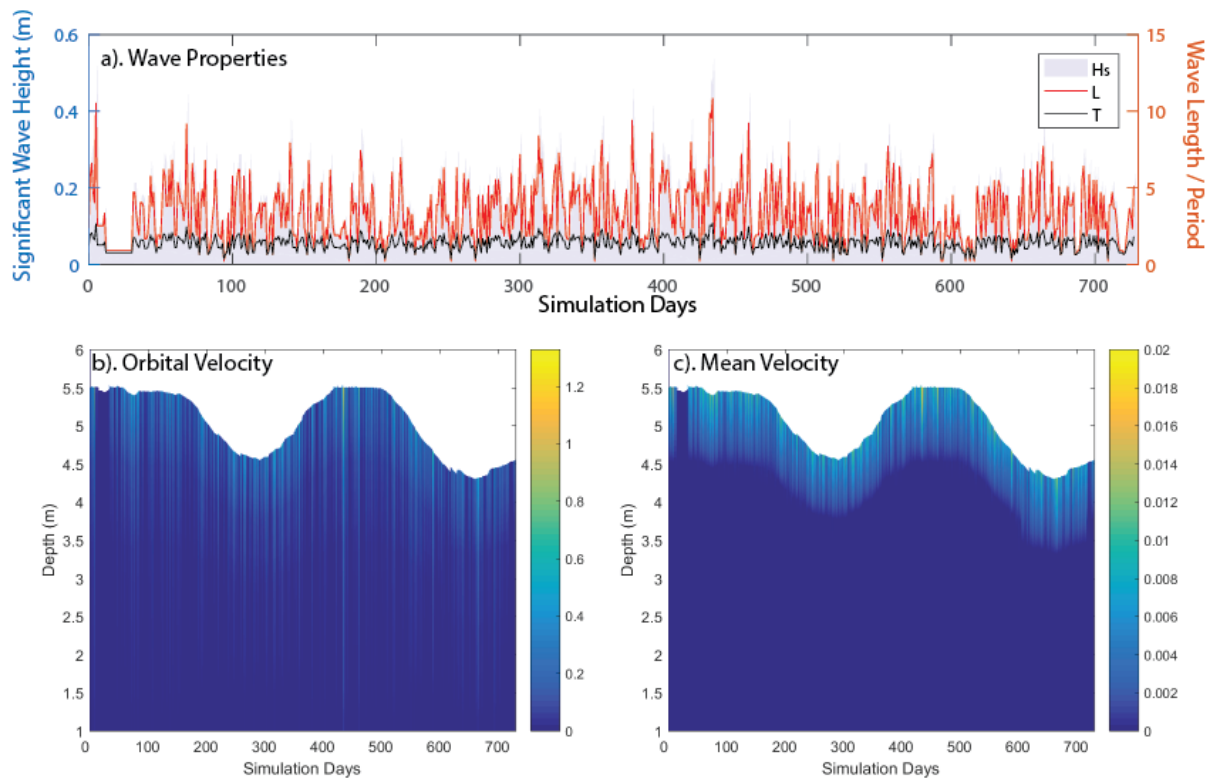


Figure 14: Simulation from Woods Lake, Australia, showing a) time-series of surface wave properties (H_s , L and T), b) orbital velocity, U_{orb} , changes over time (m/s), and c) comparison with the mean velocity, U_m (m/s).

3 Code organization and model operation

Aside from the core water balance and mixing functionality, the model features numerous options and extensions in order to make it a fast and easy-to-use package suitable for a wide range of contemporary applications. Accommodating these requirements has led to the code structure outlined in Figure 15. The model is written in C, with a Fortran-based interface module to link with Fortran-based water quality modelling libraries in Sect. 4. The model compiles with gcc, and gfortran, and commercial compilers, with support for Windows, OS X and Linux.

To facilitate the use of the model in teaching environments and for users with limited technical support, the model may be operated without any third party software, as the input files consist of “namelist” (nml) text files for configuration and csv files for meteorological and flow time-series data (Figure 16). The outputs from predictions are stored into a structured netcdf file, and this can be visualised in real-time through the simple inbuilt plotting library (libplot), or may be opened for post-processing in MATLAB or R (see Sect. 5.1). Parameters and configuration details are input through the main glm.nml text file (Figure 16) and default parameters and their associated description are outlined in Table 1.

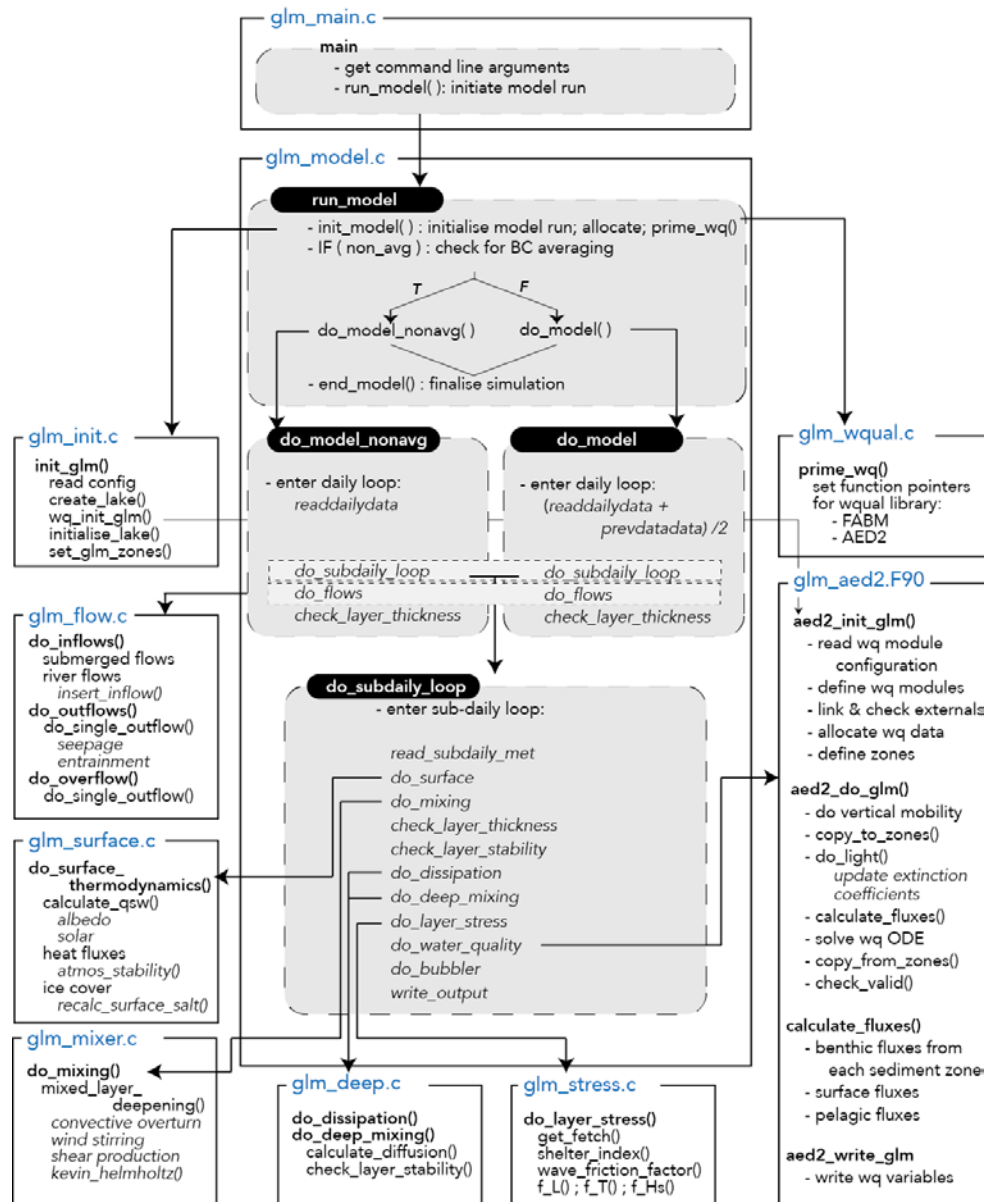


Figure 15: GLM code structure and logic flow. Each module is depicted as a box with the main routines and functions summarised.

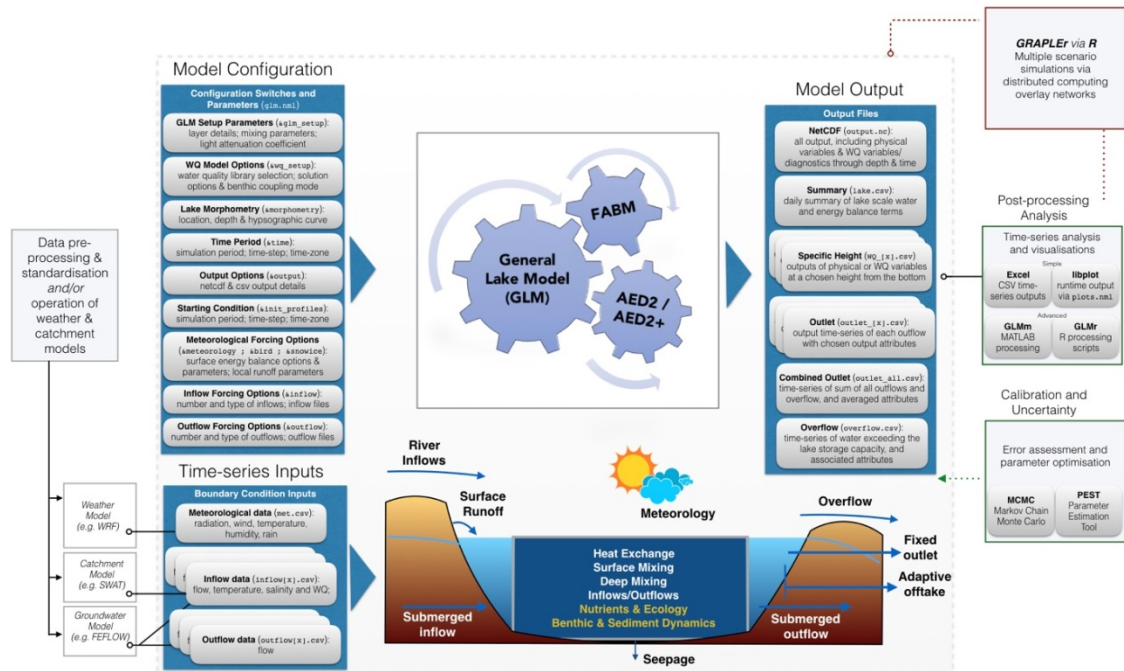


Figure 16: Flow diagram showing the input information required for operation of the model, and outputs and analysis pathways.

4 Dynamic coupling with biogeochemical and ecological model libraries

Beyond modelling the vertical temperature distribution, the water, ice and heat balance, as well as the transport and mixing in a lake, the model has been designed to couple with biogeochemical and ecological model libraries. Currently the model is distributed pre-linked with the AED2 simulation library (Hipsey et al., 2013) and the Framework for Aquatic Biogeochemical Models (FABM; Bruggeman and Bolding, 2014). Through connection with these libraries, GLM can simulate the seasonal changes in vertical profiles of turbidity, oxygen, nutrients, phytoplankton, zooplankton, pathogens and other water quality variables of interest. Documentation of these models is beyond the scope of the present paper, however, two features are highlighted here relevant to managing physical-ecological interactions.

Firstly, the model is designed to allow a user-defined number of sediment zones that span the depth of the lake. Using this approach, the current setup allows for depth-dependent sediment properties, both for physical properties such as roughness or sediment heat flux, and also biogeochemical properties such as sediment nutrient fluxes and benthic ecological interactions. Since the GLM layer structure is flexible over time (i.e., layer depths are not fixed), any interactions between the water and sediment/benthos must be managed at each time-step. The model therefore supports disaggregation and/or aggregation of layer properties, for mapping individual water layers to one or more sediment zones (Figure 17). The

weightings provided by each layer to the sediment are based on the relative depth overlap of a layer with the depth range of the sediment zone. This approach makes the model suitable for long-term assessments of wetland, lake and reservoir biogeochemical budgets, including for C, N and other attribute balances as required (Stepanenko et al., 2016).

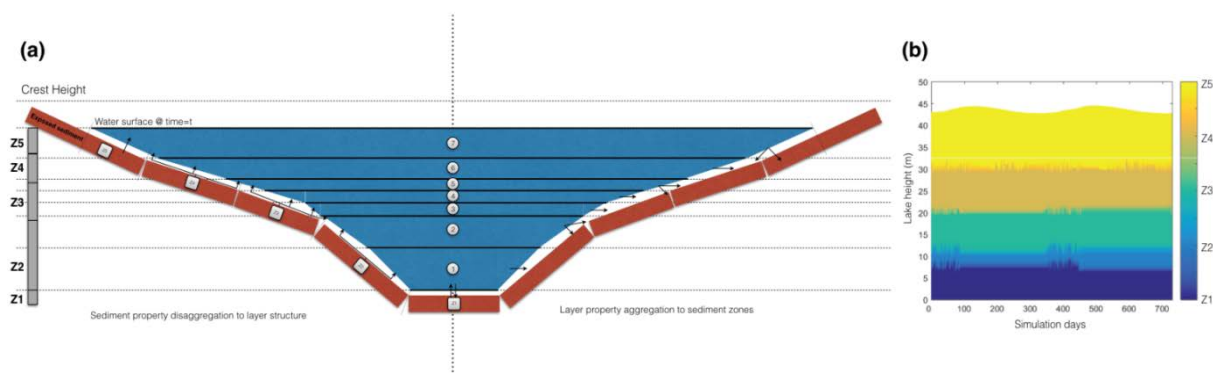


Figure 17: a) Schematic of a lake model layer structure (indicated by layers 1-7), in conjunction with five sediment “zones” (Z1-Z5) activated when `benthic_mode = 2`. The dynamically varying layer structure is re-mapped to the fixed sediment zone locations at each time step in order for the sediment zone to receive the average overlying water properties, and for the water to receive the appropriate information from benthic/sediment variables. b) example of GLM output showing the sediment zone each water layer is mapped to.

Secondly, the water quality modules feed back to GLM properties related to the water and/or heat balance. Feedback options include water density additions, bottom drag, f_w , the light attenuation coefficient, K_w , solar shading and rainfall interception.

5 Workflow tools for integrating GLM with sensor data and supporting models

The GLM model has been designed to support integration of large volumes of data coming from instrumented lakes, including many GLEON sites (cite ref, e.g., Weathers, Hanson, etc.). These data consist of high-frequency and discrete time-series observations of hydrologic fluxes, meteorology, temperature, and water quality (e.g., Hamilton et al. 2014). To facilitate research that requires running the model using these data sources, we have created GLM interfaces in the R and MATLAB analysis environments. These tools support user-friendly access to the model and include routines that streamline the process of calibrating models or running various scenarios. In addition, for assessment of lake dynamics in response to catchment or climatic forcing it is desirable to be able to connect GLM with other model platforms associated with surface and groundwater simulation, and weather prediction (Read et al., 2016).

5.1 R and MATLAB libraries for model setup and post-processing

The R and MATLAB scientific languages are commonly used in aquatic research, often as part of automated modelling and analysis workflows. GLM has a client library for both, and these tools are shared freely online. The R package is called “glmtools” (<https://github.com/GLEON/glmtools>) and the MATLAB library is called “GLMm” (<https://github.com/AquaticEcoDynamics/GLMm>). Both tools have utilities for model pre- and post-processing. The pre-processing components can be used to format and modify data inputs and configuration files, and define options for how GLM executes. Post-processing tools include visualizations of simulation results (as shown in the results figures above), comparisons to field observations, and various evaluations of model performance.

5.2 Utilities for assessing model performance, parameter identification and uncertainty analysis

In order to compare the performance of the model for varied types of lakes, numerous different metrics of model performance are relevant. These include simple measures like surface or bottom temperature, or ice thickness, however, it is also possible to compare the model’s performance in capturing higher-order metrics relevant to lake dynamics, including Schmidt Stability, thermocline depth, ice on/off dates (see also Bruce et al., 2017, for a detailed assessment of the model’s accuracy across a wide diversity of lakes across the globe). With particular interest in the model’s ability to interface with high frequency sensor data for calculation of key lake stability metrics (Read et al., 2011), then continuous wavelet transform comparisons are also possible (Kara et al., 2012), allowing assessment of the time-scales over which the model is able to capture the observed variability within the data.

As part of the modelling process, it is common to adjust parameters to get the best fit with available field data and, as such, the use of a Bayesian Hierarchical Framework in the aquatic ecosystem modelling community has become increasingly useful (e.g., Zhang and Arhonditsis, 2009; Romarheim et al., 2015). Many parameters described throughout Sect. 2 are attempts at physically based descriptions where there is relatively little variation (Bruce et al., 2017), thereby reducing the number of parameters that remain uncertain, however, for others their variation reflects imperfect formulation of some processes that are not fully considered. Therefore, within MATLAB, support scripts for GLM to work with the Markov Chain Monte Carlo (MCMC) code outlined in Haario et al. (2006) can be used to provide improved parameter estimates and uncertainty assessment (Figure 18). Wrappers and examples for use of GLM within the openDA framework and PEST are also being tested, giving users access to a wide range of uncertainty assessment and data assimilation algorithms. The PEST framework allows for calibration of complex model using highly-parameterised regularisation with pilot-points (Doherty, 2015), and sensitivity matrices

derived from the calibration process can also be utilised in linear and non-linear uncertainty analysis.

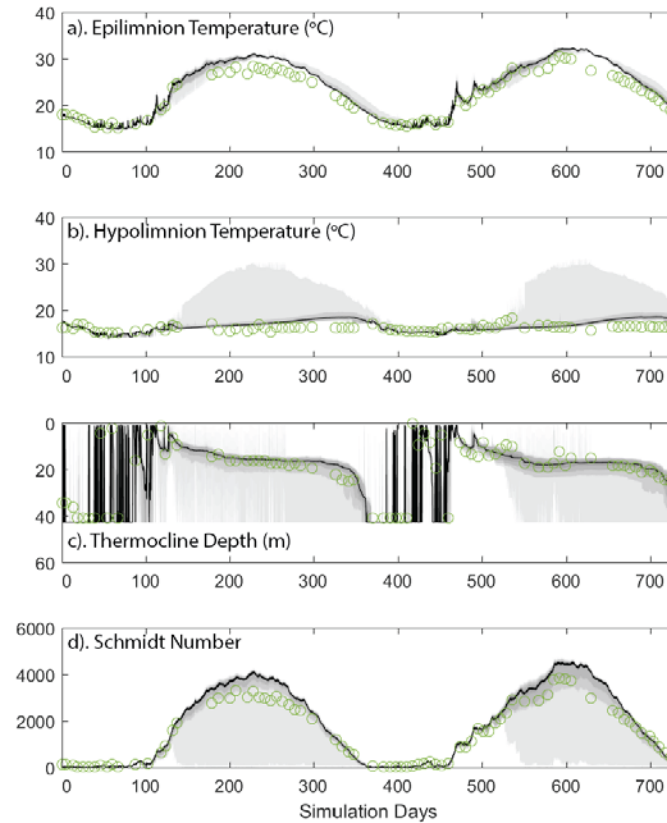


Figure 18: Depiction of parameter uncertainty for a GLM simulation of Lake Kinneret, Israel, following calibration against observations (green circles) via MCMC for a) epilimnion temperature, b) hypolimnion temperature, c) thermocline depth, and d) Schmidt number. The black line indicates the mean likelihood of the prediction, and the grey bands depict the 40th, 60th and 80th percentile.

5.3 Operation in the cloud: GRAPLER

Questions relevant to land use and climate change are driving scientists to develop scenarios for how lake ecosystem services might respond to changing exogenous drivers. An important approach to addressing these questions is to simulate lake or reservoir physical-biological interactions in response to changing hydrology, nutrient loads or meteorology, and then infer consequences from the emergent properties of the simulation, such as changes in water clarity, extent of anoxia, mixing regime, or habitability to fishes (Hipsey et al., 2015). Often, it takes years or even decades for lakes to respond fully to changes in exogenous drivers, requiring simulations to recreate lake behavior over extended periods. While most desktop computers can run a decade-long, low-resolution simulation in less than one minute, high-resolution simulations of the same extent may require minutes to hours of processor time.

When questions demand hundreds, thousands or even millions of simulations, the desktop approach is no longer suitable.

Through access to distributed computing resources, modellers can run thousands of GLM simulations in the time it takes to run a few simulations on a desktop computer. Collaborations between computer scientists in the Pacific Rim Applications and Grid Middleware Assembly (PRAGMA) and GLEON have led to the development of GRAPLER (GLEON Research and PRAGMA Lake Expedition in R), software, written in R, that enables modellers to distribute batches of GLM simulations to pools of computers (Subratie et al., 2017). Modellers use GRAPLER in two ways: by submitting a single simulation to the GRAPLER Web service, along with instructions for running that simulation under different climate scenarios, or by configuring many simulations on the user's desktop computer, and then submitting them as a batch to the Web service. The first approach provides a high degree of automation that is well suited to training and instruction, and the second approach has the full flexibility often needed for research projects. In all approaches, GRAPLER converts the submitted job to a script that is used by HTCondor (Thain et al., 2005) to distribute and manage jobs among the computer pool and ensure that all simulations run and return results. An iPOP overlay network (Ganguly et al., 2006) allows the compute services to include resources from multiple institutions, as well as cloud computing services. GRAPLER's Web service front-end shields the modeller from the compute environment, greatly reducing the need for modellers to understand distributed computing; they therefore only need to install the R package, know the URL of the GRAPLER Web service, and decide how the simulations should be setup.

5.4 Integration with catchment and climate models

GLM simulations may be coupled with catchment models, such as the Soil Water Assessment Tool (SWAT) or similar catchment models, simply by converting the catchment model output into the inflow file format via conversion scripts. Similarly, scripts exist for coupling GLM with the Weather Research Forecasting (WRF) model, or similar climate models, for specification of the meteorological input file from weather prediction simulations.

The above coupling approaches require the models to be run in sequence, however, for the simulation of lake-wetland-groundwater systems, two-way coupling is required to account for the flow of water into and out of the lake throughout the simulation. For these applications, the interaction can be simulated using GLM coupled with the 3D groundwater flow model, FEFLOW (<https://www.mikepoweredbydhi.com/products/feflow>). For this case the GLM code is compiled as a Dynamic Link Library (DLL) and loaded into FEFLOW as a plug-in module. The coupling between GLM and FEFLOW is implemented using a one-step lag

between the respective solutions of the groundwater and lake models. This approach, in most simulations, does not introduce a significant error, however, error can be assessed and reduced using smaller time step lengths. FEFLOW models can be simulated for flow-only, or including heat and/or solute transport. Depending on the simulation mode, GLM accounts for the different process variables, assigning boundaries for lake level, salinity and temperature accordingly.

The GLM module was designed to accommodate situations of variable lake geometry, by using a dry-lake/wet-lake approach. In this approach, dry-lake areas are defined as those above the current lake level and wet-lake areas as below the current lake level. Different boundary types in FEFLOW are assigned to dry-lake and wet-lake areas (Figure 19). The calibration of such coupled models is often complex, given the large number of parameters and sensitivities when different sources of information are utilised (for example flow and water level measurements). The FEFLOW-GLM coupling structure allows for a relatively straightforward integration with PEST (Doherty, 2015), based on existing FEFLOW workflows.

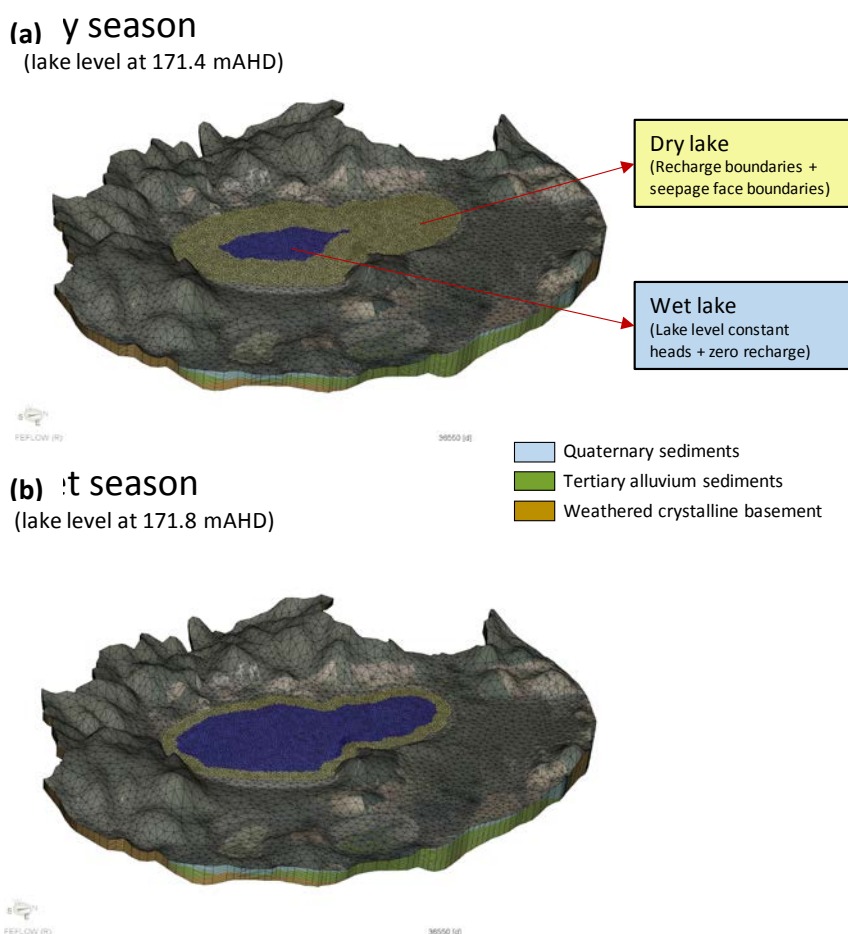


Figure 19: Example of lake boundary changes during wet and dry cycles from Lake Muir, Australia. GLM water level is communicated to FEFLOW to each time-step and used as a constant head boundary condition for all wet cells.

6 GLM as a tool for teaching environmental science and ecology

Environmental modelling is integral for understanding complex ecosystem responses to anthropogenic and natural drivers, and also provides a valuable tool for engaging students learning environmental science (Carey and Gougis, 2017). Previous pedagogical studies have demonstrated that engaging students in modelling provides cognitive benefits, enabling them to build new scientific knowledge and conceptual development (Stewart et al., 2005; Zohar and Dori 2011). For example, modelling forces students to analyze patterns in data, create evidence-based hypotheses for those patterns and make their hypotheses explicit, and develop predictions of future conditions (Stewart et al., 2005). As a result, the U.S. National Research Council has recently integrated modelling into the *Next Generation Science Standards*, which provide recommendations for primary and secondary school science pedagogy in the United States (NRC, 2013). However, it remains rare for undergraduate and graduate science courses to include the computer-based modelling that environmental scientists need to manage natural ecosystems.

A teaching module for the use of GLM within undergraduate and graduate classrooms has been developed to explore lake responses to climate change (Carey and Gougis, 2017). The GLM module, called the “Climate Change Effects on Lake Temperatures”, teaches students how to set up a simulation for a model lake within R. After they are able to successfully run their lake simulations, they force the simulation with climate scenarios of their own design to examine how lakes may change in the future. To improve computational efficiency, students also learn how to submit, retrieve, and analyze hundreds of model simulations through distributed computing overlay networks embedded via the GRAPLER interface, described above. Hence, students participating in the module learn computing and quantitative skills in addition to improving their understanding of how climate change is affecting lake ecosystems.

Initial experiences teaching GLM as well as pre- and post-assessments indicate that participation in the module improves students’ understanding of lake responses to climate change (Carey and Gougis, 2017). By modifying GLM boundary condition data and exploring model output, students are able to better understand the processes that control lake responses to altered climate, and improve their predictions of future lake change. Moreover, the module exposes students to computing and modelling tools not commonly experienced in most university classrooms, building competence with manipulating data files, scripting, creating figures and other visualizations, and statistical and time series analysis; all skills that are transferrable for many other applications. Thus, following previous studies (Schwarz and White 2005, Schwarz et al. 2009), we predict that increased experience with GLM modelling will not only build students’ understanding of lake ecosystem concepts but also their ability to interpret natural phenomena and generate new scientific knowledge.

7 Conclusions

As part of GLEON activities, the emergence of complex questions about how different lake types across the world are responding to climate change and land-use change has created the need for a robust, accessible community code suitable for a diverse range of lake types and simulation contexts. Here, GLM is presented as a tool that meets many of the needs of network participants for their individual lake simulation requirements, in addition to being suitable for application in a distributed way across tens to thousands of lakes for regional and global scale assessments. Recent examples include an application of the model for assessing how the diversity of >2000 lakes in lake-rich landscape in Wisconsin respond to meteorological conditions and projected warming (Read et al., 2014), and given its computationally efficient nature it is envisioned to be made available as a library for use within in land-surface models (e.g., the Community Land Model, CLM), allowing improved representation of lake dynamics in regional hydrological or climate assessments. With further advances in the degree of resolution and scope of earth system models, we further envisage GLM as an option suitable to be embedded within these models to better allow the simulation of lake stratification, air-water interaction of momentum and heat, and also biogeochemically relevant variables associated with contemporary questions about greenhouse gases emissions such as CO₂, CH₄, and N₂O.

Since the model is one-dimensional, it assumes no horizontal variability in the simulated water layers and users must therefore ensure their application of the model is suited to this assumption. For stratified systems, the parameterization of mixing due to internal wave and inflow intrusion dynamics is relatively simple, making the model ideally suited to longer-term investigations ranging from weeks to decades (depending on the domain size), and for coupling with biogeochemical models to explore the role that stratification and vertical mixing play on lake ecosystem dynamics. However, the model can also be used for shallow lakes, ponds and wetland environments where the water column is relatively well mixed. In order to better define the typical level of model performance across these diverse lake types, a companion paper by Bruce et al. (2017), has undertaken a systematic assessment of the model's error structure against 31 lakes from across GLEON, to which readers can refer to for further guidance. In cases where the assumption of one-dimensionality is not met for a particular lake application, then it is possible for users to apply two or three dimensional models; potentially these can be temporally nested within a longer term GLM simulation.

This paper has focused on description of the hydrodynamic model, but we highlight that the model is a platform for coupling with advanced biogeochemical and ecological simulation libraries for water quality prediction and integrated ecosystem assessments. As with most coupled hydrodynamic-ecological modelling platforms, GLM handles the boundary conditions and transport of variables simulated within these libraries, including the effects of inflows, vertical mixing, and evapo-concentration. Whilst the interface to these libraries is

straightforward, the Lagrangian approach adopted within GLM for simulation of the water column necessitates the adoption of sediment zones on a static grid that is independent from the water column numerical grid.

More advanced workflows for operation of the model within distributed computing environments and with data assimilation algorithms is an important application when used within GLEON capabilities related to high frequency data and its interpretation. The 1D nature of the model makes the run-times modest and therefore the model is suitable for application within more intensive parameter identification and uncertainty assessment procedures. This is particularly relevant as the needs for network participants to expand model configurations to further include biogeochemical and ecological state variables. It is envisioned that continued application of the model to lakes of GLEON will allow us to improve parameter estimates and ranges, and this will ultimately support other users of the model in identifying parameter values, and assigning parameter prior distributions. Since many of the users the model is intended for may not have access to the necessary cyberinfrastructure, the use of GLM with the open-source GRAPLER software in the R environment provides access to otherwise unavailable distributed computing resources. This has the potential to allow non-expert modellers within the science community to apply good modelling practices by automating boundary condition and parameter sensitivity assessments, with technical aspects of simulation management abstracted from the user.

Finally, the role of models in informing and educating members of the network and the next generation of hydrologic and ecosystem modellers has been identified as a critical element of synthesis activities and supporting cross-disciplinary collaboration (Weathers et al., 2017). Initial use of GLM within the classroom has found that teaching modules integrating GLM into classes improves students' understanding of how climate change is altering lake ecosystems.

Code availability

The GLM code is provided as open-source under the GNU GPL3 license, and version controlled via the GitHub repository: <https://github.com/AquaticEcoDynamics/GLM>.

Data availability

The five example lakes used to demonstrate the model operation are described along with model input files (and associated hydrologic and meteorological forcing data) within the GitHub repository:

<https://github.com/AquaticEcoDynamics/GLM/tree/master/Examples/2.4.0>

Acknowledgments

The primary code of GLM has been developed by MH, LB, CB, BB and DH at The University of Western Australia in collaboration with researchers participating in GLEON and benefited directly from support provided by the NSF Research Coordination Network Award. Whilst GLM is a new code, it is based on the large body of historical research and publications produced by the Centre for Water Research at the University of Western Australia, which we acknowledge for the inspiration, development and testing of several of the model algorithms that have been adopted. Funding for initial development of the GLM code was from the U.S. NSF Cyber-enabled Discovery and Innovation grant awarded to PH (lead investigator) and colleagues from 2009-2014 (NSF CDI-0941510), and subsequent development was supported by the Australian Research Council projects awarded to MH and colleagues (ARC projects LP0990428, LP130100756 and DP130104087). Funding for development of the GLM teaching module and GRAPLEr was supported from NSF ACI-1234983 and NSF EF-1702506 awarded to CC. Provision of the environmental symbols used for the GLM scientific diagrams are courtesy of the Integration and Application Network, University of Maryland Center for Environmental Science. Joanne Moo and Aditya Singh also provided support in model setup and testing.

References

- Ashton, G.D. (ed.), 1986. River and lake ice engineering. Water Resources Publications, Littleton, Colorado, U.S.A.
- Antenucci, J.P., Brookes, J.D. and Hipsey, M.R., 2005. A simple model for quantifying "Cryptosporidium" transport, dilution, and potential risk in reservoirs. *Journal of the American Water Works Association*, 97(1): 86-93.
- Babanin, A.V. and Makin, V.K., 2008. Effects of wind trend and gustiness on the sea drag: Lake George study. *Journal of Geophysical Research: Oceans*, 113(C2).
- Bird, R.E., 1984. A simple, solar spectral model for direct-normal and diffuse horizontal irradiance. *Solar energy*, 32: 461-471.
- Briegleb, B.P., Minnis, P., Ramanathan, V. and Harrison, E., 1986. Comparison of regional clear-sky albedos inferred from satellite observations and model computations. *Journal of Climate and Applied Meteorology*, 25(2): 214-226.
- Bruce, L.C., Frassl, M.A., Arhonditsis, G.B., Gal, G., Hamilton, D.P., Hanson, P.C., et al., 2017. A multi-lake comparative analysis of the General Lake Model (GLM): Stress-testing across a global observatory network. *Environmental Modelling & Software*, accepted pending final revision.
- Bruggeman, J. and Bolding, K., 2014. A general framework for aquatic biogeochemical models. *Environmental Modelling & Software*, 61: 249-265.
- Brutsaert, W., 1975. On a derivable formula for long-wave radiation from clear skies, *Water Resources Research*, 11(5): 742-744.
- Bueche, T., Hamilton, D.P. and Vetter, M., 2017. Using the General Lake Model (GLM) to simulate water temperatures and ice cover of a medium-sized lake: a case study of Lake Ammersee, Germany. *Environmental Earth Sciences*, 76(13), p.461. doi.org/10.1007/s12665-017-6790-7
- Businger, J.A., Wyngaard, J.C., Izumi, Y. and Bradley, E.F., 1971. Flux profile relationships in the atmospheric surface layer. *Journal of Atmospheric Sciences*, 28: 181-189.
- Carey, C.C. and Gougis, R.D., 2017. Simulation modeling of lakes in undergraduate and graduate classrooms increases comprehension of climate change concepts and experience with computational tools. *Journal of Science Education and Technology*, 26: 1-11.
- Chung, E. G., Schladow, S. G., Perez-Losada, J., and Robertson, D. M., 2008. A linked hydrodynamic and water quality model for the Salton Sea. *Hydrobiologia* 604:57-75.
- Chung, S.W., Imberger, J., Hipsey, M.R. and Lee, H.S., 2014. The influence of physical and physiological processes on the spatial heterogeneity of a *Microcystis* bloom in a stratified reservoir. *Ecological Modelling*, 289, pp.133-149.

- Cole, J.J., Prairie, Y.T., Caraco, N.F., McDowell, W.H., Tranvik, L.J., Striegl, R.G., Duarte, C.M., Kortelainen, P., Downing, J.A., Middelburg, J.J. and Melack, J., 2007. Plumbing the Global Carbon Cycle: Integrating Inland Waters into the Terrestrial Carbon Budget. *Ecosystems*, 10: 172–185.
- Doherty, J., 2015. Calibration and Uncertainty Analysis for Complex Environmental Models. Watermark Numerical Computing, Brisbane, Australia. ISBN: 978-0-9943786-0-6
- Dyer, A.J., 1974. A review of flux-profile relationships. *Boundary-Layer Meteorology*, 7: 363-372.
- Fischer, H.B., List, E.G., Koh, R.C.Y., Imberger, J. and Brooks, N.H., 1979. Mixing in Inland and Coastal Waters. Academic Press. New York, NY, 483 pp.
- Francey, R.J. and Garratt, J.R., 1978. Eddy flux measurements over the ocean and related transfer coefficients. *Boundary-Layer Meteorology*, 14: 153-166.
- Gal, G., Imberger, J., Zohary, T., Antenucci, J., Anis, A. and Rosenberg, T., 2003. Simulating the thermal dynamics of Lake Kinneret. *Ecological Modelling*, 162: 69-86.
- Gal, G., Hipsey, M.R., Parparov, A., Wagner, U., Makler, V. and Zohary, T., 2009. Implementation of ecological modeling as an effective management and investigation tool: Lake Kinneret as a case study. *Ecological Modelling*, 220(13), pp.1697-1718.
- Ganguly, A., Agrawal, A., Boykin, P. O. and Figueiredo, R., 2006. IP over P2P: Enabling self-configuring virtual IP networks for grid computing. In International Parallel and Distributed Processing Symposium.
- Gill, A.E., 1982. Atmosphere-ocean dynamics (Vol. 30). Academic press.
- Gu, R. and Stefan, H.G., 1993. Validation of cold climate lake temperature simulation. *Cold regions science and technology*, 22: 99-104.
- Haario, H., Laine, M., Mira, A. and Saksman, E., 2006. DRAM: Efficient adaptive MCMC, *Statistics and Computing*, 16: 339-354.
- Hamilton, D.P. and Schladow, S.G. 1997. Water quality in lakes and reservoirs. Part I Model description. *Ecological Modelling*, **96**: 91–110.
- Hamilton, D.P., Carey, C.C., Arvola, L., Arzberger, P., Brewer, C., Cole, J.J., Gaiser, E., Hanson, P.C., Ibelings, B.W., Jennings, E. and Kratz, T.K., 2015. A Global Lake Ecological Observatory Network (GLEON) for synthesising high-frequency sensor data for validation of deterministic ecological models. *Inland Waters*, 5(1): 49-56.
- Hanson, P.C., Weathers, K.C. and Kratz, T.K., 2016. Networked lake science: how the Global Lake Ecological Observatory Network (GLEON) works to understand, predict, and communicate lake ecosystem response to global change. *Inland Waters*, 6(4): 543-554.

Harvey, L.D.D., 1990. Testing alternative parameterizations of lateral melting and upward basal heat flux in a thermodynamic sea ice model. *Journal of Geophysical Research*, 95: 7359-7365.

Henderson-Sellers, B., 1986. Calculating the surface energy balance for lake and reservoir modeling: A review. *Reviews of Geophysics*, 24(3): 625-649.

Hicks, B.B., 1975. A procedure for the formulation of bulk transfer coefficients over water. *Boundary Layer Meteorology*, 8: 515-524.

Hicks, B.B., 1972. Some evaluations of drag and bulk transfer coefficients over water. *Boundary Layer Meteorology*, 3: 201:213.

Hipsey, M.R. and Sivapalan, M., 2003. Parameterizing the effect of a wind-shelter on evaporation from small waterbodies. *Water Resources Research*, 39(12): 1339.

Hipsey, M.R., Bruce, L.C. and Hamilton, D.P., 2013. Aquatic EcoDynamics (AED) Model Library Science Manual. The University of Western Australia Technical Manual, Perth, Australia, p.34.

Hipsey, M.R., Hamilton, D.P., Hanson, P.C., Carey, C.C., Coletti, J.Z., Read, J.S., Ibelings, B.W., Valesini, F.J. and Brookes, J.D., 2015. Predicting the resilience and recovery of aquatic systems: A framework for model evolution within environmental observatories. *Water Resources Research*, 51(9): 7023-7043.

Hocking, G.C. and Patterson, J.C., 1991. Quasi-two-dimensional reservoir simulation model. *Journal of Environmental Engineering*, 117: 595-613.

Hu, F., Bolding, K., Bruggeman, J., Jeppesen, E., Flindt, M., van Gerven, L.P.A., Janse, J.H., Janssen, A.B.G., Kuiper, J.J., Mooij, W.M. and Trolle, D. 2016. FABM-PCLake - Linking aquatic ecology with hydrodynamics. *Geoscientific Model Development* 9: 2271-2278

Idso, S.B. and Jackson, R.D., 1969. Thermal radiation from the atmosphere. *Journal of Geophysical Research*, 74: 5397-5403.

Imberger, J., Patterson, J., Hebbert, B. and Loh, I., 1978. Dynamics of reservoir of medium size. *Journal of the Hydraulics Division - ASCE*, 104 No HY5: 725-743.

Imberger, J. and Patterson, J.C., 1981. *A dynamic reservoir simulation model-DYRESM:5*. In: H.B. Fischer (ed.), Transport Models for Inland and Coastal Waters. Academic Press, New York: 310-361.

Imberger, J. and Patterson, J.C., 1990. *Physical Limnology*. In: T. Wu (ed.), Advances in applied mechanics 27. Academic Press. Boston. U.S.A.

Imboden, D.M. and Wüest, A., 1995. *Mixing Mechanisms in Lakes*, p. 83-138. In: A. Lerman, D.M. Imboden and J.R. Gat (eds.), Physics and Chemistry of Lakes. Springer-Verlag.

- Janssen, A.B.G., Arhonditsis, G.B., Beusen, A., Bolding, K., Bruce, L., Bruggeman, J., Couture, R.M., Downing, A.S., Elliott, J.A., Frassl, M.A., Gal, G., Gerla, D.J., Hipsey, M.R., Hu, F., Ives, S.C., Janse, J., Jeppesen, E., Jöhnk, K.D., Kneis, D., Kong, X., Kuiper, J.K., Lehmann, M., Lemmen, C., Ozkundakci, D., Petzoldt, T., Rinke, K., Robson, B.J., Sachse, R., Schep, S., Schmid, M., Scholten, H., Teurlincx, S., Trolle, D., Troost, T.A., Van Dam, A., Van Gerven, L.A., Weijerman, M., Wells S.A. and Mooij, W.M., 2015. Exploring, exploiting and evolving diversity of aquatic ecosystem models: a community perspective. *Aquatic ecology*, 49(4): 513-548.
- Jellison, R. and Melack, J.M., 1993. Meromixis and vertical diffusivities in hypersaline Mono Lake, California. *Limnology and Oceanography*, **38**: 1008–1019.
- Ji, Z.G., 2008. Hydrodynamics and water quality: modeling rivers, lakes, and estuaries. John Wiley & Sons.
- Kara, E.L., Hanson, P., Hamilton, D., Hipsey, M.R., McMahon, K.D., Read, J.S., Winslow, L., Dedrick, J., Rose, K., Carey, C.C. and Bertilsson, S., 2012. Time-scale dependence in numerical simulations: assessment of physical, chemical, and biological predictions in a stratified lake at temporal scales of hours to months. *Environmental Modelling & Software*, 35, pp.104-121.
- Kim, J-W., 1976. A generalized bulk model of the oceanic mixed layer. *Journal of Physical Oceanography*, 6: 686-695.
- Kirk, J.T.O., 1994. Light and photosynthesis in aquatic ecosystems. Cambridge University Press.
- Kirillin, G., Hochschild, J., Mironov, D., Terzhevik, A., Golosov, S. and Nützmann, G., 2011. FLake-Global: Online lake model with worldwide coverage. *Environmental Modelling & Software*, 26(5), pp.683-684.
- Kleinhans, M.G. and Grasmeijer, B.T., 2006. Bed load transport on the shoreface by currents and waves. *Coastal Engineering*, 53: 983-996.
- Klug, J.L., Richardson, D.C., Ewing, H.A., Hargreaves, B.R., Samal, N.R., Vachon, D., Pierson, D.C., Lindsey, A.M., O'Donnell, D.M., Effler, S.W. and Weathers, K.C., 2012. Ecosystem Effects of a Tropical Cyclone on a Network of Lakes in Northeastern North America. *Environmental Science & Technology*, 46 (21): 11693-11701.
- Kraus, E.B. and Turner, J.S., 1967. A one-dimensional model of the seasonal thermocline: II The general theory and its consequences. *Tellus*, 19: 98-106.
- Laenen A. and LeTourneau A.P., 1996. Upper Klamath Lake nutrient loading study – Estimate of wind-induced resuspension of bed sediment during periods of low lake elevation. *US Geological Survey Open-File Report*, 95-414, 11 pp

- Launiainen, J., 1995. Derivation of the relationship between the Obukhov stability parameter and the bulk Richardson number for flux-profile studies. *Boundary Layer Meteorology*, **76**: 165-179.
- Launiainen, J. and Cheng, B., 1998. Modelling of ice thermodynamics in natural water bodies. *Cold Region Science and Technology*, **27**: 153-178.
- Launiainen, J. and Vihma, T., 1990. Derivation of turbulent surface fluxes—An iterative flux-profile method allowing arbitrary observing heights. *Environmental Software*, **5**: 113-124.
- Le Roux, J.P., 2007. A simple method to determine breaker height and depth for different deepwater wave height/length ratios and sea floor slopes. *Coastal Engineering*, **54**: 271-277.
- Luo, L., Hamilton, D.P. and Han, B., 2010. Estimation of total cloud cover from solar radiation observations at Lake Rotorua, New Zealand. *Solar Energy*, **84**: 501-506.
- Magee, M.R., Wu, C.H., Robertson, D.M., Lathrop, R.C. and Hamilton, D.P., 2016. Trends and abrupt changes in 104 years of ice cover and water temperature in a dimictic lake in response to air temperature, wind speed, and water clarity drivers. *Hydrology and Earth System Sciences*, **20**(5), p.1681.
- Makler-Pick, V., Gal, G., Shapiro, J. and Hipsey, M.R., 2011. Exploring the role of fish in a lake ecosystem (Lake Kinneret, Israel) by coupling an individual-based fish population model to a dynamic ecosystem model. *Canadian Journal of Fisheries and Aquatic Sciences*, **68**(7), pp.1265-1284.
- Markfort, C.D., Perez, A.L.S., Thill, J. W., Jaster, D.A., Porté-Agel, F. and Stefan, H.G. 2010. Wind sheltering of a lake by a tree canopy or bluff topography. *Water Resources Research*, **46**: 1–13.
- Martynov, A., Sushama, L., Laprise, R., Winger, K. and Dugas, B., 2012. Interactive lakes in the Canadian Regional Climate Model, version 5: The role of lakes in the regional climate of North America. *Tellus, Series A Dynamic Meteorology And Oceanography*, **64**: 1-22.
- Matzinger, A., Schmid, M., Veljanoska-Sarafiloska, E., Patceva, S., Guseska, D., Wagner, B., Müller, B., Sturm, M. and Wüest, A., 2007. Eutrophication of ancient Lake Ohrid: global warming amplifies detrimental effects of increased nutrient inputs, *Limnology and Oceanography*, **52**(1), 338-353, doi:10.4319/lo.2007.52.1.0338.
- McKay, G.A., 1968. Problems of measuring and evaluating snow cover. *In: Proceedings Workshop Seminar of Snow Hydrology*. (Secretariat Canadian National Committee for the IHD, Ottawa: 49-62.
- McCord, S.A. and Schladow, S.G., 1998. Numerical simulations of degassing scenarios for CO₂-rich Lake Nyos, Cameroon. *Journal of Geophysical Research: Solid Earth*, **103**(B6): 12355-12364.

- Menció, A., Casamitjana, X., Mas-Pla, J., Coll, N., Compte, J., Martinoy, M., Pascual, J. and Quintana, X.D., 2017. Groundwater dependence of coastal lagoons: The case of La Pletera salt marshes (NE Catalonia). *Journal of Hydrology*, 552, pp.793-806.
- Mueller H, Hamilton DP and Doole GJ. 2016. Evaluating services and damage costs of degradation of a major lake ecosystem. *Ecosystem Services* 22: 370-380
- Mooij, W.M., Trolle, D., Jeppesen, E., Arhonditsis, G., Belolipetsky, P.V., Chitamwebwa, D.B.R., Degermendzhy, A.G., DeAngelis, D.L., De Senerpont Domis, L.N., Downing, A.S., Elliott, A.E., Fragoso Jr, C.R., Gaedke, U., Genova, S.N., Gulati, R.D., Håkanson, L., Hamilton, D.P., Hipsey, M.R., Hoen, J., Hülsmann, S., Los, F.J., Makler-Pick, V., Petzoldt, T., Prokopkin, I.G., Rinke, K., Schep, S.A., Tominaga, K., Van Dam, A.A., Van Nes, E.H., Wells, S.A. and Janse, J.H., 2010. Challenges and opportunities for integrating lake ecosystem modelling approaches. *Aquatic Ecology*, 44: 633–667.
- Monin, A.S. and Obukhov, A.M., 1954. Basic laws of turbulent mixing in the atmosphere near the ground. *Jr. Akad. Nauk SSSR Geofiz. Inst.*, 24: 163-187.
- National Research Council (NRC), 2013. Next generation science standards: For states, by states. Washington, DC: The National Academies Press.
- O'Reilly, C. M., Sharma, S., Gray, D. K., Hampton, S. E., Read, J. S., Rowley, R. J., Schneider, P., Lenters, J. D., McIntyre, P. B., Kraemer, B. M., et al., 2015. Rapid and highly variable warming of lake surface waters around the globe. *Geophysical Research Letters*, 42(24): 10,773–10,781.
- Patterson, J.C., Hamblin, P.F. and Imberger, J., 1984. Classification and dynamics simulation of the vertical density structure of lakes. *Limnology and Oceanography*, 29: 845-861.
- Patterson, J.C. and Hamblin, P.F., 1988. Thermal simulation of a lake with winter ice cover. *Limnology and Oceanography*, 33: 323-338.
- Paulson, C. A., 1970. The mathematical representation of wind speed and temperature profiles in the unstable atmospheric surface layer. *Journal of Applied Meteorology*, 9: 857-861.
- Peeters, F., Straile, D. Loke, A. and Livingstone, D. M., 2007. Earlier onset of the spring phytoplankton bloom in lakes of the temperate zone in a warmer climate. *Global Change Biology*. 13: 1898–1909, doi:10.1111/j.1365-2486.2007.01412.x
- Perroud, M., Goyette, S., Martynov, A., Beniston, M. and Annevillec, O., 2009. Simulation of multiannual thermal profiles in deep Lake Geneva: A comparison of one-dimensional lake models. *Limnology and Oceanography*, 54(5), pp.1574-1594.
- Porter, J.H., Hanson, P.C. and Lin, C.C., 2012. Staying afloat in the sensor data deluge. *Trends In Ecology & Evolution*, 27(2): 121-129.

- Read, J.S., Hamilton, D.P., Jones, I.D., Muraoka, K., Winslow, L.A., Kroiss, R., Wu, C.H. and Gaiser, E., 2011. Derivation of lake mixing and stratification indices from high-resolution lake buoy data. *Environmental Modelling & Software*, **26**: 1325–1336.
- Read, J.S., Hansen, G., Van Den Hoek, J., Hanson, P.C., Bruce, L.C. and Markfort, C.D., 2014. Simulating 2368 temperate lakes reveals weak coherence in stratification phenology. *Ecological Modelling*, 291: 142-150.
- Read, J.S., Gries, C., Read, E.K., Klug, J., Hanson, P.C., Hipsey, M.R., Jennings, E., O'Reilly, C., Winslow, L., Pierson, D., McBride, C. and Hamilton, D.P., 2016. Generating community-built tools for data sharing and analysis in environmental networks. *Inland Waters*, 6(4): 637-644.
- Rigosi, A., Hanson, P.C., Hamilton, D.P., Hipsey, M., Rusak, J. A., Bois, J., Sparber, K., Chorus, I., Watkinson, A.J., Qin, B., Kim, B. and Brookes, J.D., 2015. Determining the probability of cyanobacterial blooms: the application of Bayesian networks in multiple lake systems. *Ecological Applications*, 25: 186–199.
- Rogers, C.K., Lawrence, G.A. and Hamblin, P.F., 1995. Observations and numerical simulation of a shallow ice-covered mid-latitude lake. *Limnology and Oceanography*, **40**: 374-385.
- Romarheim, A.T., Tominaga, K., Riise, G. and Andersen, T., 2015. The importance of year-to-year variation in meteorological and runoff forcing for water quality of a temperate, dimictic lake. *Hydrology and Earth System Sciences*, 19(6): 2649-2662.
- Salmon, S.U., Hipsey, M.R., Wake, G.W., Ivey, G.N. and Oldham, C.E., 2017. Quantifying Lake Water Quality Evolution: Coupled Geochemistry, Hydrodynamics, and Aquatic Ecology in an Acidic Pit Lake. *Environmental Science & Technology*, 51(17): 9864-9875.
- Saloranta, T.M. and Andersen, T., 2007. MyLake—A multi-year lake simulation model code suitable for uncertainty and sensitivity analysis simulations. *Ecological modelling*, 207(1), pp.45-60.
- Schwarz, C.V. and White, B.Y., 2005. Metamodeling knowledge: Developing students' understanding of scientific modeling. *Cognition and Instruction*, 23(2): 165-205.
- Schwarz, C.V., Reiser, B.J., Davis, E.A., Kenyon, L., Achér, A., Fortus, D., Shwartz, Y., Hug, B. and Krajcik, J., 2009. Developing a learning progression for scientific modeling: Making scientific modeling accessible and meaningful for learners. *Journal of Research in Science Teaching*, 46(6): 632-654.
- Sherman, F.S., Imberger, J. and Corcos, G.M., 1978. Turbulence and mixing in stably stratified waters. *Annual Review of Fluid Mechanics*, 10: 267-288.

- Snortheim, C.A., P.C. Hanson, K.D. McMahon, J.S. Read, C.C. Carey, and H.A. Dugan. Meteorological drivers of hypolimnetic anoxia in a eutrophic, north temperate lake. *Ecological Modelling*. 343: 39-53. DOI: 10.1016/j.ecolmodel.2016.10.014
- Spigel, B., 1978. Wind mixing in Lakes. PhD thesis, University of California, Berkeley.
- Spigel, R.H., Imberger, J. and Rayner, K.N., 1986. Modeling the diurnal mixed layer. *Limnology and Oceanography*, 31: 533-556.
- Stepanenko, V., Mammarella, I., Ojala, A., Miettinen, H., Lykosov, V. and Vesala, T., 2016. LAKE 2.0: a model for temperature, methane, carbon dioxide and oxygen dynamics in lakes. *Geoscientific Model Development*, 9(5), pp.1977-2006.
- Stepanenko, V.M., Martynov, A., Jöhnk, K.D., Subin, Z.M., Perroud, M., Fang, X., Beyrich, F., Mironov, D. and Goyette, S., 2013. A one-dimensional model intercomparison study of thermal regime of a shallow, turbid midlatitude lake. *Geoscientific Model Development*, 6(4), pp.1337-1352.
- Stewart, J., Cartier, J.L. and Passmore, C.M., 2005. Developing understanding through model-based inquiry. In M.S. Donovan & J.D. Bransford (Eds.), *How students learn* (pp. 515–565). Washington, DC: National Research Council.
- Strub, P.T. and Powell, T.M., 1987. Surface temperature and transport in Lake Tahoe: inferences from satellite (AVHRR) imagery. *Continental Shelf Research*, 7: 1001-1013.
- Subratie, K., Aditya, S., Figueiredo, R., Carey, C.C. and Hanson, P.C., 2017. GRAPLER: A distributed collaborative environment for lake ecosystem modeling that integrates overlay networks, high-throughput computing, and web services. *Concurrency and Computation: Practice and Experience*, 29(13): e4139.
- Swinbank, W.C., 1963. Longwave radiation from clear skies. *Quarterly Journal of the Royal Meteorological Society*, 89: 339-348.
- Tennessee Valley Authority (TVA), 1972. Heat and mass transfer between a water surface and the atmosphere. Water Resources Research Laboratory Report 14, Report No. 0-6803.
- Tabata, S., 1973. A simple but accurate formula for the saturation vapour pressure over liquid water. *Journal of Applied Meteorology*, 12: 1410-1411.
- Thain, D., Tannenbaum, T. and Livny, M. (2005). "Distributed Computing in Practice: the Condor Experience" (PDF). *Concurrency and Computation: Practice and Experience*, 17 (2–4): 323–356.
- Ticehurst J.L., Newham LTH, Rissik D, Letcher RA and Jakeman AJ. 2007. A Bayesian network approach for assessing the sustainability of coastal lakes in New South Wales, Australia. *Environmental Modelling & Software* 22(8):1129-1139

- Tranvik, L.J., Downing, J.A., Cotner, J.B., Loiselle, S.A., Striegl, R.G., Ballatore, T.J., Dillon, P., Finlay, K., Fortino, K., Knoll, L.B. and Kortelainen, P.L., 2009. Lakes and reservoirs as regulators of carbon cycling and climate. *Limnology and Oceanography*, 54(6part2): 2298-2314.
- Trolle, D., Hamilton, D.P., Hipsey, M.R., Bolding, K., Bruggeman, J., Mooij, W. M., Janse, J. H., Nielsen, A., Jeppesen, E., Elliott, J.E., Makler-Pick, V., Petzoldt, T., Rinke, K., Flindt, M. R., Arhonditsis, G.B., Gal, G., Bjerring, R., Tominaga, K., Hoen, J., Downing, A.S., Marques, D. M., Fragoso Jr, C.R., Søndergaard, M. and Hanson, P.C., 2012. A community-based framework for aquatic ecosystem models. *Hydrobiologia*, 683: 25-34.
- UNESCO, 1981. Technical papers in Marine Science. No. 36.
- Vavrus, S.J., Wynne, R.H. and Foley, J.A., 1996. Measuring the sensitivity of southern Wisconsin lake ice to climate variations and lake depth using a numerical model. *Limnology and Oceanography*, 41: 822-831.
- Vickers, D., Mahrt, L. and Andreas, E.L., 2013. Estimates of the 10-m neutral sea surface drag coefficient from aircraft eddy-covariance measurements. *Journal of Physical Oceanography*, 43: 301-310.
- Weathers, K.C., Groffman, P.M., Van Dolah, E., Bernhardt, E.S., Grimm, N.B., McMahon, K.D., Schimel, J., Paolisso, M., Maranger, R.J., Baer, S., Brauman, K.A. and Hinckley, E., 2016. Frontiers in Ecosystem Ecology from a Community Perspective: The Future is Boundless and Bright. *Ecosystems*, 19(5): 753-770.
- Weber, M., Rinke, K., Hipsey, M.R. and Boehrer, B., 2017. Optimizing withdrawal from drinking water reservoirs to reduce downstream temperature pollution and reservoir hypoxia. *Journal of Environmental Management*, 197: 96-105.
- Weinstock, J., 1981. Vertical turbulence diffusivity for weak or strong stable stratification. *Journal of Geophysical Research*, 86(C10): 9925-9928.
- Williamson, C.E., Saros, J.E., Vincent, W.F. and Smol, J.P., 2009. Lakes and reservoirs as sentinels, integrators, and regulators of climate change. *Limnology and Oceanography*, 54(6part2), 2273-2282.
- Woolway, R.I., Verburg, P., Merchant, C.J., Lenters, J.D., Hamilton, D.P., Brookes, J., Kelly, S., Hook, S., Laas, A., Pierson, D. and Rimmer, A., 2017. Latitude and lake size are important predictors of over-lake atmospheric stability. *Geophysical Research Letters*, 44 (17), 8875–8883. DOI:10.1002/2017GL073941
- Wu J., 1973. Wind induced entrainment across a stable density interface. *Journal of Fluid Mechanics*, 61: 275-278.
- Xenopoulos, M.A. and Schindler, D.W., 2001. The environmental control of near-surface thermoclines in boreal lakes. *Ecosystems*, 4: 699-707.

Yajima, H. and Yamamoto, S., 2015. Improvements of radiation estimations for a simulation of water temperature in a reservoir. *Journal of Japan Society of Civil Engineers, Ser. B1 (Hydraulic Engineering)*, 71(4): 775-780.

Yao, H., Samal, N.R., Joehnk, K.D., Fang, X., Bruce, L.C., Pierson, D.C., Rusak, J.A. and James, A., 2014. Comparing ice and temperature simulations by four dynamic lake models in Harp Lake: past performance and future predictions. *Hydrological Processes*, 28: 4587-4601.

Yeates, P.S. and Imberger, J., 2003. Pseudo two-dimensional simulations of internal and boundary fluxes In stratified lakes and reservoirs. *International Journal of River Basin Research*, 1: 1-23.

Zhang, W. and Arhonditsis G.B., 2009. A Bayesian hierarchical framework for calibrating aquatic biogeochemical models, *Ecological Modelling*, 220(18): 2142-2161.

Zohar, A. and Dori, Y.J., 2012. *Introduction*. In: Metacognition in science education (pp. 1-19). Springer Netherlands.

Table 1. Summary of GLM physical parameters with recommended values and references.

Symbol	glm.nml ID	Description	Units	Default	Reference	Comments
Model Structure						
h_{min}	min_layer_thick	Minimum layer thickness	m	0.5	Bruce et al. (2017)	Standardised for multi-lake comparison
h_{max}	max_layer_thick	Maximum layer thickness	m	1.5	Bueche et al. (2017)	Should be estimated relative to lake depth.
Lake Properties						
K_w	Kw	Extinction coefficient for PAR radiation	m^{-1}	0.2	Lake specific	Should be measured, e.g. mean of simulation period. Can be estimated from Secchi depth.
A_C	critical_area	Critical area below which wind sheltering may occur	m^2	10^7	Xenopoulos and Schindler (2001)	
Surface Thermodynamics						
C_H	ch	Bulk aerodynamic coefficient for sensible heat transfer	-	0.0013	Fischer et al. (1979)	From Hicks' (1972) collation of ocean and lake data; many studies since use similar values. Internally calculated if atmos stability correction is
C_E	ce	Bulk aerodynamic coefficient for latent heat transfer	-	0.0013	Bruce et al. (2017)	
C_M	cd	Bulk aerodynamic	-	0.0013	Bueche et al. (2017)	

Symbol	glm.nml ID	Description	Units	Default	Reference	Comments
		coefficient for transfer of momentum				on.
λ	-	Latent heat of evaporation	J kg ⁻¹	2.453x10 ⁶	Standard	Not adjustable in glm.nml
ε_a	-	Emissivity of the water surface	-	0.985	Standard	Water only, no ice Ice or snow
σ	-	Stefan-Boltzmann constant	W m ⁻² K ⁻⁴	5.67x10 ⁻⁸	Constant	Not adjustable in glm.nml
Mixing Parameters						
C_K	coef_mix_conv	Mixing efficiency - convective overturn	-	0.2	Yeates & Imberger (2003)	Selected from a range given in Spigel et al. (1986)
C_W	coef_wind_stir	Mixing efficiency - wind stirring	-	0.23	Spigel et al. (1986)	From Wu (1973)
C_S	coef_mix_shear	Mixing efficiency - shear production	-	0.3	Sherman et al. (1978)	Best fit of experiments reviewed
C_T	coef_mix_turb	Mixing efficiency - unsteady turbulence (acceleration)	-	0.51	Bruce et al. (2017) Bueche et al. (2017)	
C_{KH}	coef_mix_KH	Mixing efficiency - Kelvin-Helmholtz turbulent	-	0.3	Sherman et al. (1978)	"a good rule of thumb..."

Symb ol	glm.nml ID	Description	Units	Default	Referen ce	Comments
		billows				
C_{HYP}	coef_mix_hyp	Mixing efficiency of hypolimnetic turbulence	-	0.5	Weinstock (1981)	General diffusivities in Jellison and Melack (1993)
Inflows & Outflows						
C_D	strmbd_drag	streambed_drag	-	0.016	Site specific	Set based on inflow stream type
G	seepage_rate	Seepage rate	m day ⁻¹	0		
Snow & Ice						
K_{w1}	-	Waveband 1, snow ice light extinction	m ⁻¹	48.0	Rogers et al., (1995),	
K_{w2}	-	Waveband 2, snow ice light extinction	m ⁻¹	20.0		
K_{b1}	-	Waveband 1, blue ice light extinction	m ⁻¹	1.5	Patterson and Hamblin (1988)	
K_{b2}	-	Waveband 2, blue ice light extinction	m ⁻¹	20.0		
K_{s1}	-	Waveband 1, snow light extinction	m ⁻¹	6	Ashton (1986)	
K_{s2}	-	Waveband 2, snow light extinction	m ⁻¹	20	Yao et al., (2014)	
D_z	-	Distance of hear	m	0.039		

Symbol	glm.nml ID	Description	Units	Default	Reference	Comments
		transfer, ice water				
ρ_{white}	-	Density, snow ice	kg m ⁻³	890		
ρ_{blue}	-	Density, blue ice	kg m ⁻³	917		
ρ_{snow}	-	Density, snow	kg m ⁻³	Variable		
c_{pi}	-	Heat capacity, ice	kJ kg ⁻¹ °C ⁻¹	2.1		
c_{pw}	-	Heat capacity, ice	kJ kg ⁻¹ °C ⁻¹	4.2		
K_c	-	Compaction coefficient	-	Variable		
K_m	-	Thermal conductivity, snow ice	W m ⁻¹ °C ⁻¹	2.0		
K_m	-	Thermal conductivity, blue ice	W m ⁻¹ °C ⁻¹	2.3		
K_m	-	Thermal conductivity, snow	W m ⁻¹ °C ⁻¹	Variable		
K_m	-	Thermal conductivity, sediment	W m ⁻¹ °C ⁻¹	1.2		
K_m	-	Thermal conductivity, water	W m ⁻¹ °C ⁻¹	0.57		
L	-	Latent heat of fusion	kJ kg ⁻¹	0334		
Bottom Stress						

Symb ol	glm.nml ID	Description	Units	Default	Referen ce	Comments
<i>D</i>	-	Typical particle diameter	m			

Appendix A: Bird solar radiation model

The Bird Clear Sky Model (BCSM) was developed by (Bird, 1984) to predict clear-sky direct beam, hemispherical diffuse, and total hemispherical broadband solar radiation on a horizontal surface. Average solar radiation is computed at the model time-step (e.g., hourly) based on ten user-specified input parameters (Table A1).

Table A1: Parameters required for the BCSM model.

Variable	Description	Example values (e.g., Luo et al., 2010)
Lat	Latitude (degrees, + for N)	-31.77
Long	Longitude (degrees + for E)	116.03
TZ	Time Zone indicated by number of hours from GMT	+7.5
AP	Atmospheric Pressure (millibars)	1013
O _z	Ozone Conc. (atm-cm)	0.279 - 0.324
W	Total Precipitable Water Vapour (atm-cm)	1.1 - 2.2
AOD ₅₀₀	Aerosol Optical Depth at 500 nm	0.033 – 0.1
AOD ₃₈₀	Aerosol Optical Depth at 380 nm	0.038 – 0.15
α _{SW}	Surface albedo	0.2

The solar constant in the model is taken as 1367 W/m². This is corrected due to the elliptical nature of the earth's orbit and consequent change in distance to the sun. This calculation gives us the Extra-Terrestrial Radiation ($\hat{\Phi}_{ETR}$), at the top of the atmosphere:

$$\hat{\Phi}_{ETR} = 1367 \left(1.00011 + 0.034221 \cos(\Phi_{day}) + 0.00128 \sin(\Phi_{day}) + 0.000719 \cos(\Phi_{day}) \right) \quad (A1)$$

where the day angle, Φ_{day} , is computed using, d , the day number:

$$\Phi_{day} = 2\pi \left(\frac{d-1}{365} \right) \quad (A2)$$

The solar declination, Φ_{dec} (radians), is computed from:

$$\Phi_{dec} = \begin{bmatrix} 0.006918 - 0.399912 \cos(\Phi_{day}) + 0.070257 \sin(\Phi_{day}) - 0.006758 \cos(2(\Phi_{day})) + \\ 0.000907 \sin(2\Phi_{day}) - 0.002697 \cos(3(\Phi_{day})) + 0.00148 \sin(3(\Phi_{day})) \end{bmatrix} \quad (A3)$$

We then solve the equation of time:

$$EQT = \begin{bmatrix} 0.0000075 + 0.001868 \cos(\Phi_{day}) - 0.032077 \sin(\Phi_{day}) \\ -0.014615 \cos(2(\Phi_{day})) - 0.040849 \sin(2(\Phi_{day})) \end{bmatrix} \times 229.18 \quad (A4)$$

in order to compute the hour angle, Φ_{hr} , calculated with noon zero and morning positive as:

$$\Phi_{hr} = 15(hr - 12.5) + Long - 15 TZ + \left(\frac{EQT}{4}\right) \quad (A5)$$

where TZ is the time-zone shift from GMT. The zenith angle, Φ_{zen} (radians), is calculated from:

$$\cos(\Phi_{zen}) = \cos(\Phi_{dec})\cos(\Phi_{hr})\cos(Lat) + \sin(\Phi_{dec})\sin(Lat) \quad (A6)$$

When Φ_{zen} is less than 90° , the air mass factor is calculated as:

$$AM = \left[\cos(\Phi_{zen}) + \frac{0.15}{(93.885 - \Phi_{zen})^{1.25}} \right]^{-1} \quad (A7)$$

which is corrected for atmospheric pressure, p (hPa),

$$AM_p = \frac{AM p}{1013} \quad (A8)$$

AM_p is then used to calculate the Rayleigh Scattering as:

$$T_{rayleigh} = e^{[(-0.0903 AM_p^{0.84}) + (1 + AM_p - AM_p^{1.01})]} \quad (A9)$$

The effect of ozone scattering is calculated by computing ozone mass, which for positive air mass is:

$$T_{ozone} = \left[1 - \left(0.1611 (Oz AM) (1 + 139.48 (Oz AM))^{-0.3035} \right) - \frac{0.002715 (Oz AM)}{1 + 0.044 (Oz AM) + 0.0003 (Oz AM)^2} \right] \quad (A10)$$

The scattering due to mixed gases for positive air mass is calculated as:

$$T_{mix} = e^{[-0.0127 AM_p^{0.26}]} \quad (A11)$$

Then the water scattering is calculated by getting the water mass:

$$Wm = WAM_p \quad (A12)$$

where W is the precipitable water vapour. This can be approximated from dew point temperature, eg.:

$$\ln W = a T_d + b \quad (A13)$$

where a and b are regression coefficients which have been taken as 0.09, 0.07, 0.07 and 0.08 for values of a while b is 1.88, 2.11, 2.12 and 2.01 in spring, summer, autumn and winter (Luo et al., 2010).

Then the water scattering effect is calculated as:

$$T_{water} = \left[1 - \frac{(2.4959 Wm)}{1 + (79.034 Wm)^{0.6828} + 6.385 Wm} \right] \quad (A14)$$

The scattering due to aerosols requires the Aerosol Optical Depth at 380 nm and 500 nm:

$$TauA = 0.2758 AOD_{380} + 0.35 AOD_{500} \quad (A15)$$

and the scattering due to aerosols is then calculated as:

$$T_{aerosol} = e^{(-TauA)^{0.873} (1+TauA-TauA^{0.7088}) AM^{0.9108}} \quad (A16)$$

We also define:

$$T_{aa} = 1 - [0.1 (1 - AM + AM^{1.06}) (1 - T_{aerosol})] \quad (A17)$$

and:

$$\frac{0.5(1 - T_{rayleigh}) + 0.84(1 - T_{as})}{1 - AM + AM^{1.02}} \quad (A18)$$

where the 0.84 value used is actually the proportion of scattered radiation reflected in the same direction as incoming radiation.

The direct beam radiation on a horizontal surface at ground level on a clear day is given by,

$$\hat{\phi}_{DB} = 0.9662 \hat{\phi}_{ETR} T_{rayleigh} T_{ozone} T_{mix} T_{watvap} T_{aerosol} \cos(\Phi_{zen}) \quad (A19)$$

$$\hat{\phi}_{AS} = 0.79 \hat{\phi}_{ETR} T_{ozone} T_{mix} T_{watvap} T_{aa} \cos(\Phi_{zen}) \quad (A20)$$

The total irradiance hitting the surface is therefore (W m^{-2}):

$$\hat{\phi}_{SW} = \frac{\hat{\phi}_{DB} + \hat{\phi}_{AS}}{1 - (\alpha_{SW} \alpha_{SKY})} \quad (A21)$$

The albedo is computed for the sky as:

$$\alpha_{SKY} = 0.068 + (1 - 0.84) \left(1 - \frac{T_{aerosol}}{T_{aa}} \right) \quad (A22)$$

Appendix B: Non-neutral bulk transfer coefficients

The iterative procedure used in this analysis is conceptually similar to the methodology discussed in detail in Launiainen and Vihma (1990). The first estimate for the neutral drag coefficient is specified as a function of windspeed as it has been commonly observed that C_{DN} increases with U_{10} (Figure A1). This is modelled by first by estimating:

$$C_{DN-10} = \begin{cases} 0.001 & U_{10} \leq 5 \\ 0.001 (1 + 0.07[U_{10} - 5]) & U_{10} > 5 \end{cases} \quad \text{Option 1 : Francey and Garratt (1978), Hicks (1972)} \quad (\text{A23})$$

$$C_{DN-10} = 1.92 \times 10^{-7} U_{10}^3 + 0.00096 \quad \text{Option 2 : Babanin and Makin (2008)}$$

and then computing the Charnock formula with the smooth flow transition (e.g., Vickers et al., 2013):

$$z_o = \frac{\alpha u_*^2}{g} + 0.11 \frac{\nu}{u_*} \quad (\text{A24})$$

where α is the Charnock constant (0.012), u_* is the friction velocity ($\sqrt{C_{DN-10} U_{10}^2}$) using Eq A23, and the final drag is re-computed using:

$$C_{DN-10} = \left[\frac{k}{\ln\left(\frac{10}{z_o}\right)} \right]^2 \quad (\text{A25})$$

where k is the von Karman constant. Note the neutral humidity/temperature coefficient, C_{HWN-10} , is held constant at the user defined C_H value and doesn't scale with wind speed.

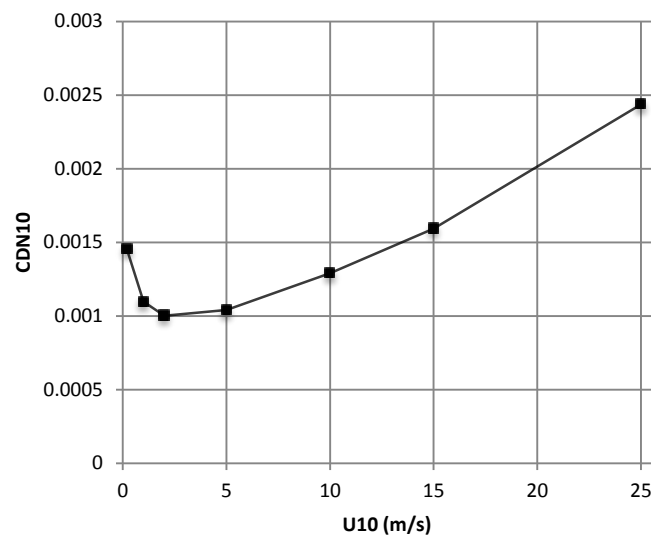


Figure A1: Scaling of the 10m neutral drag coefficient with wind speed (Eqns A23-25)

Under non-neutral conditions in the atmospheric boundary layer, the transfer coefficients vary due to stratification seen in the air column, as was parameterised by Monin and Obukhov (1954) using the now well-known stability parameter, z/L , where L is the Obukhov length defined as:

$$L = \frac{-\rho_a u_*^3 \theta_V}{kg \left(\frac{H}{c_p} + 0.61 \frac{\theta E}{\lambda} \right)} \quad (\text{A26})$$

where $\theta_V = \theta(1 + 0.61q)$ is the virtual temperature and H and E are the bulk fluxes. Paulson (1970) presented a solution for the vertical profiles of wind speed, temperature and moisture in the developing boundary layer as a function of the Monin-Obukhov stability parameter; the so-called flux-profile relationships:

$$U_z = \frac{u_*}{k} \left[\ln \left(\frac{z}{z_o} \right) - \psi_M \left(\frac{z}{L} \right) \right] \quad (\text{A27a})$$

$$\theta_z - \theta_s = \frac{\theta_*}{k} \left[\ln \left(\frac{z}{z_\theta} \right) - \psi_H \left(\frac{z}{L} \right) \right] \quad (\text{A27b})$$

$$q_z - q_s = \frac{q_*}{k} \left[\ln \left(\frac{z}{z_q} \right) - \psi_E \left(\frac{z}{L} \right) \right] \quad (\text{A27c})$$

where ψ_M , ψ_H and ψ_E are the similarity functions for momentum, heat and moisture respectively, and z_o , z_θ and z_q are their respective roughness lengths. For unstable conditions ($L < 0$), the stability functions are defined as (Paulson 1970; Businger *et al.*, 1971; Dyer, 1974):

$$\psi_M = 2 \ln \left(\frac{1+x}{2} \right) + \ln \left(\frac{1+x^2}{2} \right) - 2 \tan^{-1} x + \frac{\pi}{2} \quad (\text{A28a})$$

$$\psi_E = \psi_H = 2 \ln \left(\frac{1+x^2}{2} \right) \quad (\text{A28b})$$

where

$$x = \left[1 - 16 \left(\frac{z}{L} \right)^{1/4} \right] \quad (\text{A29})$$

During stable stratification ($L > 0$) they take the form:

$$\psi_M = \psi_E = \psi_H = \begin{cases} -5 \left(\frac{z}{L}\right) & 0 < \frac{z}{L} < 0.5 \\ 0.5 \left(\frac{z}{L}\right)^{-2} - 4.25 \left(\frac{z}{L}\right)^{-1} - 7 \left(\frac{z}{L}\right) - 0.852 & 0.5 < \frac{z}{L} < 10 \\ \ln\left(\frac{z}{L}\right) - 0.76 \left(\frac{z}{L}\right) - 12.093 & \frac{z}{L} > 10 \end{cases} \quad (\text{A30})$$

Substituting equations (17)-(18) into (A27) and ignoring the similarity functions leaves us with neutral transfer coefficients as a function of the roughness lengths:

$$C_{XN} = k^2 \left[\ln\left(\frac{z}{z_o}\right) \right]^{-1} \left[\ln\left(\frac{z}{z_X}\right) \right]^{-1} \quad (\text{A31})$$

where N denotes the neutral value and X signifies either D , H or E for the transfer coefficient and o , θ or q for the roughness length scale. Inclusion of the stability functions into the substitution and some manipulation (Imberger and Patterson, 1990; Launianen and Vihma, 1990) yields the transfer coefficients relative to these neutral values:

$$\frac{C_X}{C_{XN}} = \left[1 + \frac{C_{XN}}{k^2} \left(\psi_M \psi_X - \frac{k \psi_X}{\sqrt{C_{DN}}} - \frac{k \psi_M \sqrt{C_{DN}}}{C_{XN}} \right) \right] \quad (\text{A32})$$

Hicks (1975) and Launianen and Vihma (1990) suggested an iterative procedure to solve for the stability corrected transfer coefficient using (A32) based on some initial estimate of the neutral value. The surface flux is subsequently estimated according to (17-18) and used to provide an initial estimate for L (equation A26). The partially corrected transfer coefficient is then recalculated and so the cycle goes. Strub and Powell (1987) and Launianen (1995), presented an alternative based on estimation of the bulk Richardson number, Ri_B , defined as:

$$Ri_B = \frac{gz}{\theta_V} \left(\frac{\Delta\theta + 0.61 \theta_V \Delta q}{U_z^2} \right) \quad (\text{A33})$$

and related as a function of the stability parameter, z/L , according to:

$$Ri_B = \frac{z}{L} \left(\frac{k \sqrt{C_{DN}} / C_{HWN} - \psi_{HW}}{[k / \sqrt{C_{DN}} - \psi_M]^2} \right) \quad (\text{A34})$$

where it is specified that $C_{HN} = C_{WN} = C_{HWN}$. Figure A2 illustrates the relationship between the degree of atmospheric stratification (as described by both the bulk Richardson number and the Monin-Obukhov stability parameter) and the transfer coefficients scaled by their neutral value.

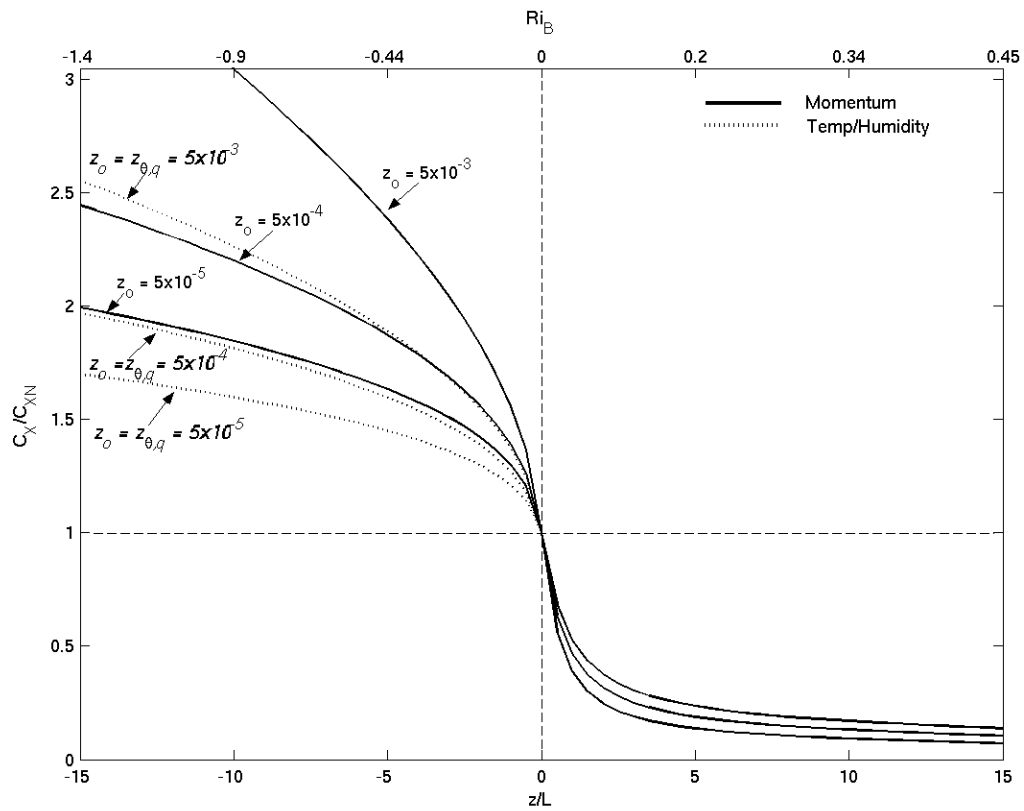


Figure A2: Relationship between atmospheric stability (bottom axis – z/L , top axis – Ri_B) and the bulk-transfer coefficients relative to their neutral value (C_X/C_{XN} where X represents D , H or W) for several roughness values (computed from Eq. A32). The solid line indicates the momentum coefficient variation (C_D/C_{DN}) and the broken line indicates humidity and temperature coefficient (C_{HW}/C_{HWN}) variation.